THÈSE

Pour obtenir le grade de

Docteur

Délivré par

UNIVERSITE DE PERPIGNAN VIA DOMITIA

Préparée au sein de l'école doctorale Energie et Environnement- ED 305
et de l'unité de recherche BioWooEB-CIRAD

Spécialité :

Sciences de l'Ingénieur

Présentée par

Xuan-Huynh PHAM

TITRE DE LA THESE

Oxidative pyrolysis of biomass pellets in a fixed bed

Soutenue **le 22 Octobre 2018** devant le jury composé de

M. Gilles FLAMANT, Professeur, PROMES, Perpignan	Président
M. Hervé JEANMART, Professeur, UCL, Louvain-la-Neuve, Belgique	Rapporteur
M. Yann ROGAUME, Professeur, ENSTIB/LERMAB, Epinal	Rapporteur
Mme. Capucine DUPONT, Docteur, HDR, UNESCO-IHE, Delft, Pays-Bas	Examinateur
M. Sylvain SALVADOR, Professeur, IMT Mines, Albi	Examinateur
M. Bruno PIRIOU, Docteur, CIRAD, Montpellier	Encadrant
M. Laurent VAN DE STEENE , Docteur, HDR, CIRAD, Montpellier	Directeur de thèse

- Page intentionally left blank -

À mes chers parents

To my beloved parents

Dành tặng bố mẹ kính yêu

- Page intentionally left blank -

ACKNOWLEDGEMENT

As quoted in a Vietnamese proverb:

"Không thầy đố mày làm nên"

I dare you to achieve success without a teacher

To complete this dissertation, first, I would like to express my great thanks to my "teachers" (my supervisors) Dr. Laurent Van de Steene and Dr. Bruno Piriou. A "MERCI BEAUCOUP" to Laurent not only for assisting in my dream of pursuing a PhD in France and for taking the time to support me in all aspects of my work, but furthermore also for supporting me to join to a great research network in both countries France and Vietnam. His rigorous supervision provided me a logical and effective methodology of doing research that I constantly apply in my current work. For example, planning for tests; publications and writing; and taking minutes for meetings. In this dissertation, he always provided me new insightful suggestions on structure, content, even some scientific terms and patiently explained me until I get the picture of everything. To Bruno, I would say thanks for all the patience he had with me at all times and for taking care of me as a brother along with my family. For all the troubles concerning equipment, experiments, measurements and administrations, whenever I was in need, he worked his magic and then everything went smoothly. He always arrived "tombe a pic" as the French people say. He taught and encouraged me that "everything is possible" and now I believe this is true. I feel very lucky to have worked with two wonderful supervisors!

A third supervisor that I would like to express my gratefulness and my respect to is Pr. Sylvain Salvador. Many thanks Sylvain for your time and your attention for me during the last three years. Your directions, comments and remarks always provided me new insight to raise my reports and communication documents up to a higher level.

A special thanks to all the members of the steering committee Dr. Gilles Vaitilingom, Dr. Jean Michel Commandré, Dr. Capuccine Dupont, and Dr. Christelle Perilhion for "piloting" the ship named "Huynh's thesis" and helping the ship to dock at the SUCCESS port.

Other special thanks to the excellent technicians Jérémy Valette, Laurent Martin, Eric Martin, and Charline Lanvin, without their help this work could have never been performed and finished.

In addition, during my thesis I received great helps for the administrative works from Nathalie Troalen, Isabelle Châlon, and later Coline Brau. Thank you all.

Thank you everyone at the research unit BioWooEB for creating a fantastic work and cross-cultural environment where you always treated me as a part of this family. Thank you Dr. Sylvie Mouras, Dr. François Pinta, Dr. François Broust, Dr. Joël Blin, and Dr. Anthony Benoist for your advices and encouragement for my work. Thank you to all the PhD students, intern students and post-doctorats at the BioWooEB, especially the three sounding boards Luke Stover, Gwendal Vonk, and Dr. Sébastien Wahl. And merci beaucoup Jérôme Singla pour les expériences "after work" exceptionnelles.

Besides the people in my institution, I would like to thank the rest of my dissertation jury for having accepted to attend my dissertation defense as well as their insightful comments, which motivated me to complete my research from various perspectives. Merci à vous Pr. Gilles Flamant, Pr. Yann Rogaume, et Pr. Hervé Jeanmart.

In addition, I would like to say thank to all my colleagues in the CleanED laboratory, University of Science and Technology of Hanoi, who helped me a lot to achieve the scholarship as well as encouraging me during my thesis.

Finally, I would like to thank my family, friends, my darling Hang and my daughter Bơ (Karine Tu Anh) for all their support, their love and their trust in me.

This work has been financially supported by CIRAD, French and Vietnamese governments.

Merci à toutes et à tous !

Chân thành cảm ơn mọi người !

Montpellier 2018

PHẠM Xuân Huỳnh

RÉSUMÉ

La gazéification étagée est une technologie innovante pour la production d'énergie renouvelable de petite et moyenne puissances, pour laquelle l'élargissement de la gamme de biomasses utilisables constitue un enjeu majeur de développement. Cette thèse porte spécifiquement sur la pyrolyse oxydante en lit fixe, première étape clé du procédé, qui conditionne fortement la performance et la fiabilité de cette technologie. Trois types de biomasses – pin, miscanthus, et paille – conditionnées sous forme de granulés ont été étudiés.

Une étude expérimentale a été réalisée sur un réacteur pilote à lit fixe de 20 cm de diamètre et 1.6 m de hauteur permettant de reproduire des conditions opératoires proches de celles rencontrées durant l'étape de pyrolyse dans les gazéifieurs industriels. Le fonctionnement du procédé pour les trois biomasses a été caractérisé par la mesure du ratio air/biomasse, des températures, des rendements en charbon, gaz permanents et condensables et de leurs compositions.

Une attention particulière a été portée à la zone d'oxydation qui se propage verticalement vers le haut dans le lit de biomasse. Une méthodologie a été développée pour mesurer la vitesse de propagation, l'épaisseur et le tassement de cette zone et étudier l'impact de la nature de la biomasse. Dans un lit de granulés de bois, la vitesse et l'épaisseur de la zone d'oxydation est 25 % plus faible que dans un lit de granulés de paille ou miscanthus. L'effet catalytique des matières minérales sur les réactions de pyrolyse primaire et secondaire et son impact sur le fonctionnement du procédé, ont également été mis en évidence.

Mots-clés : Gazéification étagée; pyrolyse oxydante; lit fixe; smoldering; biomasse, granulés.

ABSTRACT

Staged gasification is an innovative technology for small and medium renewable energy production. The expansion of the range of usable biomass remains a major obstacle to development. This thesis focuses specifically on the oxidative pyrolysis in a fixed bed, the first step of the process that strongly influences the performance and reliability of this technology. Three types of biomass- pine, miscanthus and wheat straw - in form of pellets were studied.

An experimental study was carried out in a pilot fixed bed reactor of 20 cm diameter and 1.6 m height allowing the reproduction of similar conditions to those existing in the pyrolysis step of an industrial gasifier. The process operation for the three biomasses was characterized by measuring the air/biomass ratio, bed temperature, yields and compositions of char, permanent gases and condensates.

A particular attention was paid on the oxidation zone which propagates upward towards the raw biomass. A method was developed to measure the propagation velocity, thickness and the compaction of the oxidation zone and to study the impact of the biomass nature. Velocity and thickness of this zone were 25 % lower in a fixed bed of wood pellets than in beds of wheat straw or miscanthus. Catalytic effect of the mineral matters on primary and secondary pyrolysis reactions and their impact on the process operation have been highlighted.

Keywords: *Staged gasification; oxidative pyrolysis; fixed bed; smoldering; biomass, pellets*

TABLE OF CONTENTS

- Page intentionally left blank -

GENERAL INTRODUCTION

Reliance on fossil fuels and their derived products by mankind raises many tremendous concerns on economy and environment such as energy shortages and global warming. Consequently, seeking an alternative source for the fossil fuels is necessary to overcome these problems. Along with other renewable energy sources such as wind, solar, hydropower, etc, biomass has been receiving an increased attention. Known as an abundant and reliable source, biomass plays an important role in the renewable energy domain nowadays. Depending on the type and properties of biomass, there are various types of technology for the biomass conversion into energy and material including biochemical, thermochemical and physicochemical conversion. Among them, the thermochemical processes are the most suitable technology for the conversion of the most common type of biomass, i.e. lignocellulosic biomass, into various convenient energy forms such as heat, electricity and gaseous, liquid or solid fuel. In recent years, gasification has emerged as an innovative technology to produce the synthesis gas or syngas from biomass, which is then used as fuel in an engine, electricity generator or a preliminary material to synthesize other chemical compounds.

In this manuscript, we focused on an advanced technology called air staged gasification. It shows the advantage over other gasification technologies of producing a higher efficiency and a clean syngas. The key solution of this technology lies on its specific design with two separated reactors: one pyrolyzer and one gasifier. Thus, the main stages of the biomass gasification process are separated physically that enable better control the whole gasification process. Moreover, pyrolysis stage in the pyrolyzer is particularly important as it produces the char, permanent and condensable gases that are subsequently cracked, reformed, oxidized, and gasified in the next stages in the gasifier. Understanding and controlling the pyrolysis stage was the main focus of this study.

Indeed, in the staged gasifiers, pyrolysis occurs in a continuous fixed bed. The energy needed for the heating, drying, and endothermic reactions of the conversion is provided by partial oxidation of the biomass. The pyrolysis process is said autothermal and referred here as “oxidative pyrolysis”. During oxidative pyrolysis in continuous downdraft reactors, the biomass and air are fed at the top of the reactor and char and pyrolysis gases are removed from the bottom. An Oxidation Zone (OZ) separates the unreacted biomass from the char and is the

location of several complex and coupled transformations or reactions. The stabilization of the OZ inside the bed is of particular interest for operators for two reasons:

- The top of the bed is maintained at a low temperature, thereby facilitating the control of the process and limiting the production and deposition of tar;
- A higher temperature zone is created below the OZ that favors tar cracking when crossing it.

The control of this OZ is complex as it depends on many parameters such as air and biomass flux as well as density and composition of the biomass. However, this control has been mastered by operators and constructors for a few years but only for wood chips with relatively low moisture content.

Extension of the biomass nature in such processes is clearly a big challenge for biomass gasification. Indeed, biomass with highest potential, from agricultural residues or herbaceous crop, causes technical problems due to their low density and high ash content when compared to wood chips ones. Such low-density and fibrous materials are not favorable to regular vertical flows in the reactor and are known to be responsible for bridging or channeling in the reactors and particularly when thermochemical transformations occurs. High ash content biomass affects the reactor behavior because of the inert mass of the ashes as well as its catalytic role on the transformations.

Densification is clearly the solution to meet the low-density technical issue just described regarding oxidative pyrolysis in continuous fixed beds. However, high density of biomass pellets will behave of course differently than wood chips due to significant difference in volumic energy density, heat and mass transfer mechanisms, and in a lesser extent vertical flow in the reactor. These issues have been investigated in the previous PhD [1], by comparing the behaviors of wood pellets and wood chips during oxidative pyrolysis. Furthermore, pelletization can above all open fixed bed gasification technologies to new high potential biomasses such as agricultural residues and energy crops.

In this work, we focused on the behaviors during oxidative pyrolysis of wheat straw and miscanthus pellets as the best representative of agricultural residues and herbaceous energy crops. The behavior of pine pellets as classical biomass for such process was used as reference.

Thus, the objective of this PhD was to provide practical answers to process designers and operators regarding the oxidative pyrolysis stage of a global process. In particular, we have done our best to measure some important physical quantities such as:

- Equivalence ratio (ER);
- Yields and compositions of the pyrolysis products;
- Temperature field.

The impact of the biomass nature on these quantities was another major industrial concern that we investigated.

For this purpose, in the first step, we used a pilot fixed bed reactor enabling operation in continuous mode as representative of an industrial two-stage gasifier. Process performance in terms of temperature, air/biomass ratio, equivalence ratio were quantified. Yields and compositions of pyrolysis products including char, condensates and permanent gases were determined. Mass and energy balances were established. A sensitivity study on the accuracies and impacts of some experimental and thermodynamic data on the energy balance was performed.

In the second step, we operated the reactor in batch operation mode to finely characterize some specific features of the OZ that we could not perform in continuous mode: propagation velocity, thickness, and compaction. A new methodology accompanied with data treatment tools were set up. Influence of biomass nature on such process, especially ash content and composition, was discussed through the oxidative pyrolysis of three biomasses.

This manuscript is divided into five chapters. Chapter I provides general context related to biomass-to-energy via thermochemical conversion. Chapter II highlights the most significant contributions from the literature on biomass oxidative pyrolysis. It ends with the positioning and objectives of the PhD thesis. Chapter III deals with the materials and methods. It covers three aspects: characterization of the biomass pellets; descriptions of the experimental apparatus; sampling and analyzing pyrolysis products. Chapter IV and V present the detailed experimental studies in continuous and in batch modes.

- Page intentionally left blank -

CHAPTER I

BIOMASS-TO-ENERGY

The world energy demand is currently satisfied mainly by fossil fuels including coal, crude oil and natural gas. However, these resources are limited and non-renewable. In addition, reliance on fossil fuels and their derived products forces human being to face with many tremendous concerns on economic development and environment such as energy shortage and global warming. Consequently, seeking for renewable energy sources is necessary, and biomass has been receiving increased interest as an alternative to fossil fuels.

Biomass is a renewable energy source as it is derived of living organic compounds including dedicated materials and wastes. Compared to other common forms of renewable energy sources, i.e. wind, solar, biomass is the world largest and most sustainable energy resource [3]. In addition, considering the cost effectiveness and availability factor, biomass-based technologies are becoming popular as they have edge over other renewable energy technologies. Moreover, they have a high flexibility to adapt existing fossil-fuel-based systems. They allow converting biomass into various convenient energy forms such as heat, electricity, as well as solid, liquid and gaseous fuels. Depending on the needs and the biomass properties, various technologies for the conversion were proposed.

In recent years, the development of biomass to energy processes has played an important role in easing the transition of using biomass as alternatives to the fossil fuels. For this purpose, two challenges remain essential: (i) understanding biomass conversion processes to better control the operation and optimize the performance; and (ii) expanding sources of usable biomasses.

This section aims at presenting first some basic features related to biomass and its properties, focusing on the lignocellulosic biomass. Then, the chapter describes principles of different biomass conversion processes. Finally, the main thermochemical technologies available for lignocellulosic biomass conversion are detailed.

I.1. General context

I.1.1. Biomass

Biomass includes the organic materials originating from plants, animals and microorganisms. It can be classified into three categories:

- ***Lignocellulosic biomass***

The name "lignocellulosic" refers to the main constituents of this type of biomass: cellulose, hemicellulose, and lignin. Lignocellulosic biomass feedstocks are classically divided into three sub-categories:

- *Agricultural residues*, that include food grain, bagasse, corn stalks, straw, seed husks, nutshells, and manure from cattle, poultry, and hogs;

- *Forest residues,* from harvesting or wood processing, such as branches, foliage, roots, wood waste, sawdust, timber slash, and mill scrap;

- *Herbaceous and woody energy crops*, from perennial grasses such as miscanthus, willows, switchgrass and some short rotation forest species such as eucalyptus, poplars and robinia.

- ***Non-lignocellulosic biomass***

Non-lignocellulosic biomass includes cereals, fruits, vegetables, which are a source of carbohydrates, lipids, proteins, starch, and sugar. Compared to lignocellulosic biomass, non-lignocellulosic biomass is relatively easier to convert to liquid fuels through extraction or fermentation process. Nevertheless, the production of energy from these sources must be considered carefully as it may compete with food supply.

- ***Organic wastes***

Wastes are derived from different stages of biomass/food production and use. They include municipal solid treatment, sewage sludge, animal and human wastes. They contain both lignocellulosic and non-lignocellulosic biomass. Food processing wastes are the effluents from a wide variety of industrial processes ranging from cereal bar manufacturers to fresh and frozen vegetable manufacturers or alcohol breweries. These residues and wastes can be in the form of either dry solids or watery liquids. Municipal solid waste is the main source of waste biomass, and much of it comes from renewable processes like food scraps, lawn clippings, leaves, and papers. Sewage sludge containing human excreta, fat, grease, and food wastes is a significant biomass source. Animal and human wastes are important biomass sources for many biological processes.

The sources of biomass can also be summarized as in Figure 1.

Figure 1. Main sources of biomass [4]

I.1.2. Biomass potential and worldwide usage

The estimates of the global potential of biomass energy vary widely in the literature. The variability arises from the different sources of biomass and the different methods for determining estimates for those biomasses. Fischer and Schrattenholzer [5] estimated the global biomass potential between 91 and 675 EJ.year^{-1} for the years 1990 to 2050. Their biomass included crop and forestry residues, energy crops, and animal and municipal wastes. Parikka [6] estimated the total worldwide energy potential from biomass on a sustainable basis to be 104 EJ.year^{-1}, of which woody biomass, energy crops and straw constituted 40, 36 and 17 %, respectively. Currently, according to the World Bioenergy Association factsheet: global technical biomass potential towards 2035 [7], the global supply of biomass in 2012 was 56.2 EJ compared to global energy supply of 560 EJ. This amount is expected to increase to 150 EJ by 2035. The distribution of each biomass types in the total biomass energy is shown in Table 1. Following that, agricultural residues and forestry residues are predicted to be the main biomass sources in the near future. The contribution of agricultural residues will increase ten times and forestry residues will double in 2035 compared to their values in 2012 [7].

Main sector	Sub sector	2012	2035
Agriculture	Dedicated crops	3.5	30
	By products and residues including manure	2.1	34
	Total agriculture	5.6	64
Forestry		48.9	78
Organic waste		1.7	8
Total		56.2	150

Table 1. Global technical potential of biomass in 2012 and 2035 (in EJ) [7]

The contribution of biomass in primary energy varies widely depending on the geographical and socio-economic conditions [8] (Table 2). For large portions of the rural populations of developing countries, and for the poorest sections of urban populations, biomass is often the only available and/or affordable source of energy for basic needs such as cooking and heating. In Europe, North America, and the Middle East, the share of biomass averages 2–3 % of total final energy consumption. In Africa, Asia and Latin America, which together account for three-quarters of the world's population, biomass provides a substantial share of the energy needs: one-third on average. In some of the poorest countries of Africa and Asia (e.g., Angola, Ethiopia, Mozambique, Tanzania, Democratic Republic of Congo, Nepal, and Myanmar) the share of biomass is 80–90 %.

Region	Share of biomass in final energy consumption
Africa (average)	62.0
Burundi	93.8
Ethiopia	85.6
Kenya	69.6
Somalia	86.5
Sudan	83.7
Uganda	94.6
South Asia (average)	56.3
East Asia (average)	25.1
China	23.5
Latin America (average)	18.2
Europe (average)	3.5
North America (average)	2.7
Middle East (average)	0.3

Table 2. The importance of biomass for energy purpose in different world regions [8]

However, along with the development of technologies on biomass conversion, the share of biomass in total energy consumption will increase dramatically, especially in Europe since some strong policies to encourage renewable energy are issued. For example, on the 29th of May 2011, the German government announced that it would close all of its nuclear power plants by 2022 to encourage the development of renewable energies, including biomass. France government has proposed to end sales of petrol and diesel vehicles by 2040 to promote biofuel. Table 3 presents the current and future potential bio energy contributions in 2030 for some member states of the EU [9]. As can be seen in the table, France, Germany, Italy, Poland, Spain, and UK are the countries that have the highest biomass potential. These reports highlighted the important role of biomass in the transition to a new energy system based on renewable energy.

	2010	2020	2030
Austria	6.9	7.8	8.7
Belgium	2.3	2.3	2.3
Cyprus	0.3	0.3	0.3
Czech Republic	3.8	4.5	5.0
Denmark	2.8	2.5	2.5
Estonia	1.5	2.2	2.6
Finland	9.6	9.8	9.4
France	31.4	37.2	47.4
Germany	26.2	33.8	43.2
Greece	1.6	3.4	3.8
Hungary	3.6	5.5	5.6
Ireland	1.1	1.2	1.3
Italy	16.2	18.7	24.8
Latvia	1.3	1.9	2.4
Lithuania	4.1	7.6	9.9
Malta	0.05	0.05	0.04
Netherlands	2.6	2.2	2.4
Poland	23.8	33.0	39.3
Portugal	3.6	3.9	4.1
Slovak Republic	2.2	2.4	3.6
Slovenia	1.8	1.7	1.8
Spain	16.5	22.0	25.1
Sweden	11.7	13.0	13.5
UK	13.5	19.0	24.5

*Table 3. Bio-energy potential in some member states of the EU (unit 25*Mtoe) [9]*

I.1.3. Biomass conversion processes

The bulky and inconvenient heterogeneous form of biomass are major barriers to a rapid shift from fossil to biomass fuels. There are many available technologies to overcome these barriers. For example, low energy density of biomass due to its high moisture content, low bulk density, high oxygen content, is dealt with pretreatment processes such as drying, densification (pelletization or briquetting) and torrefaction. In addition, various technologies aim at converting biomass into more convenient forms such as gas or liquid for transportation and use with high efficiency. These technologies can be divided into physicochemical, biochemical and thermochemical conversion processes (Figure 2).

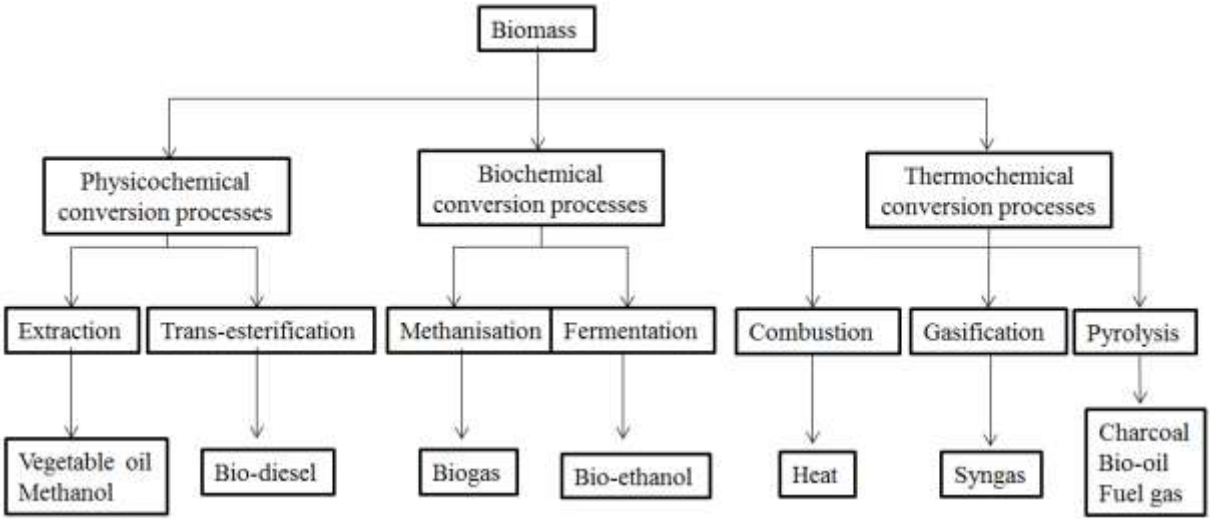

Figure 2. Simplified illustration of the three biomass conversion pathways and their final products

I.1.3.1. Physicochemical and biochemical conversion

- **Physicochemical conversion** includes extraction and trans-esterification.

Extraction is based on the separation of useful chemical compounds with physicochemical methods such as cold press extraction, supercritical fluid extraction, and microwave extraction. In the recent years, cavitation assisted (e.g. ultrasound assisted) extraction process has been utilized for the biomass pretreatment, delignification and hydrolysis, extraction of oil, fermentation and synthesis of bioalcohol.

Trans-esterification of plant or algal oil is a standardized process by which triglycerides react with methanol in the presence of a catalyst to deliver fatty acid methyl esters and glycerol. The extracted vegetable oils or animal fats are esters of saturated and unsaturated monocarboxylic acids with the trihydric alcohol glyceride (triglycerides) which can react with alcohol in the presence of a catalyst, a process known as transesterification.

- **Biochemical processes** includes methanisation and fermentation

Methanisation or anaerobic digestion is the natural biological process, which stabilizes organic wastes in the absence of oxygen and transforms them into bio-fertilizer and biogas. Biogas from this process mainly consists of methane (about 60 %) and carbon dioxide (approximately 40 %). Anaerobic digestion is a reliable technology for the treatment of wet organic waste.

Alcoholic fermentation refers to the conversion process of biomass containing sugar or starch to obtain bioethanol (or butanol) with assistance from the enzymatic treatment. Pretreatment of the biomass is followed by enzymatic hydrolysis to produce simple sugars, fermentation of sugars to produce biofuels, and then product separation.

I.1.3.2. Thermochemical conversion

Thermochemical is an important pathway for conversion of lignocellulosic biomass into energy. The three main of processes are combustion, pyrolysis and gasification (Figure 3).

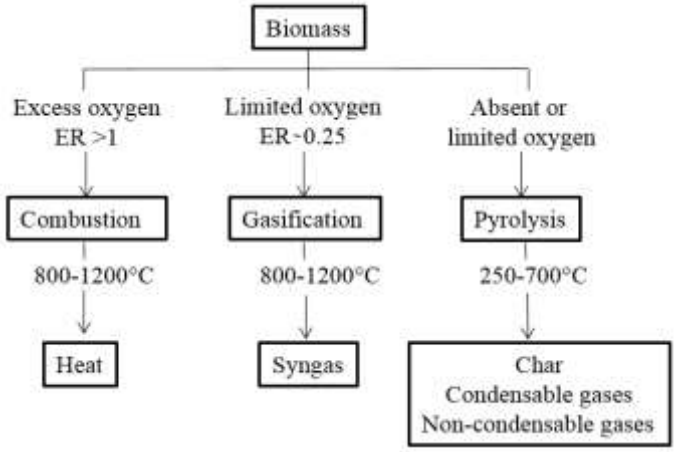

Figure 3. Details of the three types of biomass thermochemical conversion

Depending on the used amount of oxygen and on temperature, decomposition degree and/or oxidation degree are different, resulting in different products in the three processes:

- ***Combustion*** is the complete oxidation of complex hydrocarbon molecules of biomass to form carbon dioxide, water vapor. It is an exothermal process and heat releases from combustion can reach 800-1200°C. The combustion process can be used easily for heat applications, such as drying, cooking, lighting, etc... or for producing electricity.

- ***Gasification*** is the partial oxidation of biomass feedstocks under high temperature (500-1200°C) in the presence of an oxidizing agent. Oxidizing agents are typically air, steam, carbon dioxide, oxygen or a combination of them. In the presence of an oxidizing agent at high temperature, the large polymeric molecules of biomass decompose into lighter molecules and eventually to permanent gases (CO, H_2, CH_4 and lighter hydrocarbons), solid and liquid residues. The gaseous product from gasification process called synthesis gas or syngas can be used directly in gas engines for electricity production or upgraded into richer liquid or gas fuels.

- ***Pyrolysis*** is a thermochemical decomposition of biomass molecules at moderate temperature (250-700°C) without oxidizing agent or with a limited amount of oxidizing agent. During pyrolysis, large complex hydrocarbon molecules of biomass are broken down into relatively smaller and simpler molecules in gas, liquid, and solid form. The products of pyrolysis process are used as bio-char (through carbonization process) or bio-oil (through fast pyrolysis) or in subsequent stages of gasification or combustion processes.

In addition, torrefaction and liquefaction are commonly associated to low temperature pyrolysis. **Torrefaction**, a process different from carbonization, is a mild pyrolysis process carried out in a temperature range of 180- 300 °C in the absence of oxygen. This thermal pretreatment of biomass improves its energy density, grindability as well as reduces its oxygen-to-carbon (O/C) ratio and hygroscopic nature. **Liquefaction** is the direct conversion of biomass into liquid phase at low temperatures (around 300ºC), high pressures (of 200 bars) and in the presence of catalysts. This method achieves a better efficiency of the process and a good quality of the fluid produced. The main objective of these processes is to obtain a liquid with high-energy value (up to 35 $MJ.kg^{-1}$) and more stable.

Despite the clear classification above, pyrolysis can occur in almost all thermochemical processes and thus it is of particular interest and the objective of this study.

I.2. Lignocellulosic biomass and thermochemical processes

I.2.1. Lignocellulosic biomass: structure, composition and properties

Biomass composition and properties have a great impact on the performance of biomass conversion processes. A proper understanding of the physical and the chemical properties of biomass feedstock is essential for the process control and optimization. This section provides different points of view on lignocellulosic biomass from biomass structural constituents of cell walls to its composition and main properties related to the thermochemical process.

I.2.1.1. Structure of lignocellulosic biomass

Biomass is a complex mixture of organic materials with small amounts of minerals such as sodium, potassium, calcium, and iron. The main components of plant biomass are fibers or cell wall components, extractives and inorganic materials (

Figure 4). In general, lignocellulosic biomass is composed 20-60 % of cellulose, 15-40 % of hemicellulose, 10-40 % of lignin, 0-15 % of extractives and 0-20 % inorganic matters (Table 4.) [10].

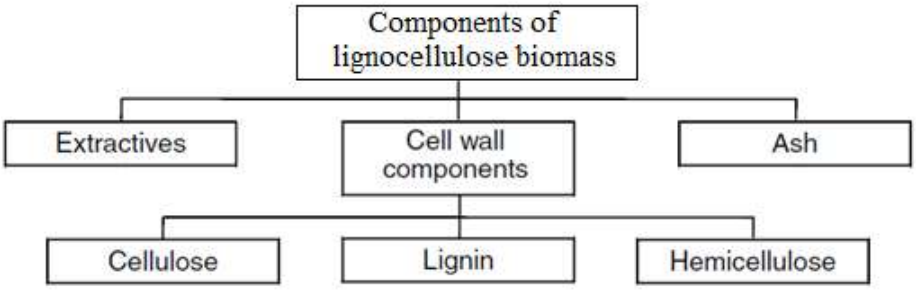

Figure 4. Constituents of lignocellulosic biomass

	Cellulose	Hemicellulose	Lignin	Extractive	Ash
Softwood biomass					
Pinus armandii Franch	48.4	17.8	24.1	9.5	0.2
Pine	46.9	20.3	27.3	5.1	0.3
Spruce	45.6	20.0	28.2	5.9	0.3
Spruce	43.0	29.4	27.6	1.7	0.6
Fir	45.0	22.0	30.0	2.6	0.5
Japanese cedar	38.6	23.1	33.8	4.0	0.3
Eastern Red cedar	40.3	17.9	35.9	5.6	0.3
Hardwood biomass					
Alder	45.5	20.6	23.3	9.8	0.7
Aspen	52.7	21.7	19.5	5.7	0.3
Willow	41.7	16.7	29.3	9.7	2.5
Poplar	49.0	24.0	20.0	5.9	1.0
Cherry wood	46.0	29.0	18.0	6.3	0.5
Beech	45.0	33.0	20.0	2.0	0.2
Beech	44.2	33.5	21.8	2.6	0.5
Japanese beech	43.9	28.4	24.0	3.0	0.6
Herbaceous and agricultural biomass					
Rice straw	37	16.5	13.6	13.1	19.8
Rice straw	34.5	18.4	20.2	10.1	13.3
Rice husk	37.0	23.4	24.8	3.2	17.3
Wheat straw	37.6	18.2	20.2	4.1	3.7
Corn straw	42.7	23.2	17.5	9.8	6.8
Corn leaves	26.9	13.3	15.2	22.0	11.0
Corn cob	34.6	15.2	18.2	10.6	3.5
Bamboo	39.8	19.5	20.8	6.8	1.2
Miscanthus	34.4	25.4	22.8	11.9	5.5
Switchgrass	40-45	31.35	6-12	5-11	5-6
Hazelnut shell	25.2	28.2	42.1	3.1	1.4

Table 4. The constituents of selected lignocellulosic feedstocks adapted from [10]

a. Polymer constituents

Cell walls are the major component of plants and lignocellulosic biomass, including cellulose, hemicellulose, and lignin (Figure 5). The compositions of cell walls vary widely among species, depending on the cell type or environmental conditions.

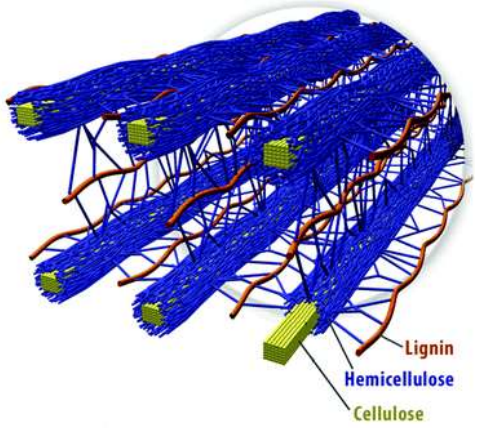

Figure 5. Spatial arrangement of cellulose hemicellulose and lignin in the cell walls of lignocellulosic biomass adapted from [11]

- **Cellulose**

Cellulose is an organic compound with the formula $(C_6H_{10}O_5)_n$, a polysaccharide consisting of a linear chain of several hundred to many thousands of β(1→4) linked D-glucose units. It has a high degree of polymerization (up to 10,000 units of glucose) as well as strong interactions due to the numerous intra- and intermolecular hydrogen bonds, which give cellulose a crystalline structure. These characteristics give cellulose a good mechanical strength and chemical stability [11]. A representation of cellulose is given in Figure 6.

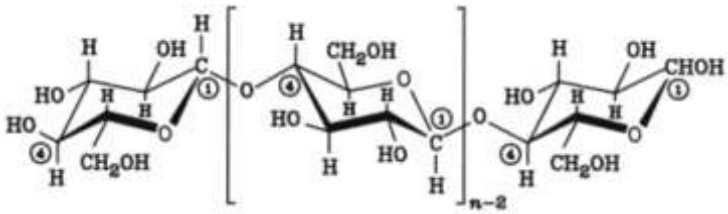

Figure 6. Structure of single cellulose molecule [11]

- **Lignin**

Lignin, is the most complex natural polymer. Unlike cellulose, lignin has an amorphous structure with phenylpropane units as the predominant building blocks. Its composition are dependent on the species and environmental conditions prevailing during the growth of the plant. Despite its apparent complexity, lignin is mainly composed of three similar aromatic hydroxylated monomers: p-coumaryl alcohol, coniferyl alcohol and sinapyl alcohol [11]. They are presented in Figure 7.

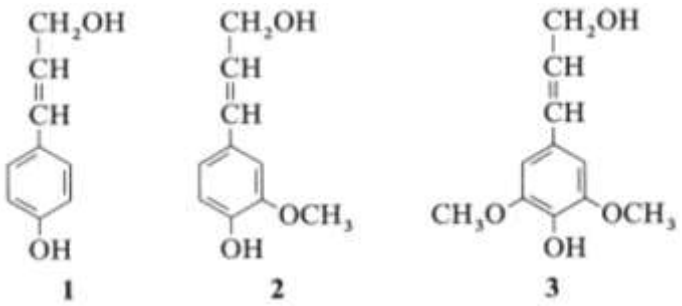

Figure 7. Three aromatic hydroxylated monomers of lignin [11]

- **Hemicellulose**

Hemicellulose is a heterogeneous group of branched polymers of various sugars having a large natural variability. Hemicellulose surrounds the cellulose fibers and stands as a connecting link between cellulose and lignin. Hemicellulose includes xylan, glucuronoxylan, arabinoxylan, glucomannan, and xyloglucan. Hemicellulose is composed of both hexose and pentose sugars: the C_6 sugars glucose, mannose, galactose and the C5 sugars xylose and arabinose (Figure 8). The degree of polymerization of hemicelluloses is low (50 to 200). While cellulose has a hydrolysis-resistant crystalline structure, hemicellulose is amorphous due to the highly branched structure and the presence of acetyl groups connected to the polymer chain. Thus, hemicellulose is more susceptible to depolymerisation than cellulose (especially in acidic conditions) [11].

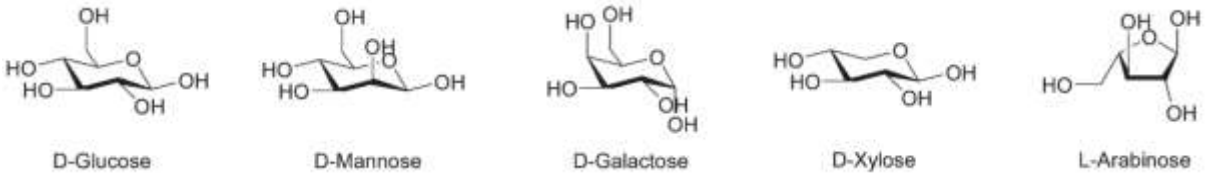

Figure 8. The hexoses and pentoses typically found in hemicellulose [12]

b. Minoritary constituents

- **Inorganic materials**

Inorganic elements are the mineral material naturally present in plants. They represent between 0.1 and 2 % for wood, and up to more than 10 % for certain agricultural residues (Table 5). The main elements are K, Na, Ca, Mg, P and Si. They exist in the form of ions or are linked to the organic structure. During the combustion of biomass, most of the inorganic elements are found in oxidized form in the ashes.

	Straw (winter wheat)	Cereals (triticale)	Bark (spruce)	Wood chips (spruce)
CaO	7.8	7.1	42.2	44.7
MgO	4.4	4.3	6.5	4.8
K_2O	14.5	14.2	5.1	6.7
Na_2O	0.4	0.5	0.8	0.6
P_2O_5	2.2	9.8	1.7	3.6

Table 5. Average concentrations of inorganic metal oxides of various biomass fuels (wt% db) [13].

- **Extractives**

Extractives are a complex mixture of organic compounds that can be removed from the wood by solvents such as petrol ether, ether, dichloromethane, benzene, acetone, ethanol and water. They are divided into two groups: primary metabolite including low-molecular weight sugars, inositol, amino acids, simple fats and carboxylic acids and secondary such as metabolite terpenes and phenolic compounds.

I.2.1.2. Composition of lignocellulosic biomass feedstock

Lignocellulosic biomass composition are characterized by elemental and proximate analyses. Table 6 shows the composition of various biomass types.

Biomass	Proximate analysis, % db			Ultimate analysis, % daf					HHV
	Ash	VM	FC	C	H	N	S	O	MJ/kg (db)
Beech	0.60	84.87	14.53	49.68	6.21	0.28	0.01	43.81	19.32
Birch	0.20	94.73	5.07	47.7	6.01	0.1	0.03	45.59	18.21
Poplar	1.22	85.07	13.71	50.03	6.07	0.23	0.05	43.6	19.50
Fir	2.20	84.80	13.00	51.53	5.93	0.1	0.10	42.02	20.05
Oak	1.40	85.60	13.00	49.67	6.13	0.15	0.02	44.10	18.65
Spruce	0.20	89.60	10.20	47.40	6.30	0.07	0.00	46.20	19.30
Pine	0.35	83.83	15.82	53.15	6.20	0.13	0.24	40.26	20.71
Wheat straw	8.24	75.54	16.22	49.06	6.17	1.00	0.2	43.29	17.68
Corn stover	5.06	80.86	14.08	49.31	6.04	0.70	0.11	43.56	18.10
Rice husk	20.60	54.40	25.00	39.60	6.00	0.70	0.00	53.70	13.40
Rice straw	20.15	65.62	14.23	49.15	6.23	1.59	0.13	42.13	14.74
Miscanthus	2.73	91.70	5.57	49.66	6.07	0.59	0.11	43.39	19.31
Switchgrass	5.40	81.50	13.10	50.74	5.71	0.49	0.17	43.76	17.61
MSW	56.00	18.00	26.00	57.27	3.64	1.36	5.00	42.27	8.18
Sewage sludge	49.70	44.15	6.15	52.70	8.15	6.28	2.21	30.72	11.44
Cattle manure	41.60	47.30	11.10	56.42	8.39	1.18	1.34	29.93	15.12

Table 6. Typical proximate (db, %) and ultimate analyses % (daf) and higher heating values for various biomass types [14]

a. Elemental analysis

From the elemental point of view, biomass is essentially composed of carbon, oxygen, hydrogen, nitrogen, sulfur and a low content of inorganic compounds. These elemental composition are provided by the elemental or ultimate analysis. The elemental composition results can be illustrated by Van Krevelen diagram, which cross-plot the hydrogen: carbon atomic ratios as a function of the oxygen: carbon atomic ratios of organic materials. This diagram provides a comparison between biomass and other fuels as well as between different biomass feedstocks (Figure 9).

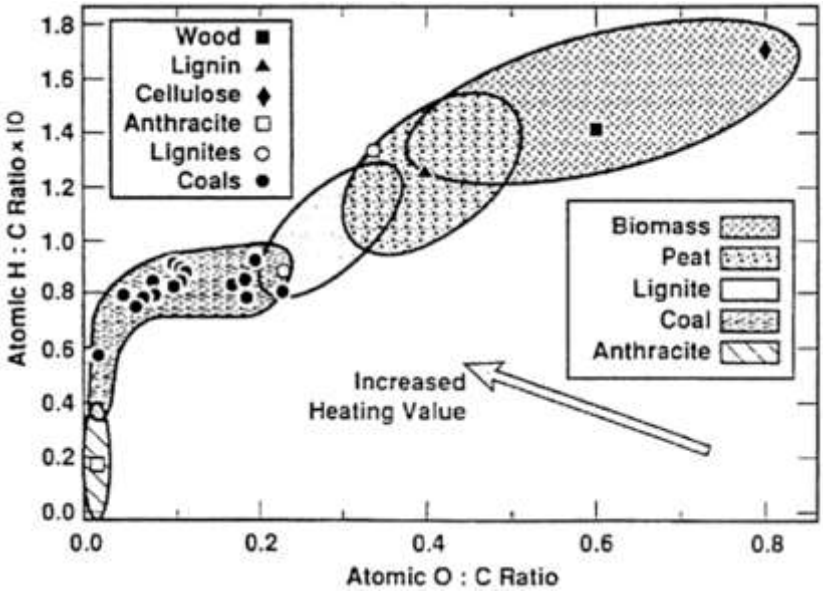

Figure 9. Van Krevelen diagram for various solid fuels

In many applications at high temperature, the elemental analysis is important in evaluating feedstocks with regarding potential pollution concerns. Nitrogen content in biomass is carefully paid attention as it shows the potential of pollution by formation of nitrogen oxide (NOx) during conversion. Moreover, in some biomass materials such as municipal solid waste and animal waste, the determination of chlorine and sulfur is particularly important because it shows possible pollutants and corrosive agents to gasification and combustion system.

b. Proximate analysis

Proximate analysis provides the amount of moisture, volatile matter, ash, and fixed carbon of biomass samples.

- **Moisture**

The moisture in biomass can remain in two forms: (i) free or external and (ii) inherent. Free moisture is that above the equilibrium moisture content. It generally resides outside the cell walls. Inherent moisture, on the other hand, is absorbed within the cell walls. When the walls are completely saturated, the biomass is said to have reached the fiber saturation point, or equilibrium moisture. Equilibrium moisture content is a function of the relative humidity and temperature. High moisture content results in low net energy content in biomass feedstocks. Thus, moisture content affects the logistics system (scale and cost) such as storage, handling and transport. In addition, moisture content must be driven off before the oxidation reactions of the hydrocarbon of biomass can start. It requires a significant energy to evaporate and thus can reduce the conversion efficiency.

- **Volatile matter**

The volatile matter of a fuel is the condensable and non-condensable vapors released when the fuel is heated to moderate temperatures, above about 150°C. The quantity of volatile depends on the type and origin of biomass (Table 6). In general, volatile matter content in biomass is higher than that in coal.

- **Ash**

Ash is the inorganic solid residue left after the fuel is completely burned. Its primary ingredients are silica, potassium, aluminum, iron, and calcium; small amounts of magnesium, sodium, and titanium maybe present. Ash is the important parameter to estimate the potential risk of slagging and fouling issues during biomass combustion or gasification. Slagging and fouling are the problems that occur when the ash begins to melt, causing deposits inside the combustion equipment. Under some conditions, the combustion ash can partially melt, forming deposits on the combustor surfaces (fouling) or hard chunks of material in the base of the combustion chamber (slagging/clinkering). Certain mineral components in biomass fuels, primarily silica, potassium, and chlorine, can cause these problems to occur at lower temperatures than might be expected. However, some alkaline metals have a positive impact on the biomass thermochemical process as they act as catalysts.

Ash content depends on the origin of biomass. In general, the ash content of herbaceous biomass is higher than that of woody biomass. Ash weight content in herbaceous biomass is in range from less than 2 % up to 10 % or even up to 20 % for rice husks while that is around 1 % for woody biomass. In waste fractions, the ash content may often be as high as 30-50 % and is only scarcely less than 10 % (Table 6).

- **Fixed carbon**

Fixed carbon is the solid combustible residue that remains after biomass is heated and the volatile matter is released. Thus, fixed carbon content in biomass is calculated value, which is determined from the following equation:

$$FC = 1 - M - A - VM \quad (1)$$

Where FC, M, A and VM are the fixed carbon, moisture, ash and volatile matter contents in biomass on the same basis of analysis.

c. Summary of expressing biomass composition

In practice, there are four types of bases of analysis commonly used for expressing biomass analysis results, i.e., as-received basis, air-dried basis, dry basis, and dry ash-free basis (Figure 10).

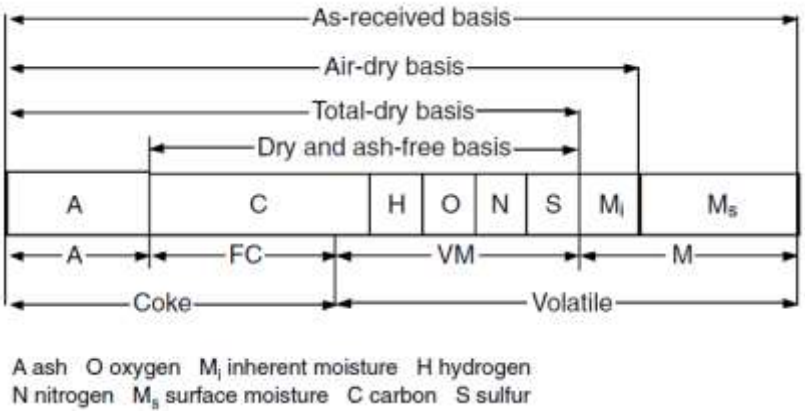

Figure 10. Bases of expressing biomass composition [15]

As-received basis is the mean of expressing an analytical result based on the total weight of sample as it arrived at the laboratory and prior to any pre-treatment.

Air-dried basis is the means of expressing an analytical result based on the condition in which the sample is in equilibrium with atmospheric humidity. Air-dried basis neglects the presence of moisture other than inherent moisture.

Dry basis (db) is the means of expressing an analytical result based on the condition in which biomass is free from moisture. Dry basis leaves all moistures including external and inherent moistures.

Dry ash-free (daf) basis is the means of expressing an analytical result based on a condition in which the sample is considered to be free from both all moistures and ash. This is frequently used in ultimate analysis to show the contents of elements in the organic fractions of the biomass sample.

d. Energy content

Results of ultimate and proximate analysis allow the calculation of an important characteristic of a fuel, *energy content*. *Energy content* of biomass indicates the amount of energy stored in a given unit of a biomass sample. It is measured as the heat of combustion, which is the total energy released as heat when it undergoes complete combustion with oxygen under standard

conditions. Calorific value (or heating value) is common used to express the energy content. There are two types of heating value: *higher heating value* and *lower heating value*.

Higher heating value (HHV) is defined as the amount of heat released by the unit mass or volume of fuel (initially at 25 °C) once it is combusted and the products have returned to a temperature of 25 °C. It includes the latent heat of vaporization of water.

Higher heating value can be measured by a bomb calorimeter or can be estimated from the results of the ultimate and proximate analysis following the equation of Chaniwala and Parikh [16].

$$HHV = 0.3491C + 1.1783H - 0.10S - 0.0134O - 0.0151N - 0.0211A \quad (2)$$

This correlation is valid within the range:

- $0 < C < 92\ \%;\ 0.43 < H < 25\ \%$
- $0 < O < 50\ \%;\ 0 < N < 5.6\ \%$
- $0 < A < 71\ \%;$
- $4745 < HHV < 55{,}345\ kJ.kg^{-1}$

Lower heating value (LHV), also known as the net calorific value, is defined as the amount of heat released by fully combusting a specified quantity less the heat of vaporization of the water in the combustion product.

The relationship between HHV and LHV is given by:

$$LHV = HHV - h_g\left(\frac{9H}{100} + \frac{M}{100}\right) \quad (3)$$

where *LHV*, *HHV*, *H*, and *M* are lower heating value, higher heating value, hydrogen percentage, and moisture percentage, respectively, on an as-received basis. Here, h_g is the latent heat of water 2260 $kJ.kg^{-1}$.

I.2.1.3. Properties of lignocellulosic biomass

a. Physical properties

- **Granulometry**

Woody and herbaceous biomasses are of irregular shapes. Shape and size of biomass feedstocks affect the flow behavior in transport and storage system and surface area for heat and mass transfers. The feedstock is usually pretreated to meet the requirement of different

thermochemical conversion technologies. For example, fast pyrolysis requires biomass with smaller particle size than slow pyrolysis. For that, grindability can be considered as one of the important properties of biomass. The grindability of a material is a measure of its resistance to grinding. The lignocellulosic components of biomass, especially cellulose and lignin, are very fibrous and difficult to grind. The grindability of biomass can be greatly improved due to increased brittleness and a reduction of the cellulose fiber length through torrefaction.

- **Density**

There are three types of density: true density, apparent density and bulk density.

True density is defined as the ratio of total mass of biomass to the solid volume in biomass. It is measured with a Helium pycnometer.

Apparent particle density is defined as the ratio of total mass of biomass to the volume of the particle (solid and internal pores). Apparent volume can be calculated from the measurement of the main dimension (diameter, side) using a micrometer.

Bulk density is the ratio of the mass of a stock of biomass particles to the total volume occupied by particles, thus including the pore space volume between and within the biomass particles.

Bulk density is a key physical property in designing the logistics system for biomass handling and transport. It depends on the biomass particle size and shape, moisture content, particle density, and surface characteristics. Table 7 shows the bulk densities of several biomass feedstocks.

Fuel	Characteristic dimension (m)	Bulk density ($kg.m^{-3}$)
Sawdust	0.0003-0.002	300
Chopped straw	0.005-0.025	60
Green wood chips	0.025-0.075	500
Wood pellets	0.006-0.008	600
Biomass briquettes	0.025-0.01	600
Cordwood	0.3-0.5	400

Table 7. Typical size and density of several biomass fuels

b. Thermochemical properties

This section presents several important thermodynamic properties of biomass that influences thermochemical conversion.

- **Thermal conductivity**

When a solid particle is heated in thermochemical conversion processes, it is subjected to heat conduction along and across its fiber, which in turn influences its thermochemical conversion behavior. Thus, the thermal conductivity of the biomass is an important parameter in this context. Di Blasi [17] reported in her extensive review on wood and biomass pyrolysis modeling that density and thermal conductivity cause the highest sensitivity of the model predictions.

Several works on thermal conductivity can be found in literature thanks to the literature survey of Hankanin et al [18]. Most studies on thermal conductivity focus on wood as a common biomass. They showed that wood is an anisotropic material, and its thermal conductivity depends on heating direction, moisture, porosity, density and temperature. In detail, Harada et al. [19] developed the following correlation for wood thermal conductivity based on their flash method experiments at a temperature range of 293 – 513 K.

$$\lambda_w = 0.00249 + 0.000145\,\rho_w\,0.000184\,(\mathrm{T} - 273) \tag{4}$$

where λ_w is wood thermal conductivity, ρ_w density and T temperature in K. The correlation indicates that thermal conductivity is linearly proportional to temperature and increases 50 % at a temperature range of 293 – 513 K.

Another correlation from Koufopanos et al. [20] is also commonly used in literature:

$$\lambda_w = 0.13 + 0.0003\,(\mathrm{T} - 273) \tag{5}$$

- **Specific heat**

Specific heat, an indication of the heat capacity of a material, is another important thermal property of biomass, required for thermodynamic calculations. It depends on the moisture content of biomass and temperature.

Within the temperature range of 0 to 106 °C, the specific heat of a large number of wood species (dry) can be expressed as (Jenkins [21]):

$$C_{p\theta} = 0.266 + 0.00116\theta \tag{6}$$

where temperature θ is in °C.

Effect of moisture on specific heat expressed as:

$$C_p = M_{wet}C_{wet} + (1 - M_{wet})C_{p\theta} \quad (7)$$

where M_{wet} is the moisture fraction on a wet basis, and C_{wet} is the specific heat of water.

Recently, Dupont et al. [22] correlated the relationship between the specific heat and temperature of 21 biomass types including wood, agricultural residue and energy crop samples with particle size below 200 µm.

$$c_{pT} = 5.34\,T - 299 \quad (8)$$

- **Standard Enthalpy of Formation**

Standard Enthalpy of Formation is the enthalpy change when one mole of compound is formed at standard state (25 °C, 1 atm) from its constituting elements in their standard state. All elements in their standard states have a standard enthalpy of formation of zero, because there is no change involved when they are formed from themselves. For example, hydrogen and oxygen are stable in their elemental form, so their enthalpy of formation is zero. If the compound is formed through multiple steps, the standard enthalpy is the sum of the enthalpy change in each process step. Table 8 shows the standard enthalpies of some common compounds.

Compound	H_2O	CO_2	CO	CH_4	O_2	$CaCO_3$	NH_3
Standard enthalpy of formation at 25°C ($KJ.mol^{-1}$)	-241.5	-393.5	-110.6	-74.8	0	-1211.8	-82.5

Table 8. Standard enthalpy of formation of some common compounds [23]

- **Enthalpy of Reaction**

Enthalpy of Reaction is the amount of heat released or absorbed in a chemical reaction with no change in temperature. In the context of combustion reactions, it is called heat of combustion, ΔH_{comb}, which can be calculated from the standard enthalpy of formation (SEF) as:

$$\Delta H_{comb} = [\text{Sum of SEF of all products}] - [\text{Sum of SEF of all reactants}] \quad (9)$$

The ΔH_{comb} for a fuel is also defined as the enthalpy change for the combustion reaction when balanced:

$$\text{Fuel} + O_2 \rightarrow CO_2 + H_2O - \Delta H_{comb} \quad (10)$$

- **Self-Ignition Temperature**

Self-Ignition Temperature (SIT) is an important property of any fuel because it shows that the combustion reaction of the fuel becomes self-sustaining only when temperature reaches a value above it. In a typical gasifier, a certain amount of combustion is necessary to provide the energy required for drying and pyrolysis and finally for the endothermic gasification reaction. In this context, it is important to have some information on the ignition characteristics of the fuel. However, SIT is not a unique property of a fuel. It depends on several other factors like oxygen partial pressure, particle size, rate of heating, and particle's thermal surroundings. Table 9 shows the SIT of some common biomass feedstocks.

Sample	Volume in cm^3	SIT in °C
Wood chips	100	210
Wood chips	200	204
Wood chips	400	196
Wood chips	800	188
Wood pellets	100	184
Wood pellets	200	180
Wood pellets	400	172
Wood pellets	800	168
Wood briquettes	200	180
Wood briquettes	400	176
Waste wood	400	188
Waste wood	800	176
Waste wood	1600	176

Table 9. Self-ignition temperature (SIT) of several biomass feedstocks [24]

I.2.2. Thermochemical conversion processes

Before going into the details for each process, we analyze an example of the conversion process efficiencies when converting one ton of a dried wood into heat and then electricity through combustion, carbonization and gasification (Figure 11).

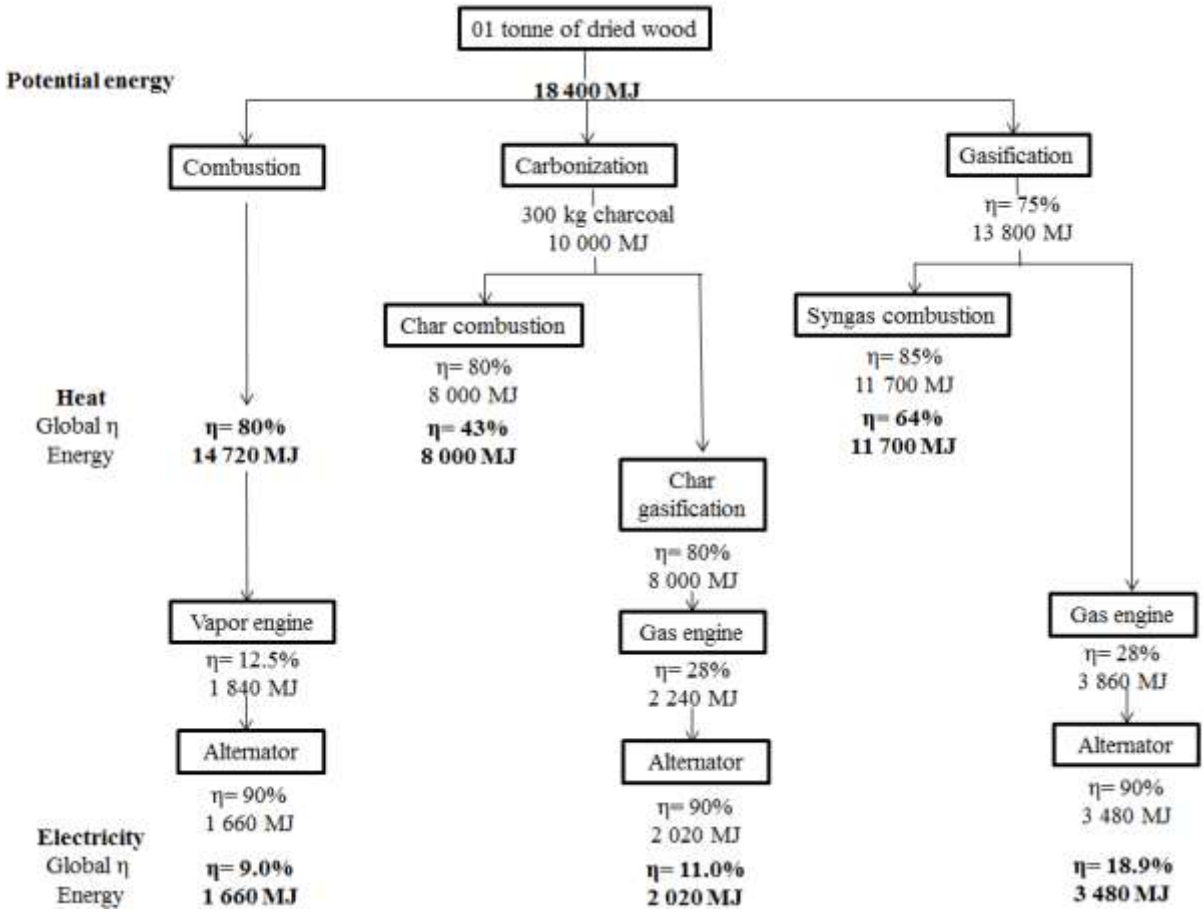

Figure 11. Quantity of thermal and electricity energies from wood conversion via different thermochemical processes [25].

The results presented in Figure 11 propose, in the technical point of view, that:

- for heat production purposes, direct combustion of wood is the best solution;
- for electricity production purpose, gasification shows the highest efficiency, followed by two other pathways: carbonization-gasification and combustion-steam engine.

Thus, the choice of thermochemical processes depends on the usage purpose and levels of the technology development.

The following sections detail these technologies.

I.2.2.1. Combustion technologies

Combustion is the most common and the oldest use of biomass. It covers a wide range of applications, including:

- Domestic use for cooking and heating by various stove and boiler systems.

- Industrial use including direct combustion and co-firing system to provide heat or electricity with boilers and steam engine/turbine.

- Waste treatment such as incineration for municipal solid waste or cleaning and preparing agricultural land by burning wastes and by-products.

In principle, combustion technologies can be classified into fixed bed combustion, fluidized bed combustion, pulverized fuel combustion [26] (Figure 12).

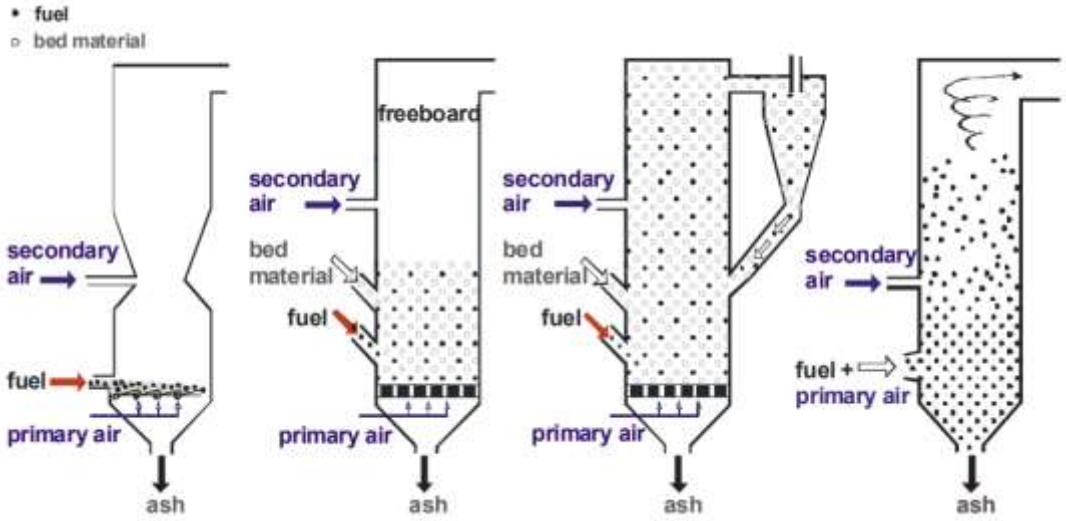

Figure 12. Overview of different combustion technologies [26]

Fixed bed combustion includes grate furnaces and underfeed stokers. Primary air passes through a fixed bed, in which drying, gasification and charcoal combustion take place. The combustible gases are burnt after secondary air injection. Fixed bed combustion system has a large flexibility concerning moisture content (10-60 %) and particle size (5 mm-10 cm). The capacity of this type of combustion technology is between 10 kW to 50 MW.

Within a fluidised bed reactor, biomass fuel is burnt in suspension of gas and solid bed materials. Depending on the fluidisation velocity, there are two kinds of fluidised bed combustion: bubbling fluidised bed and circulating fluidised bed combustion. Fluidised bed furnaces offer a large flexibility concerning moisture content (10-55 %) and fuel mixing, but a low flexibility concerning particle size (<80 mm). The boiler capacity range covers 20 MW to several hundred MW.

Pulverized fuel combustion is suitable for fuels with small particle size. A mixture of fuel and primary combustion air is injected into the combustion chamber. Combustion takes place while the fuel is in suspension and gas burnout is achieved after secondary air addition. The moisture content is usually below 20 % and particle size is limited up to 20 mm. The boiler capacity ranges from 500 kW to several hundred MW (for co-firing systems).

By capacity, combustion systems can be classified into four categories:

- Small-scale biomass combustion systems: capacity range <100 kW_{th}.
- Medium-scale combustion systems: capacity range from 100 kW_{th} to 20 MW_{th}.
- Large-scale combustion systems: capacity range > 20 MW_{th}.
- Co-firing of biomass in coal fired power stations: capacity range several 100 MW_{th}.

Figure 13. Wood pellets are metered directly on a coal conveyor before the mills at Wallerawang Power Station, Australia [27]

Figure 13 shows an example of co-firing of biomass in coal-fired power station.

In addition, combustion technologies can be also classified based on the application domains or type of feedstocks (Table 10).

Combustion systems (Capacity)	Small-scale <100 kW_{th}	Medium-scale 100 kW_{th} to 20 MW_{th}	Large-scale > 20 MW_{th}	Co-firing Several 100 MW_{th}
Applications	Residential heating	District heating Process heating and cooling CHP production	CHP production Power production	CHP production Power production
Biomass feedstocks	Log wood Wood pellets Wood pellets	Wood pellets Bark Forest residues Waste food Straw	Bark Forest residues Domestic wastes Straw Fruit stones, kernels, husks, shells	Forest residues Sawdust Wood pellets Wood pellets Straw Fruit stones, kernels, husks, shells
Technologies	Wood stoves Fire-place inserts Heat storing stoves Wood boilers	Underfeed stokers Grate-fired systems Dust burners	Grate-fired systems Fluidized beds	Co-firing of finely milled biomass mingled with coal Biomass co-firing in fluidized bed combustion systems Co-firing in separate combustion units and junction of steam Biomass gasification and utilization of the product gas as fuel in a coal combustion system

Table 10. Application domains, feedstocks and available technologies for the combustion systems [28]

I.2.2.2. Gasification technologies

Gasification converts biomass into convenient gaseous fuels, along with liquid residues (condensates) and a solid residue (char). Produced gas from the biomass gasification can be used in gas turbine, gas burner, fuel cell, or in CHP (Combined Heat and Power) systems.

Technologies for biomass gasification can be classified into three main categories: fixed bed; fluidized bed and entrained flow gasifiers. Their specification are listed in Table 11.

Reactor type	Fixed bed	Fluidized bed	Entrained flow
Power	< 5MWth	> 10 MWth	> 20 MWth
Particle sizes	> 1 cm	1-80 mm	< 1 mm
Water content	< 20 %	10-40 %	< 15 %
Temperature	120-1200°C	800-900°C	> 1300°C
Heating rate	low	very high	high
Solid residence time	> 1h	< 1 min	< 1s
Gas residence time	> 2s	< 2s	< 1s
Application	Cogeneration	Cogeneration, Methanation	Methanation, Hydrogen Fisher Tropsh synthesis

Table 11. Typical conditions in biomass gasifiers [29]

a. Fixed bed gasifiers

There are many types of fixed bed reactors, but they can be grouped into updraft, downdraft, and multi-staged gasifiers.

Updraft gasifiers are characterized by an upward gas flow inside the reactor. Biomass is fed from the top while air is introduced from the bottom (Figure 14). Gas is produced in a high temperature zone close to the grate, travels up to cooler zone of pyrolysis and drying of biomass and then leaves out from the top of the reactor. The produced gas accompanied with tar (condensates) travels upward through cooler regions and therefore has no opportunity for conversion into gases and secondary tar. For this reason, updraft gasifiers generate the highest amount of tar compared to other fixed bed gasifier types, typically 10 to 20 % by weight of the initial feedstock.

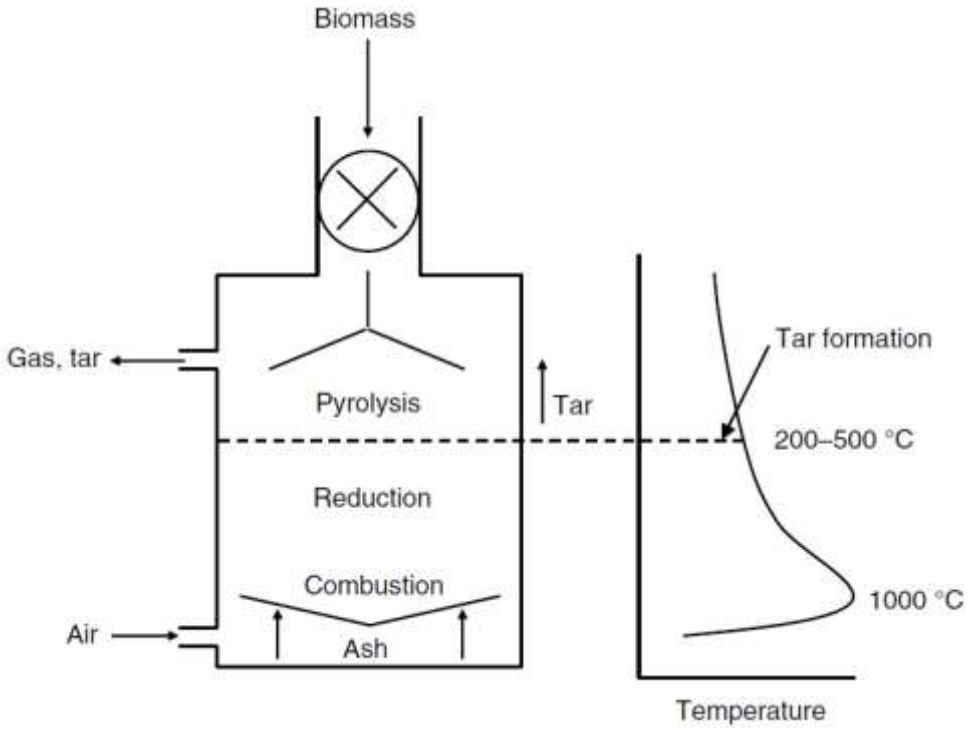

Figure 14. Updraft gasifier configuration and temperature profile [15]

In downdraft gasifiers, the pyrolysis zone is above the combustion zone and the reduction zone is below the combustion zone (Figure 15). Fuel and gas travel downward. Tar and gas produced in the pyrolysis zone pass through the highest temperature zones: combustion and reduction zones. Thus, this configuration allows the tar cracking easily, resulting in a very low tar production (<1 $g.Nm^{-3}$).

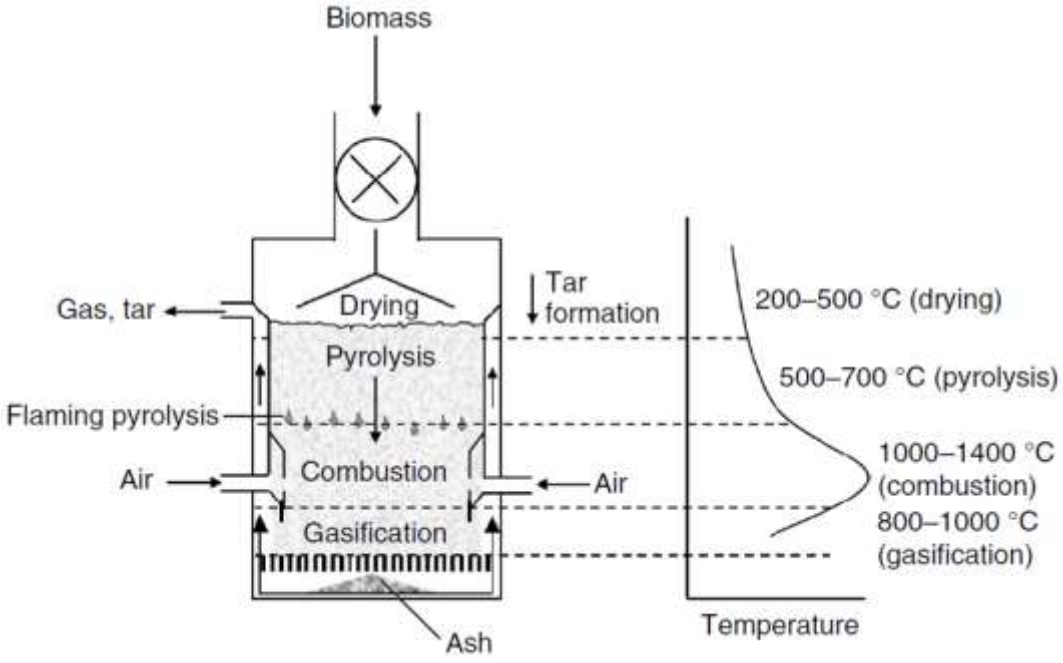

Figure 15. Downdraft gasifier configuration and temperature profile [15]

Multi-staged gasifier include two-staged gasifiers or three-staged gasifiers such as the NOTAR® reactor developed by Xylowatt® or the Viking gasifier developed by the DTU (Danish Technical University).

Here, we introduce a typical example of the two-staged fixed bed gasifier, the NOTAR® (300 kW_e or 600 kW_{th}) (Figure 16), previously described in [29].

Figure 16. The staged fixed bed gasifier NOTAR® developed by Xylowatt®

This type of gasifier allows the separation of the different stages in a gasification process:

- The pyrolysis of biomass takes place in a fixed bed reactor. Biomass and air are fed into the first reactor on top. Partial oxidation of biomass and the pyrolysis products allows the autothermal operation and temperature can reach 500-700°C. A reaction zone in the first reactor of pyrolysis, which produces char, volatile matters and tends to propagate upward, is maintained stable by extracting char from this reactor to the second reactor of gasification.
- The volatile pyrolysis products are passed into the second reactor where they are oxidized (and/or cracked) by adding the secondary air injection. A part of the produced char from the first reactor can also be oxidized here. Temperature in this combustion zone can reach about 1200 °C.
- The gasification of the char takes place in a second reactor downstream of the combustion zone, at a temperature of about 1000 °C. The synthesis gas leaves the reactor at about 700 °C.

b. Fluidized bed gasifiers

In a typical fluidized bed (bubbling or circulating) air enters from the bottom, but fuel is fed from its sides or top (Figure 17).

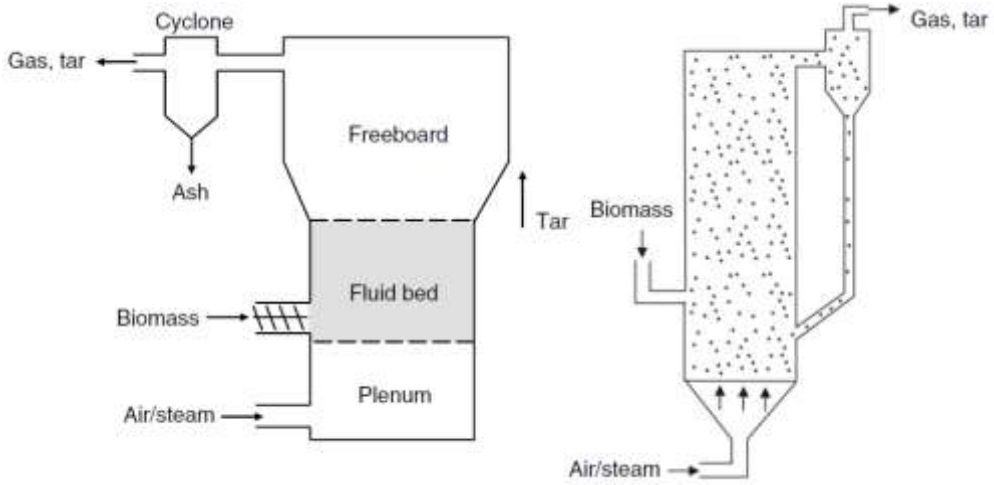

Figure 17. Schematic diagram of (a) bubbling fluidized bed gasifier and (b) circulating fluidized bed gasifier [15]

In a bubbling fluidized bed gasifier, when the gas velocity is increased (1-2 $m.s^{-1}$), a situation is reached when the particles are suspended by the upward flowing gas. Gas moves through the bed in voids and in bubbles with higher velocity. Particles are entrained into the freeboard along with these fast moving bubbles. Some fine particles are transported with the produced gas and leave the reactor at the top. However, most of the entrained particles fall back and can be continuously removed from the fluidized bed with the remaining ash at the bottom. A uniform temperature zone can be reached. The produced gas can be characterized by high particulate loadings and medium tar contents [15].

In a circulating fluidized bed gasifier, when the gas velocity is increased beyond the bubbling fluidized bed regime (5-10 m/s), the solid is distributed across the whole volume and entrained by the gas at the top of the gasifier. Particles are separated from the gas in a cyclone and are returned to the fluid bed near the bottom. This configuration allows a longer overall residence time. Circulating fluidized bed gasifiers are normally used for large applications. It has enhanced flexibility over bubbling fluidized bed gasifier for firing multi-fuels with high moisture content and significantly higher efficiency [15].

c. Entrained flow gasifier

Entrained flow gasifier (Figure 18) requires a very small biomass particle such as dust fuels or slurry. It works at high temperatures (>1200°C) and the gasification reactions end within a few

seconds. The producer gas is characterized by a low methane and low tar concentration. Entrained flow gasifiers are well suitable for the syngas production with high efficiency, e.g. Fisher-Tropsch-Synthesis.

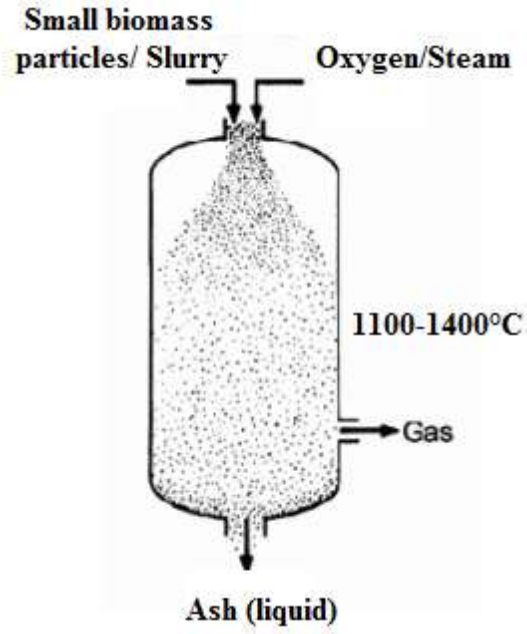

Figure 18. Basic sketch of entrained flow gasifier for biomass [15]

To sum up, the advantages and disadvantages of the different types of gasification reactor are given in Table 12.

Types of reactor		Advantages	Disadvantages
Fixed bed	Updraft	•Simple and robust construction •Higher particle size limit for feedstocks •High conversion efficiency •Greater flexibility with respect to fuel water content (<50 %)	•High risk of condensation because of low exhaust gas temperature •High tars in the produced gas
	Downdraft	•Simple design and suitable for a wide range of biomass feedstocks •Good carbon conversion efficiency •Produced gas with relatively low tar content	•Not very flexible with regard to fuels in terms of size and water content (low content required) •Limited installation size (350 kWe) •Possibility of ash melting in the grate of reactor
Fluidized bed	Bubbling	•Good in control of temperature •Better transfers of material and heat than in fixed beds. •Possible to use catalytic treatment •Moderate tar content •Proven construction	•Minimum size to be economical •Require small particles •Require low moisture content in biomass (<20 %) •Sensitive to the particle size distribution of the fuel.
	Circulating	•Good temperature control and reaction rate •Better control in feeding than the bubbling fluidized bed •High tolerance with respect to fuel (type, size) •Moderate tar content •Proven construction •High conversion rate	•High particle content in produced gases •Minimum size to be economical
Entrained flow		•Very high speed of reactions (very high temperature) •High ability to gasify high ash fuels •High conversion rate •Low tar in the produced gases	•High cost of pretreatment the biomass (powder or liquor, 70 % <70µm) •High temperature produces clean gases but reduces the heating values of the gases •Risk of the ash fusion

Table 12. Advantages and disadvantages of the different type of gasification reactors [30–32]

I.2.2.3. Pyrolysis technologies

Pyrolysis process can be found in the carbonization system for charcoal production or in fast pyrolysis system for bio-oil production or multi-staged gasification system. Technologies for

biomass pyrolysis can be divided into two main categories: fixed bed and fluidized bed (Table 13).

Reactor type	Fixed bed	Fluidized bed
Process	Carbonization	Fast pyrolysis
Main product	Charcoal	Bio-oil
Particle sizes	> 10 cm	1-2 mm
Temperature	400-500°C	500°C
Heating rate	Low	very high
Solid residence time	> 1h	< 1 min
Gas residence time	> 2s	< 2s

Table 13. Main characteristics of fixed bed and fluidized bed pyrolysis

a. Carbonization for charcoal production

Carbonization is typically a slow pyrolysis process. The purpose of these processes is to maximize the production of solid residue, i.e. charcoal. For that, the reactor is maintained at low temperature and long residence time. Table 14 presents some main carbonization processes and their charcoal yields.

Traditional reactors	Charcoal yield
Earth pits and mounds	> 10 %
Industrial reactors	
Brick, concrete, and metal kilns	20- 25 %
Retorts (Lambiotte)	30-35 %
Multiple hearth reactors (Herreshoff)	25-30 %

Table 14. Some main carbonization processes and their charcoal yields

Traditional mounds (Figure 19) are common reactors for carbonization. In these reactors, energy needed for the carbonization process is provided by partial combustion of wood feedstocks or produced chars. Thus, combustion must be supervised to avoid its run away so as not to consume too much wood. Air supply can be limited by modifying the air inlets at the base of the wood log. The reactor is usually covered with straw and soil, and the pyrolysis can last from 6 to 24 hours depending on the size and arrangement of the feedstocks.

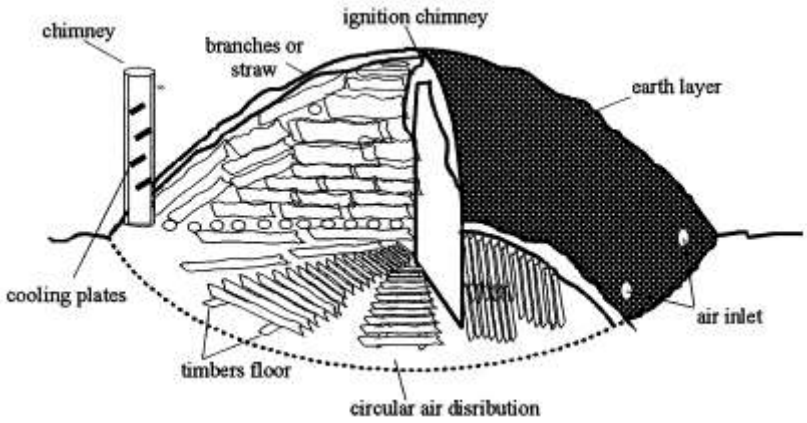

Figure 19. Traditional mound

For industrial reactors, various types of technology can be found depending on the way that heat is provided to the reactor. In general, there are three principle ways:

- Heating by partial combustion
- Heating by contact with hot gases
- Indirect heating (through a reactor wall or internal radiators)

b. Fast pyrolysis for bio-oil production

Fluidized bed reactors are used in fast pyrolysis processes. The purpose of these processes is to maximize the production of condensable vapors, so called bio-oils. In contrast to carbonization reactors, the heating rate is maximized and the residence times of solids and vapors are low. Small particles, usually less than 2 mm, are required to compensate for the low thermal conductivity of wood and achieve high heating rates. These reactors make it possible to obtain condensable yields of the order of 70 to 80 % of the incoming dry biomass.

Several types of reactors make it possible to work according to the operating conditions described above [33]. Bubbling fluid bed and circulating fluid and transported bed are two kinds of the most efficient and successful reactors (Figure 20).

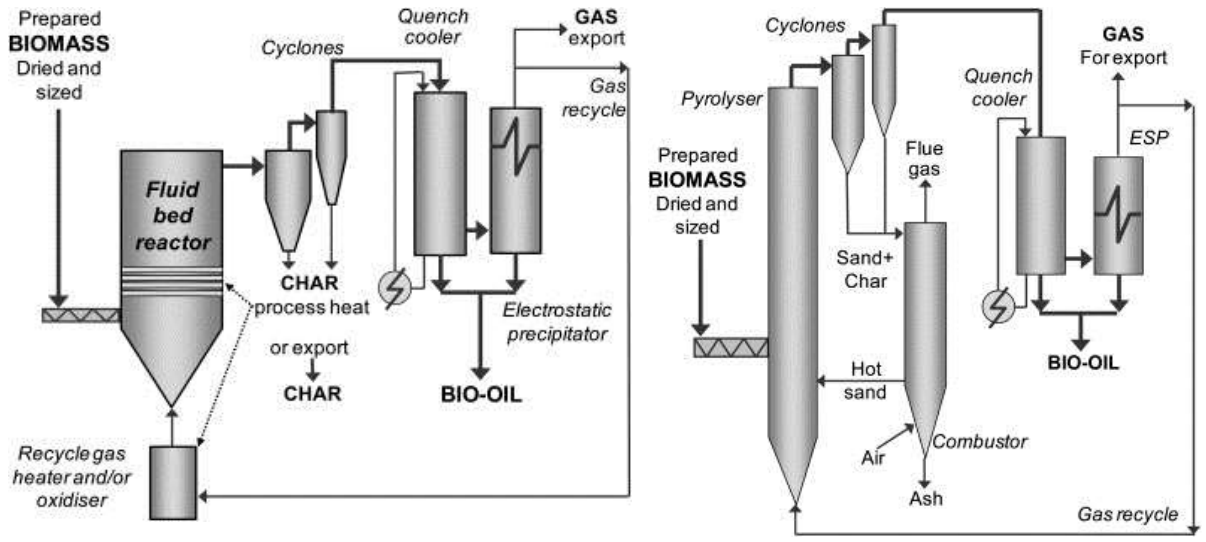

Figure 20. Fluidized bed reactors: (a) Bubbling fluid bed and (b) Circulating fluid and transported bed [33]

I.3. Conclusion

The problems associated with the use of fossil fuels demand a transition to renewable sources for energy and materials. Biomass is the most reliable and abundant sources, which can be directly burned to produce heat or can be transformed into other convenient fuels or chemical products for our modern life. Thermochemical conversion is shown as the most effective pathway for the lignocellulosic biomass conversion and pyrolysis is the most important stage of thermochemical conversion. Pyrolysis can be considered as a separated process for charcoal or bio-oil production as well as a precursor stage in combustion and gasification processes. This chapter aimed at providing a basic background on biomass characteristics and biomass conversion processes. Pyrolysis technology is the key point of this thesis and will be detailed in incoming chapter.

- Page intentionally left blank -

CHAPTER II

OXIDATIVE PYROLYSIS OF BIOMASS IN A FIXED BED

Interests in pyrolysis process for charcoal or bio-oil production as well as for gasification processes promoted the set-up of many research works for decades. Many studies have been performed to achieve a better understanding of the reactions and mechanisms involved in the pyrolysis process as well as to quantify the impact of process parameters on the yields and qualities of the pyrolysis products.

The present chapter details the most significant contributions from the literature on biomass pyrolysis with a particular attention paid to the impact of oxygen on the transformation. Finally, the chapter ends with stating the positioning and objectives of the PhD thesis.

II.1. Biomass pyrolysis

Pyrolysis consists in the conversion of lignocellulosic biomass under the action of heat into three main sets of products: permanent gases, condensable vapors and char (Figure 21).

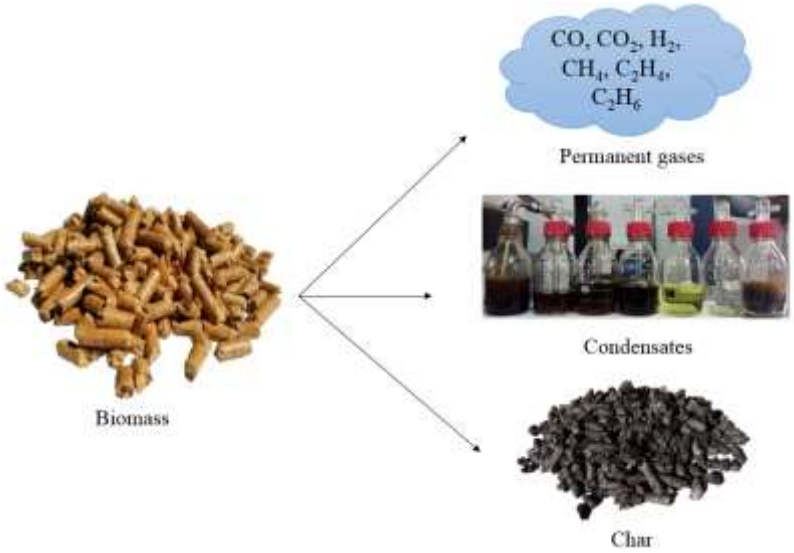

Figure 21. Biomass pyrolysis products

Permanent gases (or non-condensable gases) mainly consist of H_2, CO_2, CO and CH_4 together with traces of light hydrocarbon species such as C_2H_4 and C_2H_6.

Condensates are a complex mixture of water and oxygenated aliphatic and aromatic compounds. For lignocellulosic biomass feedstocks, the condensates usually contain native resins, intermediate carbohydrates, acids, aromatics, alcohols, aldehydes, ketones, esters, heterocyclic derivatives and phenolic compounds.

Char is the porous carbon structure that remains after the hydrogen and oxygen fractions left the fuel. Char is thus defined as the solid residue after pyrolysis. It contains unconverted organic solid, carbonaceous residues and mineral fractions.

Depending on the operating conditions, i.e. temperature, heating rate, solid residence, pyrolysis processes are usually classified into three categories: slow, fast and flash (Table 15).

Pyrolysis process	Solid residence time (s)	Heating rate ($K.s^{-1}$)	Particle size (mm)	Temperature (K)	Product yields		
					Condensable vapors	Char	Permanent gases
Slow	450-550	0.1-1	5-50	550-950	30	35	35
Fast	0.5-10	10-200	<1	850-1250	50	20	30
Flash	<0.5	>1000	<0.2	1050-1300	75	12	13

Table 15. Typical operating parameters and products for pyrolysis process [34]

- **Slow pyrolysis**

Slow pyrolysis has been conventionally applied for the production of charcoal. In slow pyrolysis, biomass is typically heated to about 550-950 K at low heating rates (up to 1 $K.s^{-1}$). The char yield related to the total biomass used can reach 35 %, depending on the type of biomass [34]. Yields and properties of the produced char are affected not only by pyrolysis operating conditions but also by properties of the parent biomass. For example, a higher yield in charcoal is obtained from biomass feedstocks with higher lignin contents [35]**.**

Char can be used in a wide range of applications, such as:

- Domestic fuel for cooking and heating;
- Activated carbon for depollution, and catalyst support;
- Fertilizer (biochar);
- Reducing agent in metallurgy.

- **Fast and flash pyrolysis**

Fast and flash pyrolysis aim at maximizing yield of liquid products. The essential features of these pyrolysis processes lie on particle size of biomass and operating conditions. First, very high heat transfer rates (10–1000 $K.s^{-1}$) are needed. Thus, a fine granulometry of biomass (<1mm) usually is required. Second, carefully controlled pyrolysis reaction temperature of around 773 K is recommended. Finally, short residence times (0.5–10 s, typically less than 2 s)

are necessary to minimize secondary reactions, that would lower liquid yield. Fast and flash pyrolysis process produce about 60-75 % of bio-oil, 15-20 % of char residue and 10-30 % of non-condensable gases [33,34]. Heating value of the produced liquid from these processes is comparable to the one of the biomass and about half of the conventional oil fuel as it contains significant amount of oxygen. Moreover, liquid fuel is of interest regarding application in chemistry through upgrading.

II.2. Fundamentals of biomass pyrolysis

Fundamental reactions during biomass pyrolysis can be classified in two groups: primary and secondary ones. Primary reactions consist in the breaking of different chemical bonds within the polymers of biomass. They result in the carbon rearrangement within the solid matrix and the release of volatile compounds. Then, these unstable volatile compounds undergo additional conversions during secondary reactions (Figure 22).

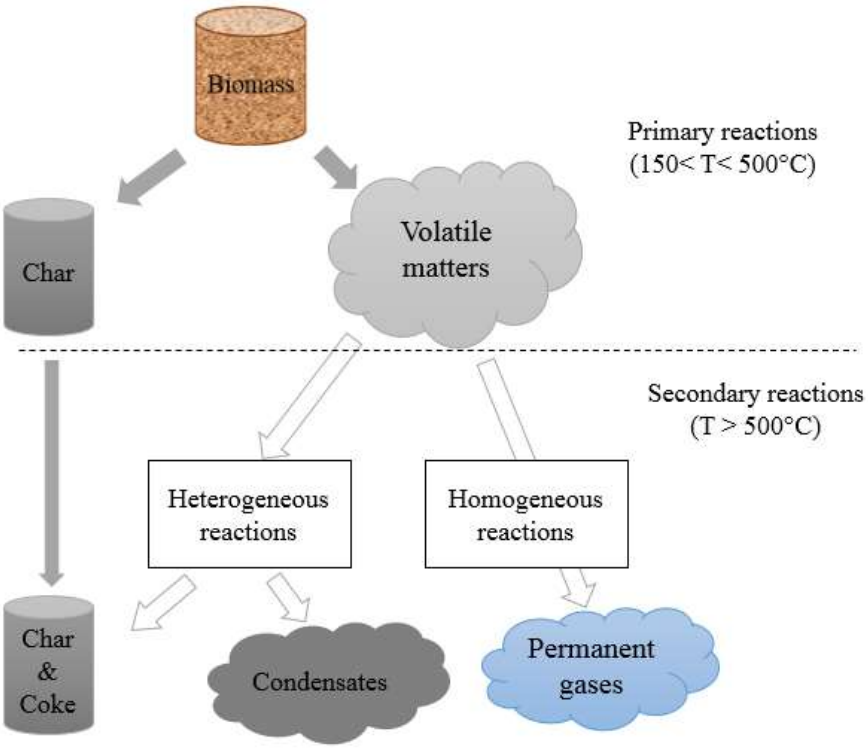

Figure 22. Global pyrolysis reaction, adapted from [29]

II.2.1. Primary pyrolysis reactions

Primary reactions consist mainly in char formation, depolymerization, and fragmentation. First, *char formation* refers to the conversion of the biomass into a solid residue (char), which presents an aromatic polycyclic structure. This pathway is generally favored by intra- and intermolecular rearrangement reactions resulting in a higher degree of reticulation and in a higher thermal

stability of the residue. The main steps of this pathway are the formation of benzene rings and the combination of these rings in a polycyclic structure. All these rearrangement reactions are generally accompanied by the release of water and incondensable gas. Second, *depolymerization* consists in the breaking of the bonds between the monomer units of the polymers. After each rupture, stabilization reactions of the two new chain ends occur. Depolymerization results in a decrease of the polymerization degree of the chains until the produced molecules become volatile. These condensable molecules at ambient temperature are most frequently found in the liquid fraction in the form of derived-monomer, dimer or trimer. Third, *fragmentation* is the linkage of many covalent bonds of the polymers, even within the monomer units, and results in the formation of incondensable gas and of a diversity of small chain organic compounds, which are condensable at ambient temperature [36].

Studies on pyrolysis of the primary reactions aim at the determination of the intrinsic kinetics as well as of the products distribution and compositions. Challenge is to avoid any secondary reactions of pyrolysis products and limitations by heat and mass transfers to occur. For these purposes, experimental apparatuses have the following characteristics:

- The sample is spread in a thin layer to avoid both internal limitations and occurrence of secondary reactions inside the sample.
- The heating rate is low (<10 $K.min^{-1}$) to avoid temperature gradients within the sample.
- An inert gas is swept to evacuate the pyrolysis products as soon as they are produced.

Microscopic approach is commonly considered to investigate the primary reactions behavior and products. Microscopic approach takes into account the main constituents (cellulose, hemicellulose, and lignin) of the biomass and focus on the behavior of each one as well as on their interactions.

- **Pyrolysis kinetic**

Cellulose, hemicellulose, and lignin have distinct pyrolysis behavior. In general, decomposition of hemicellulose and cellulose occurs quicker and at lower temperature than lignin. As an example, Figure 23 shows TGA (Thermo-Gravimetric Analysis) and DTG (Differential Thermal Analysis) of the decomposition of the three constituents [3]. In this example, samples were heated to 900 °C with a heating rate of $10°C.min^{-1}$.

In the case of **hemicellulose**, despite its heterogeneity in composition, most of the mass loss occurs between 220 and 315°C. **Cellulose** decomposition happens mainly between 310 and 400

°C [35,37], and the highest decomposition rate is found in a temperature range between 330 and 370°C. Cellulose is the most thermally stable constituent of lignocellulosic biomass since its decomposition begins at the highest temperature. **Lignin** was the most difficult one to decompose. Its decomposition is slow under the whole temperature range from 160°C to 900 °C [35].

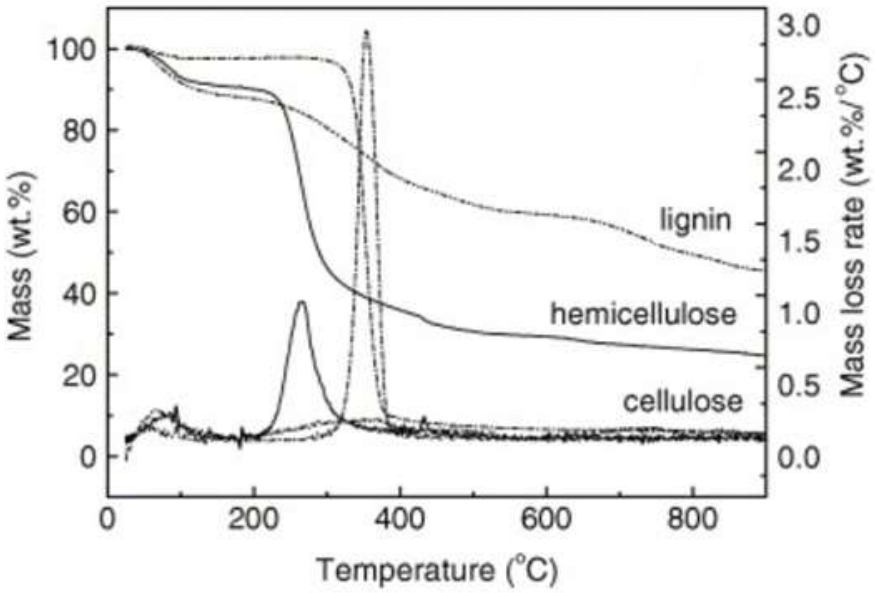

Figure 23. TGA and DTG of cellulose, hemicellulose, and lignin [35]

- **Pyrolysis products**

Regarding the pyrolysis products from the three constituents, lignin pyrolysis shows a higher yield in char than hemicellulose and cellulose. Some authors have shown that at 900°C, char yield was 22-45 % for lignin [35], 20 % for hemicellulose [35] and 5-10 % for cellulose [37,38]. It was also observed that hemicellulose had higher CO_2 yield, cellulose generated higher CO yield, and lignin produced more H_2 and CH_4 [35].

The main reactions and products from the decomposition of each constituent as function of temperature, based on an executive review of Collard and Blin [36], are presented below.

- Hemicellulose

As presented in the previous chapter, hemicellulose consists in various branched polymers, including xylan, glucuronoxylan, arabinoxylan, glucomannan, and xyloglucan. Xylan, as the main polymer component of hemicellulose, has been particularly investigated. We discuss in the following the decomposition of this specific hemicellulose compound.

At low temperatures (150-240°C), dehydration and breaking of less stable linkages happen resulting in release of H_2O and CO_2.

At moderate temperatures (240-320°C), rapid depolymerization occurs resulting in an increase of furan ring in the pyrolysis condensates. Some of the light volatiles can form H_2O, CO and CO_2 at these temperatures.

At high temperatures (320-800°C), mainly charring process occurs. When temperature higher than 300°C, the structure of the solid residue becomes more and more aromatic. Some benzene rings produced methyl or oxygenated compounds. CH_4 is mainly produced at temperature around 550°C while CO is produced at higher temperature. H_2 is produced at temperature of 480-800°C as result from dehydrogenation reactions. The solid residue resulting from the pyrolysis of xylan at 500 °C is approximately 30 % of the initial mass. The main condensable product formed is water up to 30 %. Incondensable gases are mainly CO and CO_2, for up to 30 % of the initial mass of the sample.

- Lignin

At low temperature (<300 °C), conversion of the alkyl chains from lignin and rupture of some linkages between units happen. These results in the formation of oxygenated compounds such as CO, CO_2 and H_2O as well as phenolic compounds.

For temperature between 300°C and 400°C, decomposition of lignin mostly results in the formation of phenolic compounds.

At higher temperature (380°C-800°C), the short substitution of the aromatic rings and charring process happen. CH_4 and water are produced at 430°C while CO are mainly released between 500 and 800°C.

When temperature is higher than 800°C, most of the aromatic rings of volatile compounds and solid residue are deoxygenated, resulting in a significant increase in H_2 production. In addition, CO and H_2 are the result of the steam gasification of the char.

- Cellulose

At low temperature (<300 °C), reactions of cellulose dehydratation occur to form the active cellulose or anhydrocellulose. While H_2O molecules are already released from a heating temperature of 200°C, CO, CO_2 and organic compounds are rarely detected in the volatile phase before 280°C. Dehydration reactions are also responsible for the formation of the solid residue. In fact, dehydration reactions can be intermolecular or intramolecular, resulting in the formation

of additional covalent bonds or C=C double bonds which promote the formation of the benzene rings composing the char [39]. Although being relatively slow, depolymerization reactions are also possible before 300°C due to the rupture of the glycosidic linkages between the monomer units. This leads to the formation of levoglucosan (1,6-anhydro-β -D-glucopyranose, $C_6H_{10}O_5$).

At temperature from 300 to 390 °C, depolymerization and decarboxylation reactions occur. The breakdown of acetal bonds between cellobiose units results in the formation of sugar derivatives, the main representative being levoglucosan [39]. Some unstable compounds containing new functions such as carbonyl and carboxyl can undergo dehydration and fragmentation reactions during this temperature range to form H_2O, CO, CO_2 and small chain compounds (hydroxyacetaldefyde, acetaldehyde, hydroxyacetone).

At high temperature from 380 to 800 °C, charring process occurs. The structure of the char from cellulose pyrolysis changes drastically. The first benzene rings appear at 300 °C and their concentration in the char becomes preponderant at 400 °C. To these benzene rings are linked some remaining aliphatic and oxygenated groups (hydroxyl and ether), giving to the cellulose char a structure relatively close to the one of the lignin char at 400 °C. The aliphatic groups progressively disappear between 400 °C and 600 °C. The production of CH_4 occurs in the temperature range 500–600 °C while CO and H_2 released from the char of cellulose between 500 °C and 800 °C.

Interactions between the three constituents do exist and have a significant influence on their pyrolysis behaviors. First, the presence of lignin remarkably suppressed the tendency of thermal polymerization and carbonization of the cellulose pyrolysis as well as decrease the formation of 2-furaldehyde and C=O containing compounds in hemicellulose pyrolysis. Second, the presence of cellulose suppressed char formation from lignin, while enhanced the conversion of lignin to phenols and promoted the formation of hemicellulose-derived acetic acid and 2-furaldehyde [40]. Although great efforts have been made to investigate the interactions of these biomass constituents, the detailed interaction mechanisms are still not clear.

II.2.2. Secondary pyrolysis reactions

When the released volatile compounds are not stable under the reactor temperature, they can undergo secondary reactions such as cracking or recombination. By simplification, these secondary reactions can be classified into homogeneous or heterogeneous reactions. Homogeneous reactions refer to the reactions within gas phase (condensable vapors and permanent gases).

II.2.2.1. Homogeneous reactions

Homogeneous reactions include thermal cracking and/or recombination reactions of the primary volatile products. Reforming reactions are involved also if steam is present in the atmosphere.

To study the homogeneous reactions, specific reactors were developed [29,41]. In general, it contains two separated reactors as in the example given in Figure 24 [29]. Pyrolysis vapors from the primary reactor go through the secondary reactor, where operating parameters such as temperature, resident time, and steam concentration are controlled. The system can also be equipped with a Micro-GC system to analyze the produced gases [29].

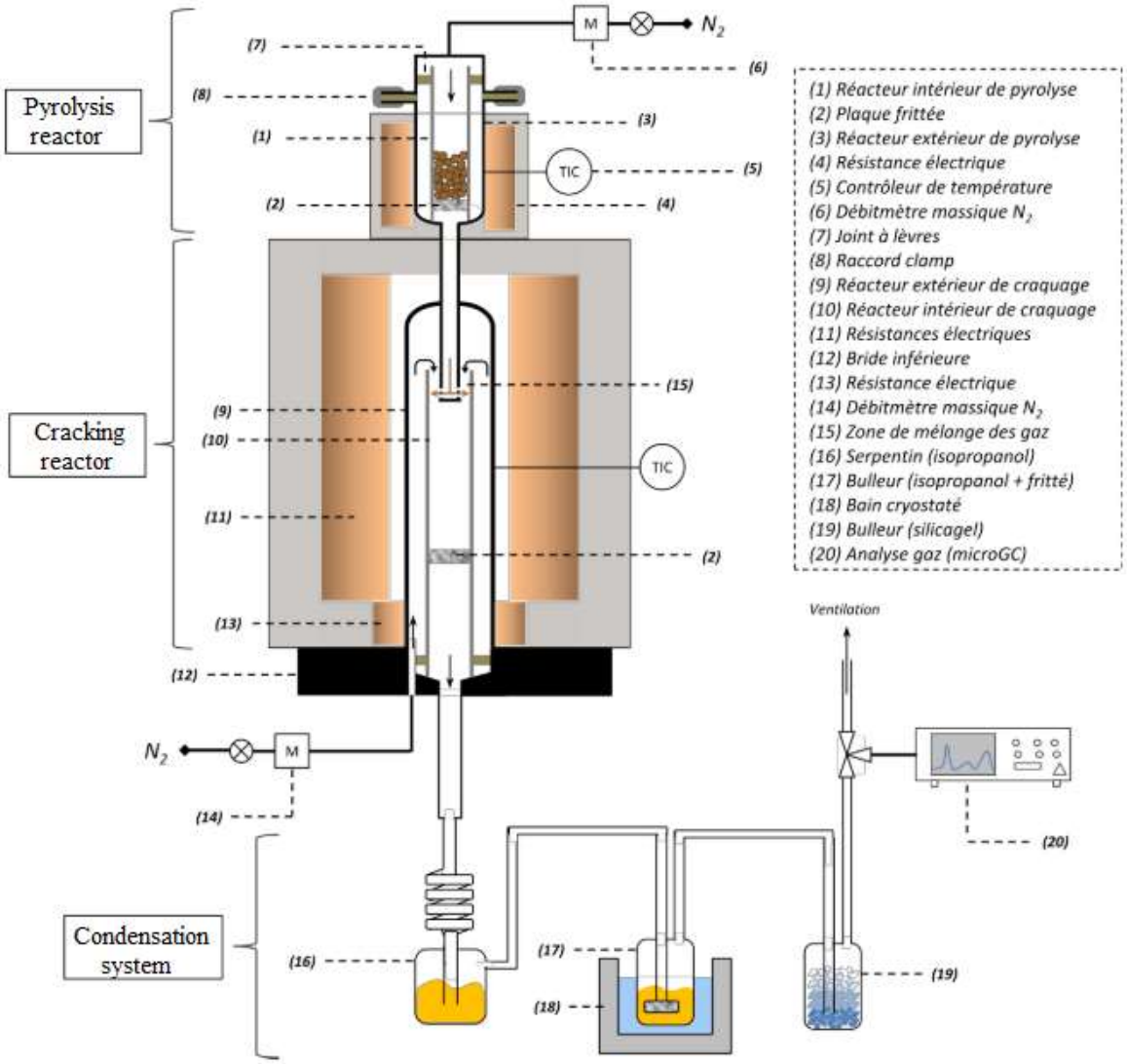

Figure 24. A specific reactor for studying the homogeneous cracking [29]

- **Kinetic of the thermal cracking reactions**

Due to the wide variety of primary pyrolysis products, the description of the thermal cracking reactions is complex. In general, they are described by a simple reaction scheme consisting of one or two reaction pathways [17,42] (Figure 25). The first reaction refers to cracking reaction and consists in the breaking of chemical bonds within the primary pyrolysis vapor compounds. It results in the formation of lower molecular weight molecules, i.e. light gases. The second pathway consists in the recombination of some volatile compounds to form higher molecular weight molecules, which has a higher thermal resistance, called refractory tars. However, many authors [41,43–47] focus on the kinetic of the homogeneous cracking while considering only the first reaction pathway.

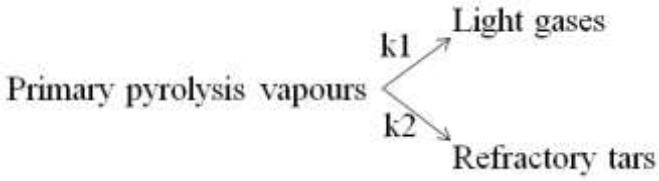

Figure 25. Homogeneous cracking of pyrolysis vapors [42]

The cracking reactions are thus generally estimated by comparing the yields of primary pyrolysis vapors or light gases before and after cracking. The thermal cracking reactions are usually grouped into a single first-order reaction with respect to the concentration of pyrolysis vapors (Equation 11). Where $\rho_v(t)$ (kg.m^{-3}) is the concentration of vapors and k (s^{-1}) is the kinetic constant of the reaction, expressed according to the Arrhenius law. The values of the kinetic parameters determined in the literature are summarized in Table 16 with the specific operating conditions.

$$\frac{d\rho_v}{dt} = -k.\rho_v(t) \tag{11}$$

Authors	Cracking conditions	k_o (s^{-1})	E_a (kJ.mol^{-1})
Liden et al. [44]	450-550°C	1.28.106	107.5
Boroson et al. [41]	500-800°C 0,9-2,2 s	6.3.104	93.3
Font et al. [45]	705-850°C	4.5.106	110.1
Cozzani et al. [46]	500-900°C	4.1.104	102.3
Garcia et al. [48]	700-850°C < 5 s	1.9.106	99.5
Morf et al. [49]	500-1000°C < 0,2 s	4 .104	76.6
Fagbemi et al. [50]	400-900°C 0,3-4 s	4.34	23.4
Baumlin et al. [47]	560-1030°C 0,3-0,5 s	1.9.103	59

Table 16. Kinetic parameters determined by different authors (adapted from [42])

- **Products of the thermal cracking reactions**

Thermal cracking of pyrolysis vapors results in an overall decrease of amount of condensable compounds in favor of lighter gases. For example, guaiacol derivatives, produced mainly by the decomposition of lignin, are likely to evolve into catechol derivatives or phenol. This cracking results in an increased production of CH_4 and CO and a change in the composition of condensates. Levoglucosan, the main decomposition product of cellulose, is cracked with formaldehyde and with CO.

The products of cracking reactions have been classified into three categories [51]:

- Primary tars, as the products of primary pyrolysis, are a complex set of oxygenated organic compounds. They contain carboxylic acids, aldehydes and ketones, sugars, furans or guaiacol derivatives.

- Secondary tars become the majority above 650°C. They are mainly represented by the families of phenols and mono-aromatic hydrocarbons (benzene, toluene, and xylene).

- Tertiary tars appear above 800 °C and become the majority after 900 °C. These are mainly polycyclic aromatic hydrocarbons (PAHs) such as naphthalene or pyrene, and alkylated aromatic compounds (indene, methylnaphthalene, fluorene). These compounds have very high dew points and cause problems of condensation and accumulation in downstream processes. They are refractory and therefore difficult to destroy when they are formed, even at temperatures above 1000 °C.

Milne et al. [51] shown that thermal cracking resulted in an overall decrease of primary tars in favor of secondary and tertiary ones with increasing temperature. Consequently, the relative importance of these classes of tars in the condensates depends on the cracking temperature (Figure 26).

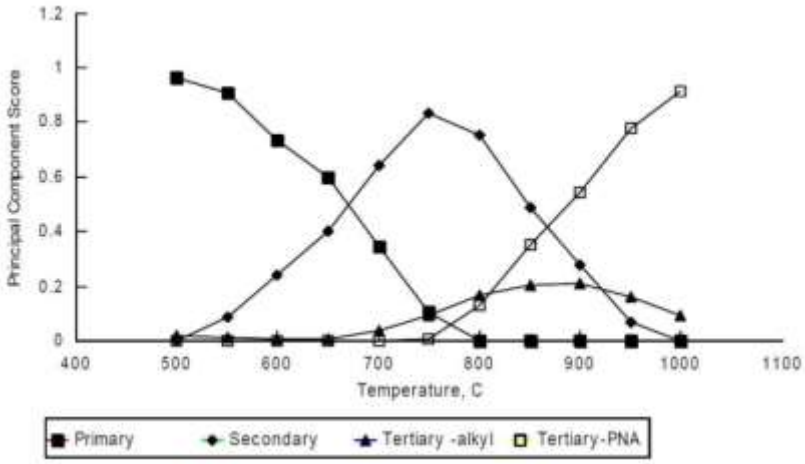

Figure 26. Relative composition of pyrolysis oils by tar class as a function of cracking temperature [51]

The light gases produced by cracking reactions of pyrolysis vapors are, according to Boroson et al. [52] , mainly composed of CO (more than 2/3 by mass of cracked vapors), followed by CO_2 and CH_4. However, for Baumlin [53], Fagbemi [54] or Morf [55], CO_2 was not a product revealing the cracking of condensable vapors (Figure 27).

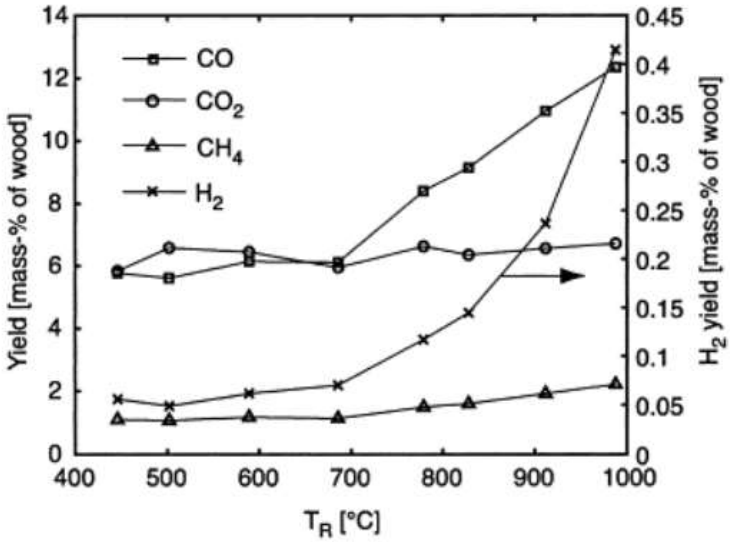

Figure 27. Gas production vs. cracking temperature of pyrolysis vapors [55]

II.2.2.2. Heterogeneous reactions

The heterogeneous reactions occur during the contact of a solid (char) and a reacting gas following two mechanisms:

- Physisorption or adsorption: the reagent, in the gas phase, is adsorbed at the surface of the solid. The bond between the reagent and the solid is weak (Van der Walls forces). This phenomenon is favored by the existence of large specific surfaces and a large

porosity. This is the case, for example, with zeolites, which can serve as molecular sieves (separation of light compounds).

- Chemisorption or absorption: the reagent reacts with a catalyst (could be inorganic matters in the char) to form covalent bonds. This step makes it possible to create complexes between active surface sites and molecules in the fluid phase, and thus accelerates the kinetics of the reactions.

The role of the char bed on the cracking of pyrolysis vapors was studied at low temperatures, between 400 and 700°C, considering primary and secondary compounds at high concentrations [52,56]. Although the operating conditions are different from one study to another, in all cases, the addition of a char bed in the cracking zone causes an increase in the production of permanent gases, in particular of CO_2. Sun et al. [56] observed also a decrease in the production of condensable vapors with the presence of a char bed. They indicated that the cracking of the vapors was selective and concerns mainly the lightest compounds produced during the primary pyrolysis (acids, ketones, furans). Boroson [52] hypothesized that only a part of the vapors was reactive: the aromatic compounds resulting from the decomposition of lignin (guaiacols).

II.2.2.3. Influence of oxygen on the pyrolysis reactions

Pyrolysis of biomass in an oxidative environment, so called *oxidative pyrolysis*, has been studied by several authors [57–61]. Compared to the pyrolysis in an inert atmosphere, the mass loss during pyrolysis is greater when oxygen is present.

As an example, Figure 28 shows the pyrolysis behavior under different oxygen concentration. First, the main mass loss occurred at a lower temperature in the presence of oxygen. Second, the peak, generally between 350 and 400°C in DTA and attributed to the decomposition of cellulose, was shifted to temperatures below 350 °C in the presence of oxygen. Moreover, the amplitude of this shift increased with the oxygen concentration. The second peaks were due to char oxidation when oxygen was used.

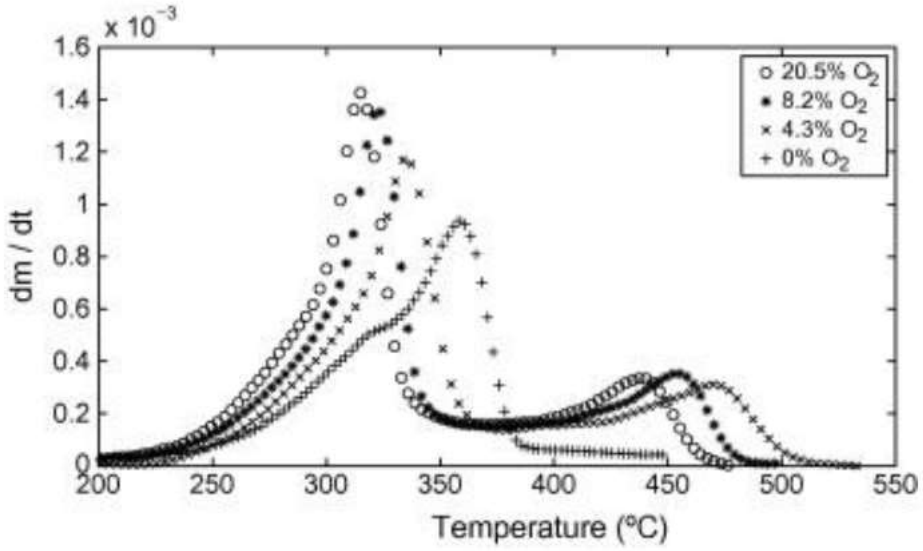

Figure 28. Comparison of pine pyrolysis DTA curves in an inert atmosphere and in the presence of O_2 at different concentrations in Nitrogen [57]

However, the observed kinetics are not well modeled by a superposition of kinetics of biomass pyrolysis and char oxidation. Anca-Couce et al. [58] and Amutio et al. [57] have shown that the oxidation of biomass should also be considered. Thus, there would be a competition between biomass pyrolysis and biomass oxidation as shown in the proposed model from Ohlemiller (Figure 29) [62].

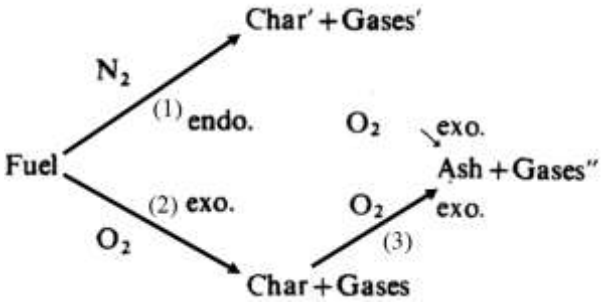

Figure 29. Kinetic model proposed by Ohlemiller [62]

Anca-Couce et al. [58] tried to determine the existence of this biomass oxidation reaction by the measurements of the enthalpie by calorimetry. Their work showed that the pyrolysis of biomass in the presence of oxygen was exothermic, with a reaction enthalpy measured at -6.5 $kJ.g^{-1}$, whereas the enthalpy of biomass pyrolysis in an inert atmosphere was endothermic of +0.2 $kJ.g^{-1}$ under the same conditions. In addition, the increase of the oxygen concentration in the pyrolysis atmosphere leaded to an increase in CO_2 production and of CO_2 /CO ratio, which confirms the existence of oxidation reactions.

II.3. Oxidative pyrolysis in a fixed bed

Oxidative pyrolysis in a fixed bed consists in a set of complex and coupled transformations or reactions (Figure 30):

- Homogeneous and heterogeneous reactions between the char and the primary and secondary pyrolysis products.

- Heat and mass transfers through conduction, convection and radiation take place between solid phases; solid and gas within the bed and between the bed, the walls and the reaction zone within the bed.

- Hydrodynamic of the solid bed and gaseous flows through the porous media.

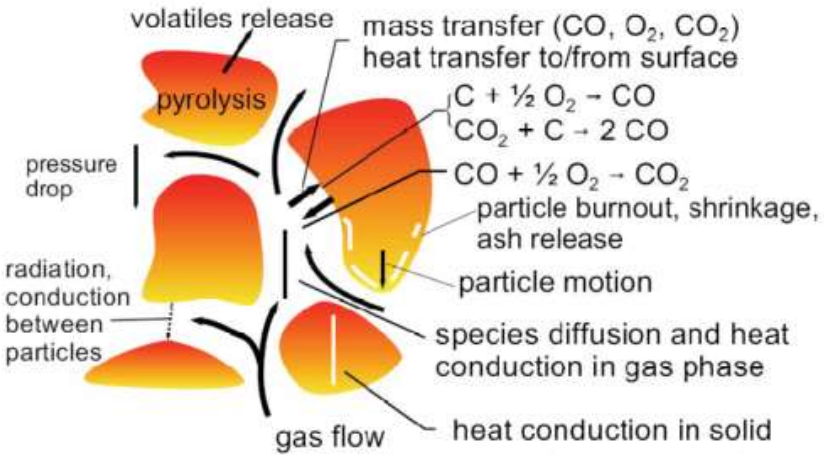

Figure 30. Coupled phenomena of heat and mass transfer, hydrodynamic, and chemical reaction in a reactive porous medium [63]

These phenomena occurred mainly in a zone that propagates into the bed. In the literature, this zone is referred to “reaction zone”, “ignition zone” or “ignition front”. In our current work we proposed to call it the Oxidation Zone (OZ). It can be described by several specific features:

- Propagation rate,

- Temperature,

- Thickness and shape,

- Yields and compositions of the products.

In this section, the main literature contributions related to the oxidative pyrolysis in a fixed bed were highlighted. We focused on the characterization of the main features just listed above, and paying particular attention to the influence of operating parameters on these values.

II.3.1. Propagation of the oxidation zone in a fixed bed.

The propagation of an oxidation zone in a porous medium is classically called "*smoldering*". Smoldering refers to a flameless form of combustion with a slow propagation of an oxidation zone in a porous medium. It has been studied in many contexts, such as forest fires [2,3] organic soil or houses fires [62], in underground fires for mining [66], in waste and biomass incineration [7,8] as well as in biomass combustion and gasification [62]. Smoldering is also said natural or forced according to the way the air penetrates into the porous media. Depending upon the relative directions of the oxidation zone propagation and the air supply, the smoldering is said: co-current and counter-current. In detail, in co-current smoldering, the oxidation zone propagates in the same direction of the air supply, unlike the counter-current smoldering where the oxidation zone propagates reversely to the direction of the air supply (Figure 31).

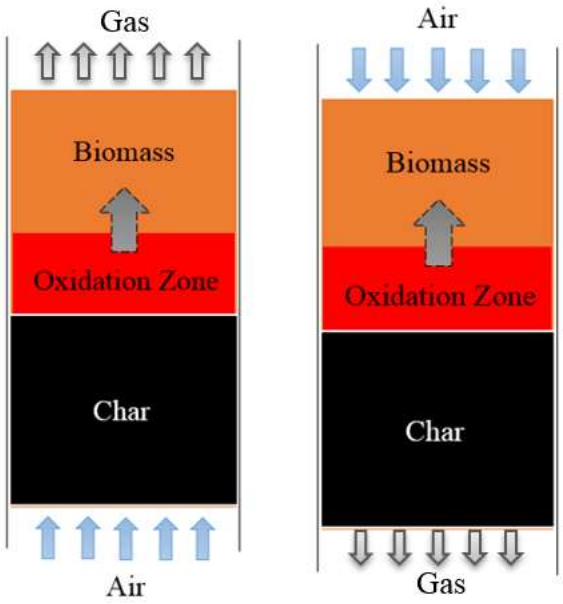

Figure 31. Illustration of co-current (left) and counter-current smoldering (right)

In both cases, the oxidation zone propagates towards biomass and converts biomass into char, condensates and gases. Ohlemiller and Lucca [69] compared the propagation rates of the oxidation zone in these two configurations. They showed that the propagation rate in counter-current smoldering was ten times faster than in co-current smoldering. Following their work, the rate of counter-current smoldering spread appeared to be dominated by the heat transfer processes (conduction and radiation) which bring each successive fuel layer into the temperature range of exothermic oxidation. Oxygen was fully consumed by the reaction front so its rate of heat generation (and, therefore, its rate of propagation by heat transfer to the next fuel element) was ultimately controlled by the rate of oxygen supply. However, in the case of co-current smoldering, the spreading rate of the oxidation front was controlled by the fact that

the incoming oxygen first sees hot char and apparently cannot penetrate this zone without being totally consumed. This left no oxygen on the front end of the spreading smolder wave. Even though the heat generated by oxidation moved forward into the fuel bed, the lack of oxygen allowed it to produce only thermal pyrolysis. The char oxidation front progresses only at the rate at which oxygen could move forward. This process was set by the stoichiometry of char oxidation, since this reaction went to completion; no oxygen was available to the next fuel layer until the outermost layer of char stopped consuming it.

In the following part of this section, we focus on the counter-current smoldering as existing in the processes investigated in the current work. Fatehi and Kaviany [70] investigated the counter-current combustion in a wood packed bed of 43 mm diameter and 0.14 m length (Figure 32-a). Air was introduced at the bottom; the oxidation zone propagated from the top to the bottom, which could be observed by the increase of the temperature along the reactor (Figure 32-b).

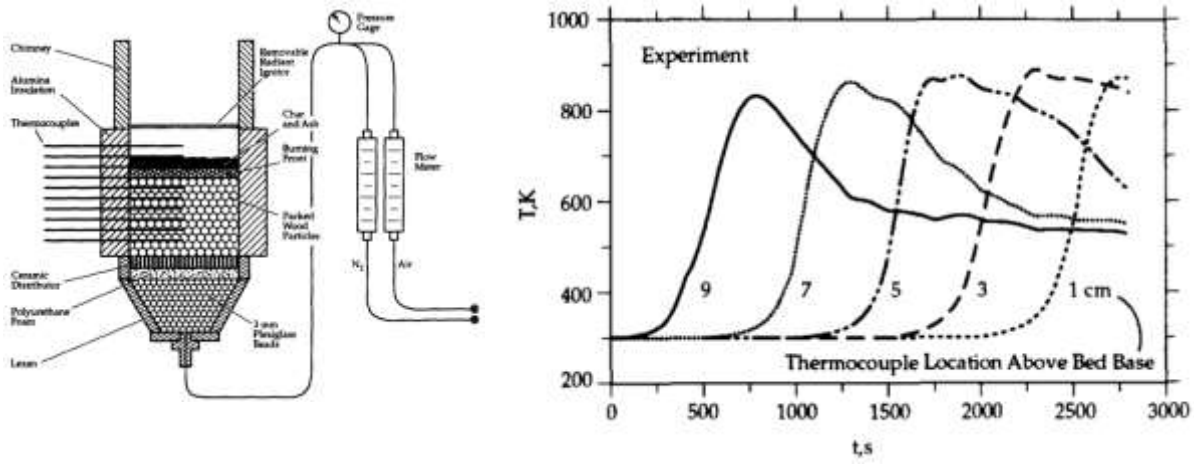

(a) (b)

Figure 32. Experimental equipment (a) and typical temperature for the counter-current smoldering (b) [70].

Air mass flux is acknowledged by many authors as the key process parameter that controls the propagation rate. Porteiro et al. [71] classified the propagation in three regimes depending on the air mass flux: oxygen-limited, reaction-limited and extinction by convection regimes (Figure 33). When the air flowrate is small, the propagation of the ignition front is controlled by the amount of oxygen and is linearly proportional to the air flow-rate. In the reaction-limited regime, the propagation rate is limited by the reaction rate of the fuel. As the air supply increases further, the convective cooling of particles around the ignition front slows down the propagation rate and finally causes extinction of the flame.

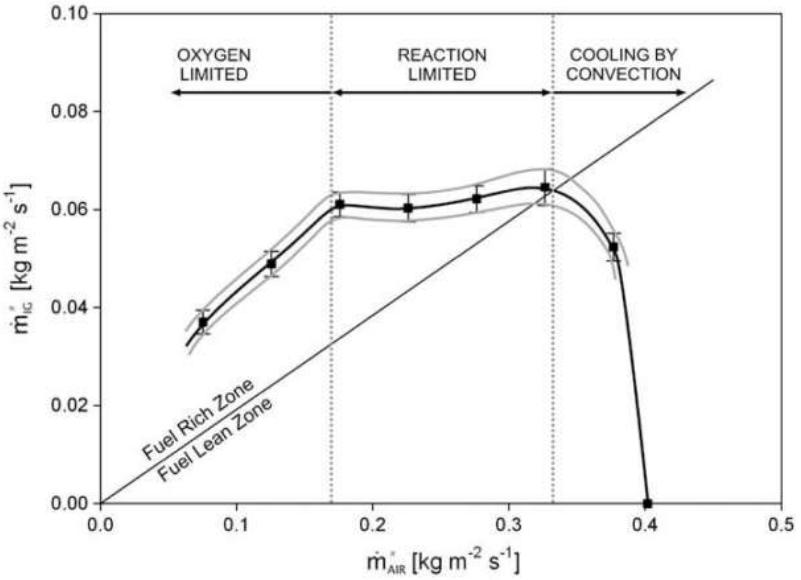

Figure 33. Effect of air flux on the propagation rate of the oxidation zone in a fixed bed

This three-regime description was then applied in many works of other researches [9,14,15]. However, the values of air flow rate and front propagation rate varied between these studies. Some studies [1,9–13] showed that the propagation rate not only depends on the air mass flux but also on fuel and bed properties.

Concerning the influence of biomass properties on the propagation rate, several studies have been performed. First, the authors [9,14,15] showed that the propagation rate is reversely proportional to particle size of biomass. Moisture, ash content and density are also the other parameters having negative impacts on the propagation rate. It is shown that the propagation rate is high when moisture content [8,13,15], ash content [71] and bulk density [1,72,78] are low. In contrast, high propagation rate is found in the bed of biomass with high heating value [13,15].

II.3.2. Structure of the oxidation zone

The structure of the Oxidation Zone (OZ) refers to its form and thickness. It is of interest for gasifier design and control. However, its characterization is not obvious and several methods to measure for example the OZ thickness can be found in literature.

Porteiro et al. [75] determined front thickness as well as different zones using temperature thresholds. They defined three distinguished zones (Figure 34):

- Drying zone in which solid fuel is dried under the temperature in range of 303 to 373 K because of heat transfer within the oxidation zone.

- Devolatilisation zone in which temperature is above 373 up to 773K. The solid fuel starts pyrolyzing to produce volatiles and char.

- Combustion zone refers to a burning zone of biomass and its products. Reactions with oxygen are highly exothermic and result in a sharp rise of the temperature up to 973 - 1473K.

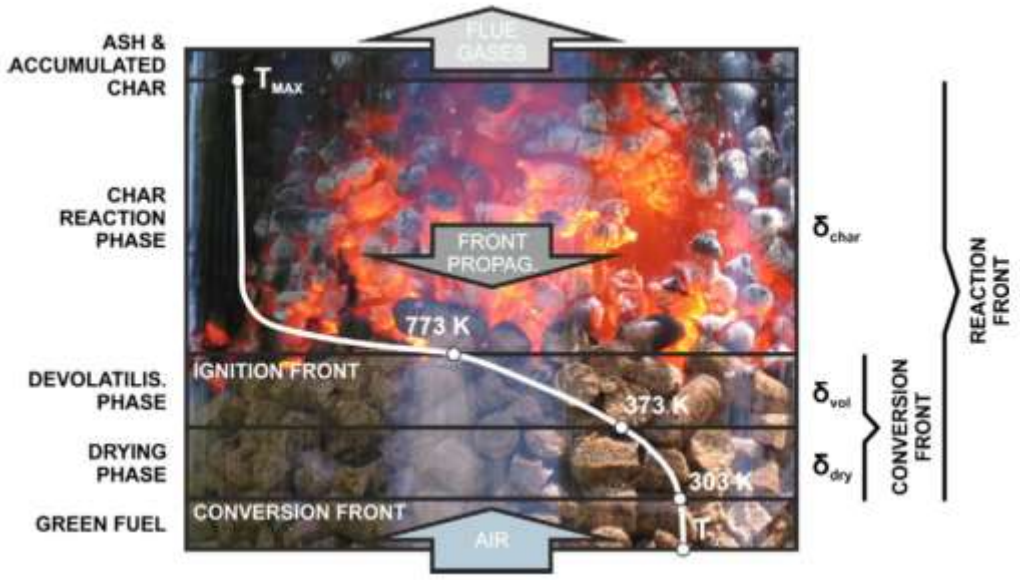

Figure 34. Structure of the oxidation zone [75]

Yang et al. [79] also used the temperature profile to estimate the reaction zone thickness in their works on municipal solid wastes and wood chips combustion. They calculated the thickness based on the propagation rate and the temperature profile in which temperature rises from 30 °C to the peak value [79] . They showed that reaction zone thickness ranged from 20 to 50 mm.

We could also mention Fatehi and Kaviany [70], who used a modelling approach to estimate the OZ thickness. Using a single-step reaction with a kinetic model of char oxidation, they defined the front thickness as the length along which 90 % of the char conversion rate occurred.

Several parameters affecting the OZ thickness were reported in literature. Fatehi and Kaviany [70] normalized the front thickness regarding the initial diameter and showed that it was proportional to the air flow rate (Figure 35). However, Porteiro et al. [75] showed that the thickness of the oxidation zone was proportional to particle size, and was not sensitive to the air mass flux. Yang et al. [79] shown that the thickness of the oxidation zone was almost an inversely linear function of the moisture level (Figure 36).

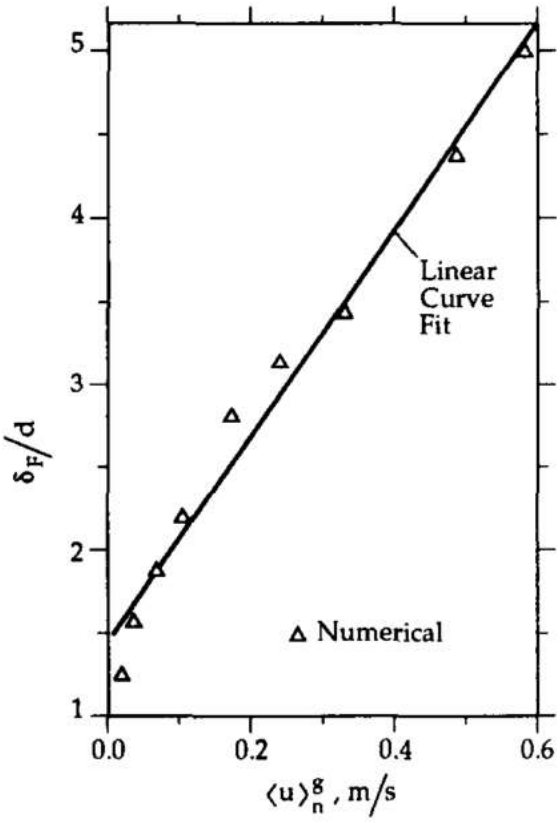

Figure 35. Variation of the predicted normalized front thickness with respect to the air flow rate [70]

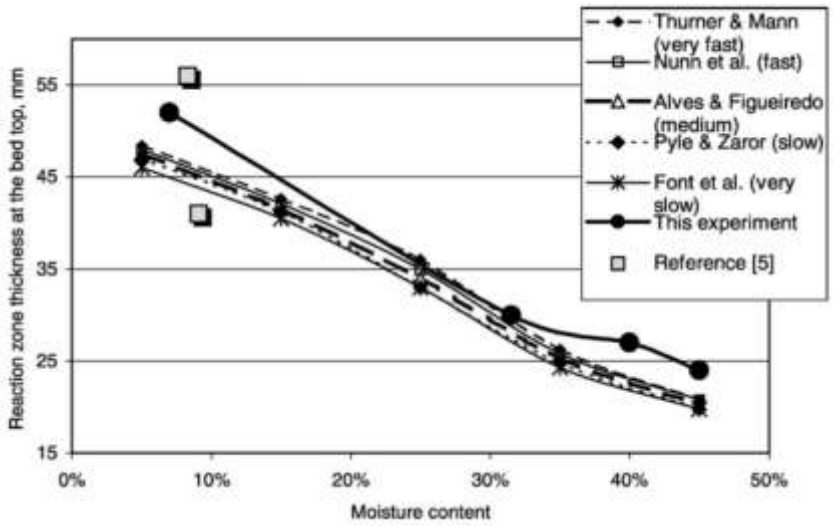

Figure 36. Reaction zone thickness inside the bed as a function of moisture content in the fuel [79]

Regarding the shape of the oxidation zone, no information was found in the literature except the works from the same research group. In a previous study, they investigated reverse smoldering in a continuous fixed bed fed with wood pellets and wood chips. They showed that the shape of the oxidation zone was flat and horizontal in a wood pellets bed but inclined and less stable in a wood chips bed [1].

II.3.3. Oxidative pyrolysis products

Knowledge of yields and properties of the oxidative pyrolysis products are of high interests regarding applications. Comparison of oxidative and inert pyrolysis was investigated by few authors. Results showed that the presence of oxygen improved the yields of permanent gas and water, and lowered the yields of char and condensable vapor [12,17, 51]. As an example, Figure 37 shows the distribution of pyrolysis products from autothermal (oxidative) pyrolysis and allothermal (inert) pyrolysis [59]. Yields of the pyrolysis products are calculated on the basis of dry inlet biomass. Moreover, these changes in yields during oxidative pyrolysis were amplified when the oxygen concentration was increased (Figure 38).

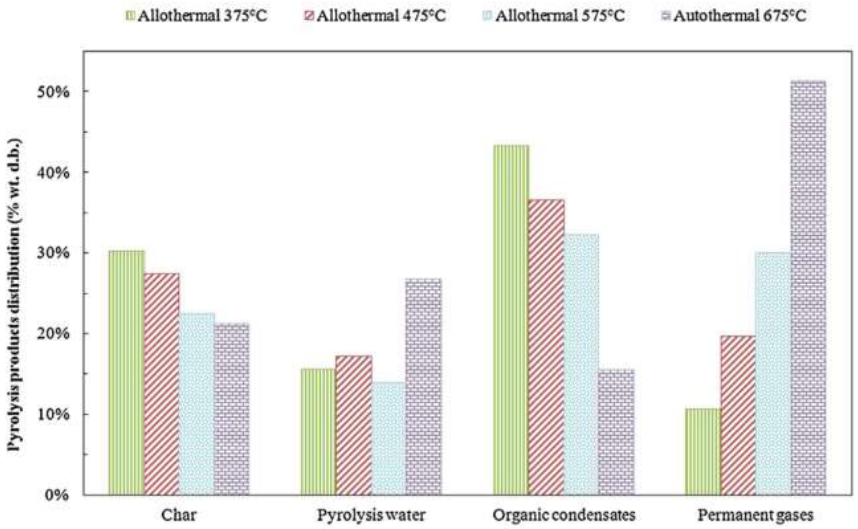

Figure 37. Distribution of pyrolysis products; yields are calculated on the basis of dry wood chips [59]

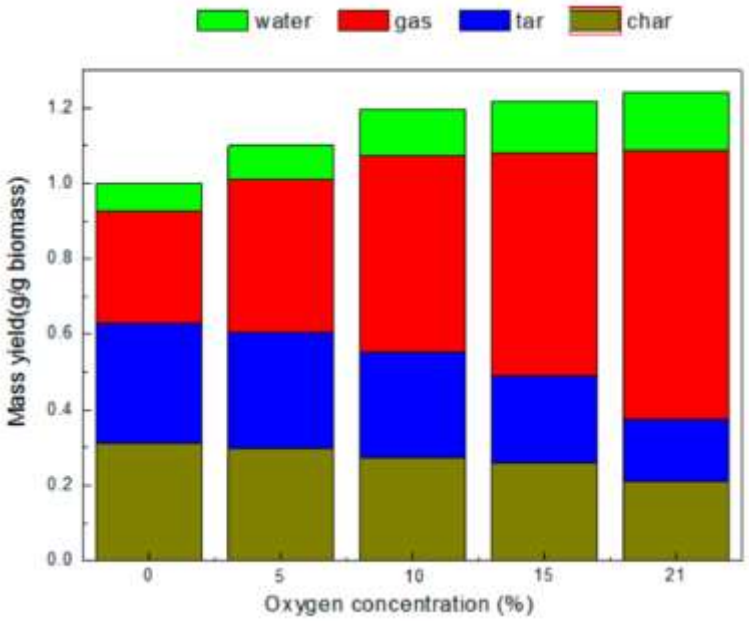

Figure 38. Product distribution of pinewood 500 °C pyrolysis under different oxygen concentrations [77]

II.4. Positioning and objectives of the thesis

II.4.1. Positioning of the PhD thesis

Based on the literature review presented above, it is important to highlight that all the works from the literature consider counter-current smoldering in which the oxidation zone is ignited at the surface of a biomass bed and then propagate downward into the bed (downward counter-current smoldering). To the best of our knowledge no work has been performed on upward counter-current smoldering, except the previous works from the research team [1,59,61]. This PhD thesis is in the same direction as the Milhé's and Daouk's doctoral studies [29,80]. We focused on the pyrolysis of biomass as a key step in the fixed bed staged gasification process. These previous works can be briefly summarized below.

First, M. Milhé [29] performed an experimental study of the pyrolysis of wood chips in inert and oxidative conditions. Part of his work concerned the homogeneous and heterogeneous cracking of tars passing through a hot charcoal bed. This investigation was carried out at lab and pilot scale. At lab scale, he showed that homogenous tar cracking is significant only above 500°C while heterogeneous tar cracking in the char bed is significant above 400°C. At pilot scale, he compared allothermal and autothermal (or oxidative) pyrolysis of wood chips in a continuous operation mode.

Second, E. Daouk [81] focused on the oxidative pyrolysis of wood chips and wood pellets both at particle and at bed scale. At the particle scale, he investigated the influence of oxygen

concentration, particle size and density. At pilot scale, oxidative pyrolysis was performed in batch and continuous mode. However, several experimental results in batch mode remain questionable because the bed compaction was not considered.

Moreover, some additional remarks have to be done before positioning the present work.

First, one should highlight that almost all of the research related to forced counter-current smoldering was performed at high air flux compared to those involved in oxidative pyrolysis. Indeed, in those studies, air flux varied from stoichiometry conditions (equivalence ratio equals to 1) to fit with combustion applications, down to gasification ones with equivalence ratio close to 0.25. Some authors investigated lower air flux but no one has gone down to the level of the present study 0.022 $kg.m^{-2}.s^{-1}$, chosen for its similarity to the one in a two-staged industrial gasifier. Thus, information is missing on the propagation rate, geometry, and conversion during counter-current smoldering in packed bed in very low air flux conditions. Moreover, it is also said that in such extreme small air mass flux, steady state regime is difficult to reach [75].

Second, very little information is available on the influence of biomass nature on the features of the oxidation zone; especially quantitative results would be useful to enhance understanding.

And finally, in counter-current smoldering in a downdraft reactor, compaction occurs in the oxidation zone and thus needs to be considered carefully applications.

Therefore, this PhD focused on the oxidative pyrolysis of various biomass types at fixed bed scale. Experimental study was performed in both continuous and batch modes. Experiments in continuous mode allowed approaching real process in an industrial gasifier while the batch mode enabled the fine characterization of main oxidation zone features.

II.4.2. Biomass pellets for valorization of new biomass sources

Extending the usable biomass range for the air-staged gasification is an objective of this study. Indeed, in current years, operators and constructors succeeded to control the air-staged gasification process, but only for wood chips with relatively low moisture content. Extending the range of biomass to the agricultural residues or herbaceous crop biomass with higher potential raises many technical problems due to their low density and high ash content when compared to wood chips ones.

Considering non-woody biomass, irregular shape, size, and low bulk density cause many difficulties for handling, storage and conversion [82,83]. Densification could be a solution as it provides multi-advantages over the raw biomass. First, densified biomass reduces the cost of

handling and storage [83–85]. The first reason for this is that the densification reduces significantly the bulk volume of the raw biomass, thus less space is needed for transporting and storing. Second reason lies on its uniform shape and size that allow the easy handling and storing steps by using standard equipment. In addition, higher energy density in the densified biomass enables to adapt to various existing energetic conversion technologies. Moreover, densification brings the possibility of using different biomass resources since densified biomass can be produced from a wide range of raw biomass materials including residues from forestry and agricultural sectors, industrial and domestic solid wastes, and also the blends between them [85–87].

Thus, in this PhD thesis, the process performances with agricultural residues and herbaceous crop biomasses pellets were studied in detail. Wood pellets were also investigated as reference biomass.

II.4.3. Industrial challenges and PhD scientific objectives

- *Industrial challenges*

This PhD thesis approaches the biomass pyrolysis step in two-staged gasifiers or possibly in future advanced carbonization processes. Regarding the industrial applications aimed at, the challenges in development or optimization of these technologies are many and varied; the most urgent are for sure:

- Improvement of the reliability of the technologies;

- Widening of the type of biomass usable;

- Increase of the process performance in terms of energy efficiency and environmental concerns.

- *Industrial objectives*

In this global challenge, the specific industrial objectives of the present work were to provide practical answers to process designers and operators regarding the oxidative pyrolysis stage of the process. In particular, the work aimed to measure some important physical quantities such as:

- Equivalence ratio (ER);

- Thickness of the oxidation zone;

- Yields and compositions of the pyrolysis products;

- Temperature field.

The impact of the biomass nature on these quantities was another major industrial concern of the PhD.

- *Scientific objectives*

As discussed in the beginning of this chapter, oxidative pyrolysis of biomass in a downdraft fixed bed reactor is so complex that researchers are today far away to be able to predict its behavior. Such a final goal will for sure require in the future the setup of strong and robust CFD models. Therefore, the scientific objective of our work was to contribute to this final goal by providing an experimental database that could be useful for CFD model developers.

However, our experimental work aimed also at improving by itself scientific knowledge on the oxidative pyrolysis in a downdraft fixed bed reactor. Indeed, the quantification of the physical quantities listed above was a strong scientific objective. Moreover, a particular attention was paid to the influence of biomass nature as well as its composition on the global behavior of the fixed bed during oxidative pyrolysis.

II.4.4. Methodology

The experimental study was carried out in a fixed bed reactor of 20 cm diameter and 1.6 m height, under similar conditions as in an industrial staged gasifier. Three types of biomass pellets, as representatives for the different biomass sources, were selected to investigate the influence of the biomass nature on the oxidative pyrolysis. Two operation modes: continuous and batch were performed.

At the first step, the continuous mode was studied to reproduce the industrial operation mode with the different biomasses. Fixing the airflow rate at 0.022 $kg.m^{-2}.s^{-1}$ (as in an industrial gasifier), the biomass consumption rate as well as the produced char flowrate were measured. The oxidation zone was stabilized at a given elevation in the fixed bed by action of char extraction. The Tar protocol [2] was adapted to sample and analyze the pyrolysis vapors including condensable and permanent gases during the course of the experiments. We compared the behavior of herbaceous and agricultural residues pellets with classical wood pine pellets, by measuring some important process performances such as yield and compositions of the products, air/biomass ratio, as well as mass and energy balances.

At the second step, the batch mode was set up to allow a fine characterization of the oxidation zone that we could not obtain with the continuous mode. The specific features of the oxidation

zone: propagation velocity, thickness, and compaction, were measured for three types of biomass. Similar to the continuous mode, we fixed the airflow rate and feed the biomass into the reactor up to about 80 cm. After ignition step at the bottom of the reactor, the oxidation zone propagated within the fixed bed of biomass. The propagation of the oxidation zone was followed by the temperature evolution in the thermocouples located along the bed fixed bed. Bed height was monitored continuously thanks to a laser beam located on the top of the reactor. In this study, we developed a method to characterize the oxidation zone features and a Matlab program for the experimental data treatment. The pyrolysis products including char, condensates and gas were also quantified and analyzed.

- Page intentionally left blank -

CHAPTER III

MATERIALS AND EXPERIMENTAL METHODOLOGY

III.1. Biomass

We selected three biomasses with different origin and nature: pinewood as a representative of forestry residues, miscanthus as a representative of herbaceous energy crops and wheat straw as an agricultural residue. The pinewood was used as a reference. Three commercial biomass pellets types were chosen: pine pellets from Bioforest®, miscanthus pellets from Jardi'nova® and wheat straw pellets from RAGT®. The biomass pellets particles were measured to 20 mm length and 6.1, 6.3 and 5.6 mm diameter for pine, miscanthus and wheat straw, respectively (Figure 39).

Figure 39. Three types of biomass pellets chosen for this study

Proximate and ultimate analyses of these biomasses are given in Table 17. Proximate analyses were carried out in a muffle furnace according to standards AFNOR NF EN 1860-2 and AFNOR XP CENT/TS 14775. Ultimate analyses (C, H, N, S content) were performed using a Vario Macro Cube Element analyzer. The O content was calculated by difference. Heating values of biomasses were measured using a calorimeter (Parr Instrument, Parr-6200).

Biomass	Pine	Miscanthus	Wheat straw
Proximate analysis (wt%, d.b)			
Moisture (wt%)	7.0	7.9	8.2
Ash	0.3	3.0	8.2
Volatile matter	82.1	84.8	78.8
Fixed carbon	17.6	12.2	13.1
Ultimate analysis (wt%, d.a.f)			
C	51.0	53.3	53.8
H	6.9	6.7	6.9
N	0.1	0.2	1.0
O (by difference)	42.1	39.8	38.4
LHV ($MJ.kg^{-1}$, d.b)	21.8	20.0	19.1

Table 17. Characteristics of the biomass pellets

The main difference between the biomasses is their ash content; varying from 0.3 % for wood to 8.2 % for wheat straw.

Bulk density was calculated for each sample from the measurement of their mass and volume. The bulk density of pine pellets was 657 $kg.m^{-3}$ and that of miscanthus and wheat straw pellets were lower with 584 $kg.m^{-3}$ and 549 $kg.m^{-3}$, respectively (Table 18).

Biomass	Pine	Miscanthus	Wheat straw
Bulk density, ρ_b ($kg.m^{-3}$)	657	584	549

Table 18. Bulk density of biomass pellets

The composition of Ash in the three biomass pellets were analyzed using Inductively Coupled Plasma (ICP) method. Results are given in Table 19.

ppm, db	SiO_2	Cl	P	K	Ca	Mg	Fe	Na	Zn	Al
Pine	1,540	80	39	510	710	240	0.4	0.6	0.1	0.4
Miscanthus	12,600	360	350	4,000	3,180	530	1.7	1.3	0.1	2.3
Wheat straw	47,300	1,450	1,320	10,180	3,800	820	1.9	2.3	0.1	2.3

Table 19. ICP analysis of ash content in the three biomasses

III.2. Fixed bed reactor

The fixed bed reactor was designed and installed at CIRAD. This reactor was originally designed to study char gasification [88–90]. Later on, Milhé et al. [29], adapted the reactor to study the autothermal and allothermal pyrolysis of wood chips and then Daouk et al. [81] studied the oxidative pyrolysis of wood chips and wood pellets.

The reactor was composed of several components: reactor chamber, feeding system, char extraction, air supply, and products sampling (Figure 40).

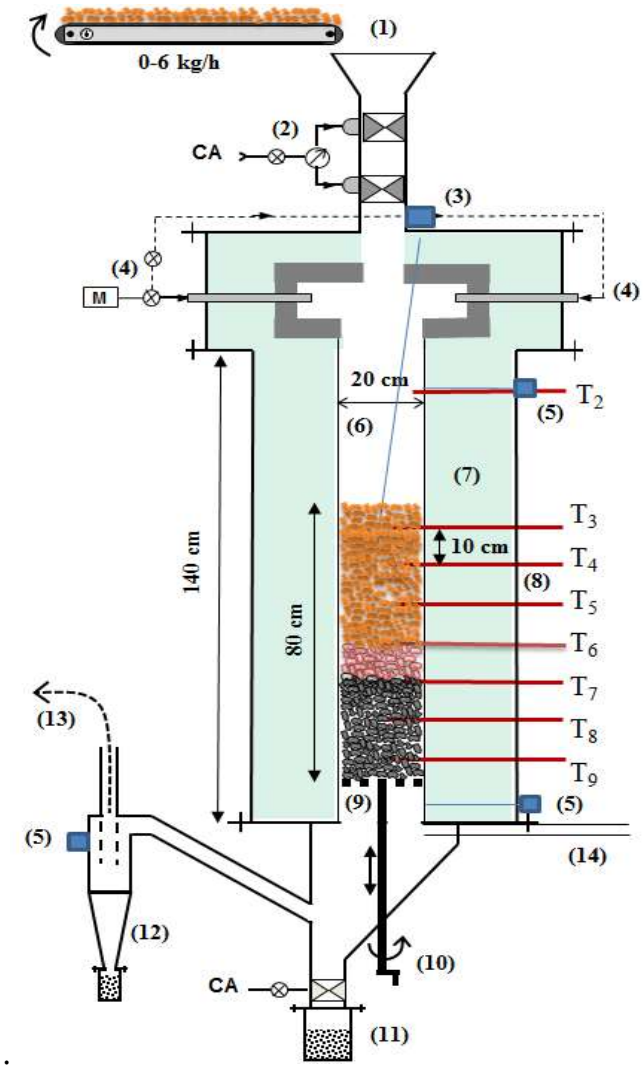

Figure 40. The schematic diagram of the fixed bed reactor

1- Convoyer; 2- Pneumatic valves; 3- Laser system; 4- Air entrances; 5- Pressure transducers; 6- Reactor tube; 7- Wool insulation; 8- Thermocouples; 9- Grate; 10- Char extraction system; 11- Char tank, 12- Cyclone; 13- To post-combustion system; 14- Sampling pipe; M- Mass flowmeter; CA- Compressed air

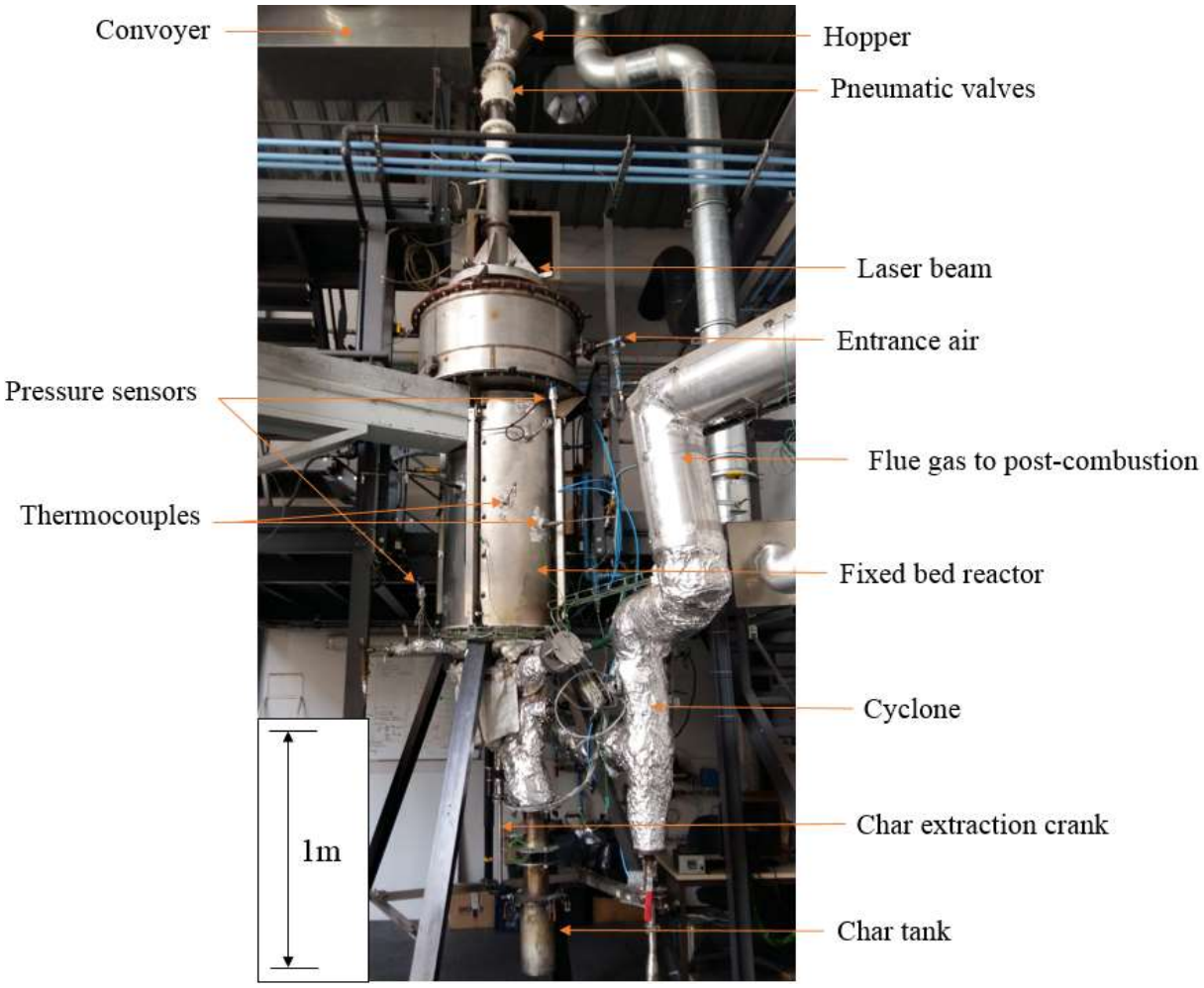

Figure 41. Photo of the fixed bed reactor

It allows operation in both batch and continuous mode. The difference between the two modes of operation is illustrated in Figure 42.

III.2.1. Two operating mode: batch and continuous

Batch mode (Figure 42-a) consists in a sequence of several steps including feeding, ignition and propagation of the oxidation zone in a fixed bed of biomass. Biomass was initially fed into the reactor to form a bed of about 80 cm height. Char was not extracted and remained in the reactor during the propagation: it was extracted only at the end of the test to be weighed and analyzed.

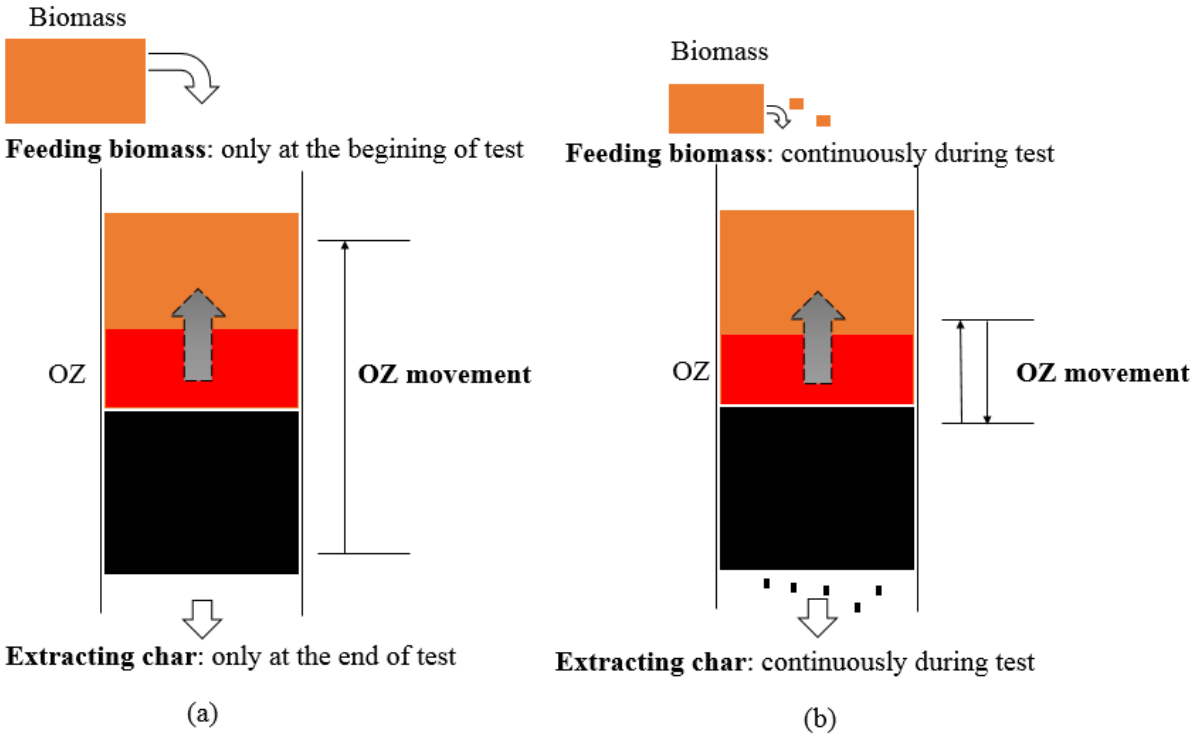

Figure 42. Illustration of two operating modes with the fixed bed reactor: (a) batch (b) continuous

Continuous mode (Figure 42-b) started as the batch mode but it was performed differently when the oxidation zone reached a given elevation inside the reactor, at the position of the thermocouple T6 (Figure 40) in this study. The char was extracted to lower the oxidation zone and to maintain it at the middle of the fixed bed (between T6 and T7). Decrease of the bed height due to extraction and compaction was compensated by the automatic biomass feeding system thanks to a convoyer and a laser beam. Details of the experimental procedure for both of two operating modes are presented in the next sections.

III.2.2. Reactor chamber

The reactor chamber consisted of a 310-type refractory steel tube of 20 cm diameter and 160 cm of length. It was surrounded by 30 cm of refractory wool insulation. Temperature and pressure measurement as well as gas sampling could be performed every 10 cm as the reactor was equipped with eight tapping pipes containing 1-mm K-type thermocouples. Figure 43 shows an illustration of the integrated temperature, pressure measurement and sampling pipe. These tapping pipes (labeled T2 to T9 in Figure 40) were placed helicoidally along the reactor to avoid disrupting of the solid flow downwards and hence to avoid channeling or dead volumes creation. Another pipe (numbered 14, Figure 40) was situated at the lower part of the reactor to allow sampling of pyrolysis products. All these tapping pipes could also be moved horizontally. In addition, to measure the external wall temperature, using for calculation of the heat losses,

three thermocouples were installed at the same elevation as T5, T6 and T7 (presented in Section IV.4 later).

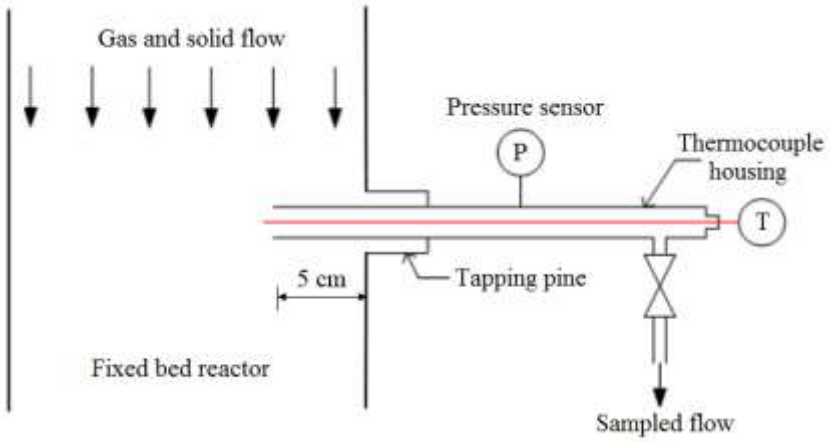

Figure 43. Illustration of the temperature, pressure measurement and sampling line

The biomass was fed at the top of the reactor chamber and formed a packed bed. The bed was supported by a grate situated at the bottom of the reactor chamber. The grate was linked to a char extraction system (Figure 44) allowing the manual extraction of the char at the end of the tests in batch mode or during the course of the tests in continuous mode.

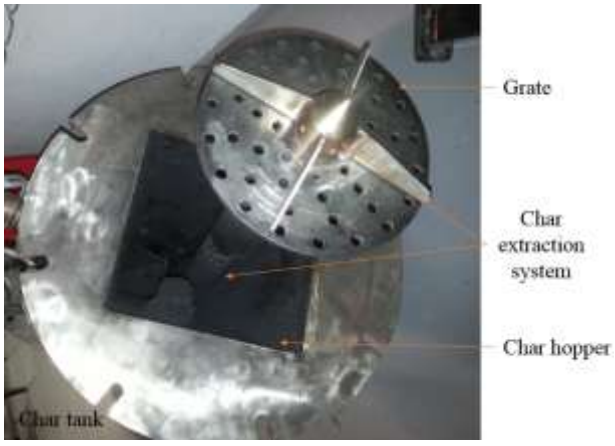

Figure 44. Grate and char extraction system

The height of the biomass bed was continuously measured during experiments by a laser beam located on the top of the reactor chamber.

Air supply in the reactor was controlled by a mass flowmeter (Brooks 5851S). It guaranties all experiments run with a controlled airflow rate of 34 $NL.min^{-1}$; that is to say 0.022 $kg.m^{-2}.s^{-1}$ close to the operating airflow rate in an industrial gasifier. In addition, two pressure transducers was located before and after the biomass/char bed in order to check plugging or bridging formation during experiments.

At the outlet of the reactor, the gases passed through a cyclone (numbered 12, Figure 40) where the fine solid particles were removed before being sent to a post-combustion chamber. The line leading the gaseous products to the post-combustion was heated to 350°C by electrical resistances in order to avoid condensation of pyrolysis vapors and eventual plugging.

II.2.3. Biomass feeding

Biomass feeding was carried out differently according to the operating modes. In batch mode, after preliminary weighing, biomass was fed manually to reach a certain height of 80 cm. In continuous mode, the oxidation zone was maintained at the middle of the bed, between T6 and T7 (Figure 40). A biomass bed of at least 35 cm was maintained above the oxidation zone. The feeding process was controlled and performed automatically thanks to the conveyor (numbered 1, Figure 40), two pneumatic valves (numbered 2, Figure 40) and the laser system (numbered 3, Figure 40). Here, we will detail the feeding process for the continuous operating mode.

Biomass was arranged on the conveyor belt of 2 m long and 12 cm large to be fed into the reactor (Figure 45). The velocity of the conveyor belt was kept constant. The mass flow- rate of this feeding system depends on the height of biomass in the conveyer, its velocity, and the bulk density of the biomass. Considering these parameters, the feeding system capacity can be adjusted between 1.0 and 6.0 $kg.h^{-1}$ of biomass.

Figure 45. The conveyer belt (used in continuous operation mode): front view (left) and side view (right)

During the feeding process, the sealing of the reactor was ensured by the presence of two pneumatic valves. The two pneumatic valves and the conveyor were operated automatically when a low bed level value was detected by the laser system. Briefly, when the bed height was lower than 65 cm, the upper valve opened, the conveyer ran and biomass was fed into the zone between the two valves for 1 minute. Then, the conveyer stopped, the upper valve closed, and

the lower valve opened to allow biomass entering the reactor. The feeding process stopped when the bed height reached 70 cm.

At the bottom of the reactor, char extraction was carried out manually with the help of the crank connected to the scrapers above the grate (Figure 44). By turning the crank, the char was extracted from the reactor and collected in a char tank. During experiments in continuous mode, the char tank could be opened and weighted; the sealing of the reactor was ensured by a pneumatic valve located between the reactor chamber and the char tank.

III.3. Analysis and instrumentation

III.3.1. Sampling system

A sampling line was inserted below the grate to collect both condensable and non-condensable gases (Figure 46). Adapted from the tar protocol [2], this line allows sampling of the gas at the output of reactor. Condensable gases (condensates) were condensed in a series of impingers. Non-condensable gases (permanent gases) were analyzed during the experiment. The sampling flow rate was kept constant during experiments between 2.0 and 4.0 $L.min^{-1}$. The flow rate had to be high enough to collect a significant mass of the condensates but low enough to avoid rapid clogging of filters and porous frit in the sampling line as well as disturbance of gas flow in the reactor.

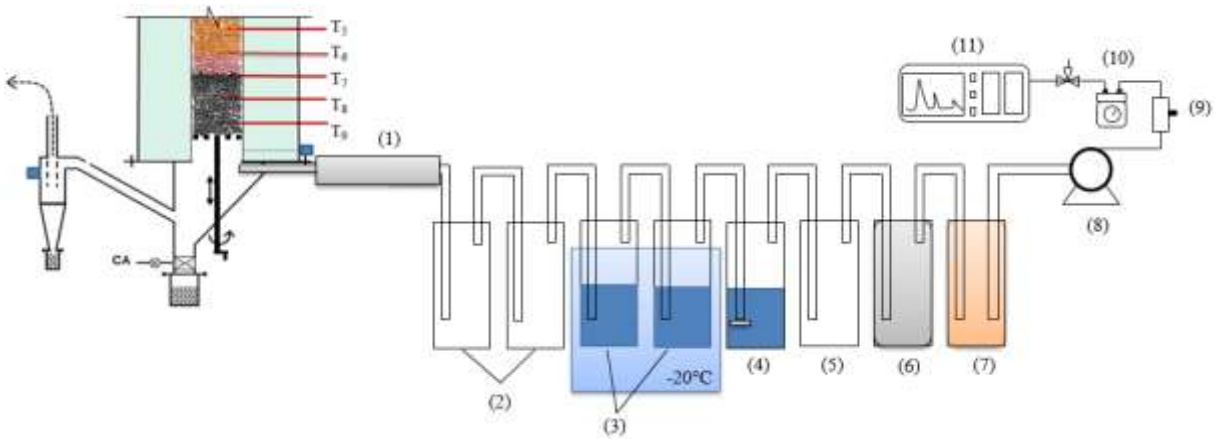

Figure 46. Sampling system for condensable and non-condensable gas

(1) heated sampling line, (2) empty impingers, (3) impingers with isopropanol, (4) impinge with isopropanol and a porous frit, (5) empty impinger, (6) impinger with cotton fiber, (7) impinger with silica gel, (8) Pump, (9) Flowmeter, (10) Volumetric counter (11) Micro-GC analyzer

Volatile matters, including condensates and permanent gases, were sampled through a pipe heated up to 350°C (1) to avoid condensation. Then, they passed through a set of eight

impingers to trap the condensable gases. First, the two empty impingers (2) were maintained at ambient temperature to condensate majority of vapor and heavy molecules. Then, the following three impingers were filled up with around 100ml of isopropanol. Two were maintained at -20°C (3) and the third one was equipped with a porous quart frit at ambient temperature (4) to collect the lighter molecules of condensates and the remaining of steam. An empty impinge at ambient temperature (5) was added to extend the residence time of the sampled gas (5). In addition, one impinger at ambient temperature filled with cotton (6) and one filled with silica gel (7), allowed the complete absorption of the residual condensates and water to protect the Micro-GC system. The dried gases were pumped (8) before entering a mass flowmeter (9) a volumetric counter (10), and finally, they were continuously analyzed by a Micro-GC system (11).

The photo of the whole sampling system for condensable gases is shown in Figure 47.

Figure 47. Photo of the sampling system for condensable and gas

Figure 48 shows the impingers before and after a test with Pine pellets in continuous mode. Water and organic condensates differed from one impinger to another. Thus, before sampling and analyzing, all the condensates in the eight impingers need to be mixed well together by pouring isopropanol from the impringers illustrated in (3) and (4) into the other ones.

Figure 48. The impingers before (left) and after (right) a test with Pine pellets in continuous mode.

III.3.2. Permanent gases

The produced permanent gases were characterized in terms of mass flow rate and composition.

- *Flow rate*

Nitrogen in the fed air ($\dot{m}_{N_{2,i}}$) was used as a tracer to calculate the total mass flow rate of the permanent gases ($\dot{m}_{pg}$) at the outlet of the reactor, according to Equation 12.

$$\dot{m}_{pg} = \frac{\dot{m}_{N_2}}{Y_{N_2}} \tag{12}$$

$\dot{m}_{N_2}$[kg.m^{-2}.s^{-1}] was calculated from the inlet air mass flowrate.

Y_{N_2}[%m] is the N_2 mass fraction in the produced permanent gases, calculated from its volumic concentration as follows:

$$Y_{N_2} = \frac{M_{N_2} * [N_2]}{M_{pg}} \tag{13}$$

M_{N_2}[g.mol^{-1}] is N_2 molar mass.

M_{pg} [g.mol^{-1}] is the average permanent gas molar mass calculated as follows:

$$M_{pg} = \sum_j M_j Y_j \tag{14}$$

where, j= {N_2, O_2, CO_2, CO, H_2, CH_4, C_2H_2, C_2H_6}

Y_j [%v] is the volumic fraction of gas j, measured by the micro-GC.

M_j [g.mol^{-1}] is the molar mass of gas j.

Finally, the mass flow rates of each gas ($\dot{m}_j$) in the permanent gases was calculated using Equation 15.

$$\dot{m}_j = Y_j . \dot{m}_{pg} \quad (15)$$

- *Composition*

Gas chromatography (GC) was used to analyze the concentration of the permanent gases. A typical GC system consists of a carrier gas bottle, a sample injector, a column, and a detector (Figure 49).

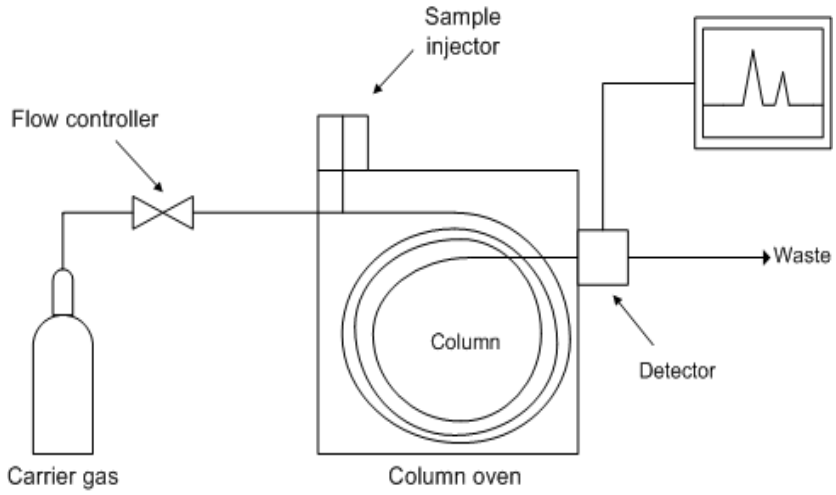

Figure 49. Schematic diagram of the gas chromatograph (illustrated with a column)

A sample of the gaseous mixture is mixed with a carrier gas, which typically is an inert gas such as helium or argon gas. This carrier gas is called the mobile phase of the gas chromatograph. A GC has several columns including packed columns and capillary columns, where the separation of sample components takes place. Inside the columns, it exists an active layer, which consists of a coating chosen for its affinity with the chemical species of interest. Each gas has a different absorption and release rate in presence of this active layer, so it leaves the columns at different times: this is called the *retention time*. The columns are exposed to different temperature levels, which influences the rate of release and transportation through the columns.

After the gases are separated in the columns, they go through a Thermal Conductivity Detector (TCD). This detector identifies the thermal conductivities of the various gases.

In this work, we used a µGC VARIAN CP 4900 system, equipped with a TCD detector with two columns: MolSieve 5 Å and PoraPlot Q. Column 1, MolSieve 5Å, used Argon as the carrier

gas and measures major gases such as O_2, N_2, CH_4, CO, and H_2. Column 2, PoraPlot Q, used Helium as the carrier gas and measures CO_2, CH_4, C_2H_4, C_2H_6 and C_2H_2. The gas chromatograph parameters for each column are shown below in Table 20.

	Column 1: MolSieve 5Å	Column 2: PoraPlot Q
Detector	TCD	TCD
Carrier gas	Argon	Helium
Column temperature	140°C	50°C
Column pressure	150 kPa	150 kPa
Detection time	70 s	70 s
Sampling time	15 s	15 s
Injection time	50 ms	50 ms

Table 20. Gas chromatograph parameters of column Molsieve 5Å and PoraPlot Q 10 m

III.3.3. Char

- Mass flow-rate

Char collected in the char tank was weighted and kept for analysis. The mass flow-rate of char was determined differently following two different methods:

- By weighing of the char after each extraction. The average flow rate of char $\dot{m}_{ch}$ was calculated from the total char mass m_{ch} and the test duration.

- By ash tracer method, i.e. by comparing the ash content in the char sample at the output of the reactor to the one in the initial biomass. It is based on the hypothesis that all the mineral matters in biomass remain in the solid residue. The calculation of the char production flux $\dot{m}_{ch}$ (in $kg.m^{-2}.s^{-1}$) using the ash tracer method as follows:

$$\dot{m}_{ch} = \frac{\dot{m}_b . ASH_b}{ASH_{ch}} \quad (16)$$

where:

+ ASH_b and ASH_{ch} [%m] are the ash fraction in respectively the biomass and the produced char;

+ $\dot{m}_b$ [$kg.m^{-2}.s^{-1}$ db] is the average biomass consumption flux during experiments.

- Proximate and ultimate analyses

Proximate analyses were carried out in a muffle furnace (Figure 50-a) according to standards AFNOR NF EN 1860-2 and AFNOR XP CENT/TS 14775. Ultimate analyses (C, H, N, S content) were performed using a Vario Macro Cube Element analyzer. The O content was calculated by difference.

(a) (b)

Figure 50. Muffle furnace (a) and calorimeter (b)

Ultimate analyses (C, H, N, S content) were performed using a Vario Macro Cube Element analyzer. The O content was calculated by difference.

In addition, heating values of the produced char were measured using the calorimeter Parr Instrument, Parr-6200 (Figure 50-b).

III.3.4. Condensates

- *Flow rate*

The flowrate of condensates were determined by difference between inlet and outlet in order to check the mass balance.

Inlet:

- Biomass, daf
- Air

Outlet:

- Char, daf
- Permanent gases
- Condensates
- Water

- *Water content in the condensates*

Karl Fischer titration method [91] was used to measure the water content in the condensates. This method is suitable for the water content from 100 ppm to 100 %. In the laboratory of our research unit, the METTLER TOLEDO V20 system was used (Figure 51).

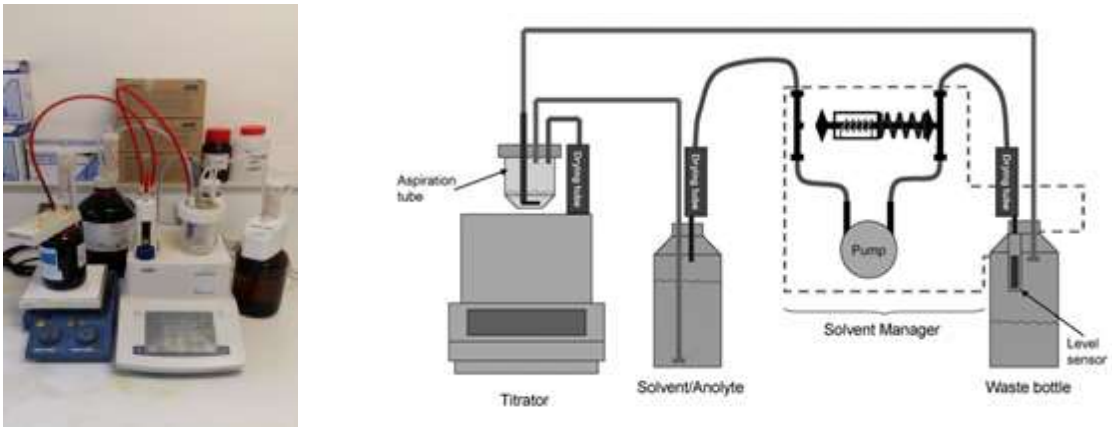

Figure 51. METTLER TOLEDO V20 system

For samples of the condensates from pyrolysis process, we used the HYDRANAL™-Composite 5 reagent ("titrant"). It is the specific reagent for condensates from pyrolysis and gasification processes. About 0.3 mL sample was used for each run.

The contribution of drying water (originating from moisture in the biomass) was subtracted to obtain the yield of pyrolysis water only.

$$\dot{m}_{H_2O}^{pyro} = \dot{m}_{H_2O}^{tot} - \dot{m}_{H_2O}^{dry} \quad (17)$$

- *Elemental composition of the condensates*

Composition of condensates was presented here by CHO content. C and H contents in condensates were determined by elemental balances. Oxygen content in condensates was determined by difference.

III.3.5. Temperature measurement

The K type thermocouples were located inside thermocouple housings (Figure 43), which protect the thermocouples and enable the insertion of the thermocouple at a given position inside the bed every 10 cm. In addition, three thermocouples were installed on the reactor wall to measure the external temperature during experiment in order to calculate the heat losses.

During experiments, temperature from each thermocouple was recorded continuously each 0.17 minute by the Data Acquisition 34970A and was visualized by the software Bench Link Data Logger 3 (Figure 52). The temperature data were then exported into an excel file and treated with MATLAB Software.

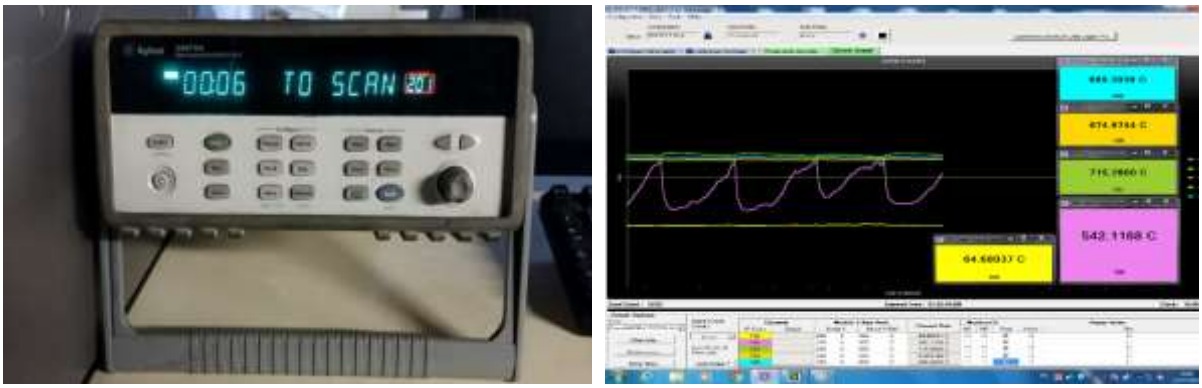

(a) (b)

Figure 52. (a) Data Acquisition 34970A and (b) Visualization by BenchLink Data Logger 3 software

Example of temperature recording during an experiment in batch mode is given in Figure 53.

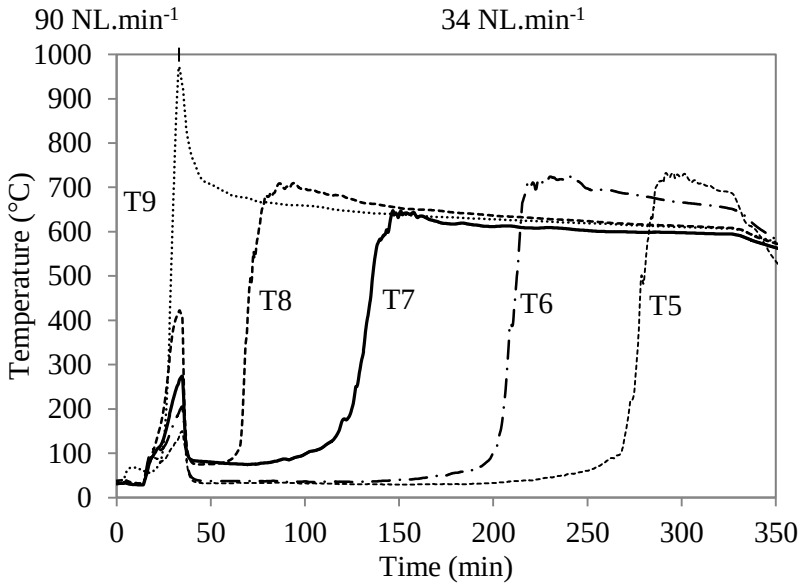

Figure 53. A typical temperature versus time profile obtained from an experiment in batch with pine pellets, 0.022 kg.m^{-2}.s^{-1} air flux.

Figure 53 shows a typical temperature versus time profile for an experiment in batch operating conditions. Temperature was recorded when the oxidation zone was ignited at T9 and propagated from T8 to T5. At T9, we observe first a rising in temperature up to 950-1000°C at 30 minutes, indicating the ignition step (detailed in the Chapter V). Then, the temperature

dropped to about 650 °C because of both the reduction air flux to 34 NL.min^{-1} and the introduction of biomass. Temperature at T9 remained stable while the OZ propagated upward to the other thermocouple positions. The oxidation zone reached T8, resulting in a rise in temperature at T8 from 50°C to a peak of about 720°C. This phenomenon was repeated when the oxidation zone propagated to T7, T6 and T5, successively. Thus, the temperatures versus time allowed the determination of the oxidation zone velocity and thickness in the fixed bed of biomass.

III.3.6. Bed height measurement

During experiments in both continuous and batch modes, bed height was observed continuously thanks to a laser beam.

In continuous mode, bed height measurement enabled to control the feeding process. The bed height was maintained between 65 cm and 72 cm thanks to the feeding and monitoring systems. Figure 54 shows the bed height evolution during a typical test with wheat straw pellets. Biomass feeding stopped automatically when the bed height reached a height higher than 70 cm and started again when the level dropped to lower than 65 cm. This figure also shows the bed compaction, char extraction, and biomass feeding during the experiment.

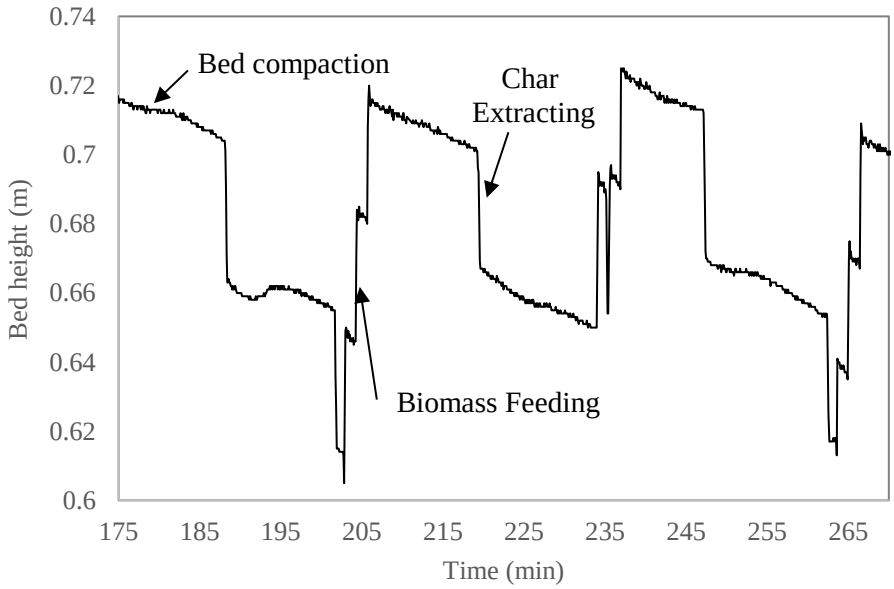

Figure 54. Bed height evolution during a test with wheat straw pellets in continuous operating condition, 0.022 kg.m^{-2}.s^{-1} air mass flux

In batch mode, the data of the bed height measurement allows the estimation of the bed compaction, which is an important value to establish the effective propagation velocity of the oxidation zone in this study. The details of this method will be presented in the chapter V.

- Page intentionally left blank -

CHAPTER IV

OXIDATIVE PYROLYSIS OF BIOMASS IN CONTINUOUS OPERATING CONDITIONS

This chapter focuses on the oxidative pyrolysis in a continuous fixed bed as existing in some industrial gasifiers. In these gasifiers, oxidative pyrolysis occurs in an oxidation zone (OZ) in which several complex and coupled reactions take place. This OZ produces char, condensates and gas for the next steps of the gasification process, as well as it provides energy for the pyrolysis process. In a downdraft continuous fixed bed, the OZ trends to propagate upward towards the raw biomass but is maintained still at a given elevation thanks to the char extraction (Figure 55).

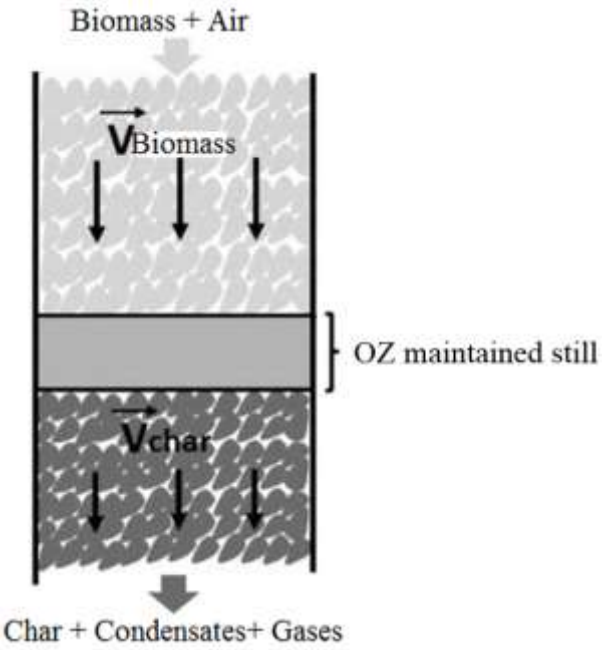

Figure 55. Oxidation zone in a continuous fixed bed

The stabilization of the oxidation zone inside the bed is of particular interest for operators for two reasons:

- The top of the bed is maintained at a low temperature, thereby that facilitates the control of the process and limits the production and deposition of tar;

- A higher temperature zone is created that favors tar cracking when crossing it.

This chapter presents the oxidative pyrolysis in a continuous fixed bed of three different biomass pellets: pine, miscanthus and wheat straw. First, the experimental procedure is

presented. Then, the results regarding process parameters, compositions of the products, and mass and energy balances are discussed. The chapter ends with a detailed enthalpy balance.

IV.1. Experimental procedure

A typical experiment consisted in two periods: transient and stationary. First, the transient period was considered as the preparation step for the experiment. Then, the oxidation zone was maintained still at the middle of the reactor and sampling system was turned on: this was the stationary period that we investigated.

Temperature along the reactor are used to follow and control the experiments (Figure 56).

IV.1.1. Transient period

Transient period includes the following steps:

- *Ignition (1)*

  About 1.3 kg of the char was introduced in the reactor to form a char bed of about 12 cm height (above the T9). Note that the char was previously dried to 105°C during 12h and sieved above 4 mm to eliminate fine particles. Then, we dropped one or two pieces of ignited barbecue-lighter briquettes on the char bed surface from the top of the reactor. Airflow rate was set to 20 $NL.min^{-1}$ to maintain the oxidation reaction. Temperature at the thermocouple T8 increased to about 350°C when the combustion spread on the surface of the char bed.

- *Creation of the Oxidation Zone (2)*

  The airflow rate was increased to 90 $NL.min^{-1}$ to speed the combustion in the char bed surface and create the OZ. When the temperature at T9 reached about 950°C, we considered that the OZ was created and was homogeneous in the char bed.

- *Biomass feeding (3)*

  Airflow was then decreased to the experimental operating flow rate of 34 $NL.min^{-1}$. Then, biomass pellets were fed into the reactor manually until the bed height reached about 80 cm. It resulted in a decrease in temperature of T9 to around 650°C.

- *Raising the Oxidation Zone to the middle of the bed (4)*

  The OZ propagated upward in the fixed bed of biomass and reached T8, T7 and T6, successively. This propagation of the oxidative pyrolysis was monitored by temperature

measurements. The OZ was supposed to reach a given thermocouple when its temperature increased rapidly to 650°C.

This step aimed at raising the oxidation zone to the middle of the bed of 35 cm above the grate. When the OZ reached T6, we maintained it still at this position by controlling char extraction.

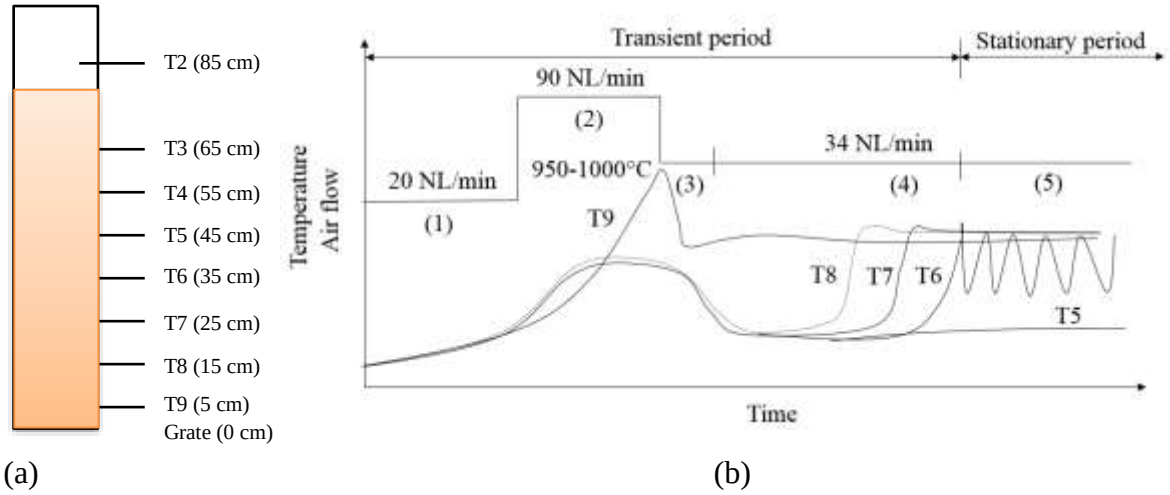

Figure 56. (a) Thermocouple positions and (b) typical temperature profile versus time during experiment in continuous operating mode

IV.1.2. Stationary period

This period corresponded to the step (5) in Figure 56. The actions in this period aimed:

- to maintain the oxidation zone still at the middle of the reactor, near T6;

- to maintain a biomass bed of 30 cm minimum above the oxidation zone;

- to sample the produced char, condensates and permanent gases.

Thus, when T6 reached 650°C, we extracted the char from the bottom of the reactor by turning three rounds of the crank to lower the OZ position of a few cm in the bed. The char collected in the tank at the bottom of the reactor was weighed. The OZ propagated upward; when it reached T6 again, a new extraction of char was performed.

During the experiments in continuous mode, the bed height decreased due to the char extraction and the bed compaction. The level of the bed height was measured continuously by a laser beam located on the top of the reactor. The measured data of the bed height were recorded and used to control the biomass feeding system automatically. The feeding system allowed maintaining a biomass bed of 30 cm minimum above the oxidation zone. In detail, we set a maximum bed

height of 70 cm and a minimum of 65 cm. When the measured value was lower than 65 cm, the feeding system was run to fill biomass into the reactor; when this value is greater than 70 cm, the feeding system was stopped.

The biomass consumption rate was measured from the total biomass injected into the reactor over a period of experiment. To determine this period, the bed height at the beginning and the one at the end of the considered period had to be similar.

IV.2. Bed temperature

During the experiments, the Oxidation Zone (OZ) was maintained at a given position (near T6, about 35 cm above the grate), and we measured the temperature via the thermocouples located all along the fixed bed. From this temperature measurement and the location of these thermocouples, we established the temperature profile. Figure 57 presents the average values recorded in the three biomass pellets beds.

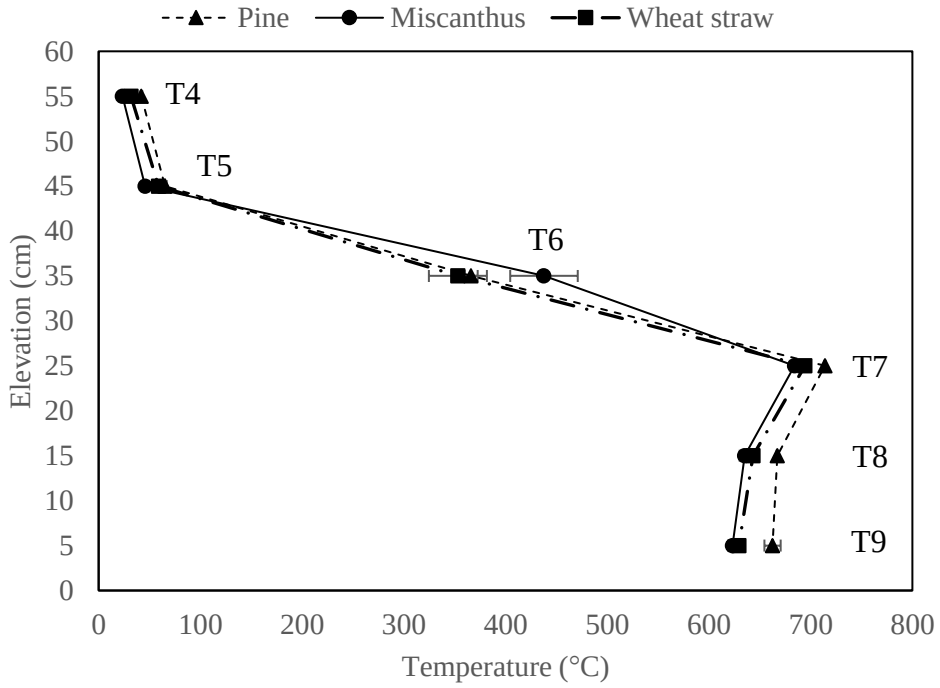

Figure 57. Temperature profile in different pellets beds during tests in continuous mode

Globally, measured temperature increased from about 30°C to 650°C along the bed from the top to the bottom. Temperatures at T6 fluctuated between a minimum value to a maximum value due to the successive char extraction and upward propagation of the OZ. Temperature below the position of T6 was in range of 620-720°C while temperature above the position of T6 was between 30-60°C.

Comparing the temperature in the beds of the biomasses, it was slightly higher for the pine than for the other biomasses. For example, at T7, average temperature was around 715°C in wood pellets bed while about 690°C in miscanthus or straw pellets beds.

Furthermore, we compared these results on wood pellets with those obtained with wood chips by Daouk et al. [1] in the same reactor and similar conditions. Temperature with wood chips of 680°C was lower than the 725°C for wood pellets. The difference in the bulk density of 657 $kg.m^{-3}$ for wood pellets and 220 $kg.m^{-3}$ for wood chips can explain the difference. Indeed, Yang et al [107] showed that in a given volume, high-density fuels have more combustible mass. Thus, in similar combustion conditions, denser biomass produces higher temperature than lighter one do.

Note that this temperature profile provides an information on the thickness of the oxidation zone, less than 10 cm. This point is detailed more precisely in the chapter V, using batch operating mode.

IV.3. Air/biomass ratio and equivalent ratio

Biomass consumption rate, air/biomass ratio and equivalence ratio are given in Table 21 on a dry basis (db).

	Pine	Miscanthus	Wheat straw
Air mass flux ($kg.m^{-2}.s^{-1}$)	0.022	0.022	0.022
Average biomass consumption rate ($kg.m^{-2}.s^{-1}$) (db)	0.032	0.033	0.034
Air/biomass ratio (db)	0.69	0.67	0.65
Air/biomass stoichiometry (db)	5.42	5.83	5.78
Equivalence ratio (db)	0.13	0.11	0.11

Table 21. Air/biomass ratio and equivalence ratio during oxidative pyrolysis of the three biomasses

The air mass flux was adjusted to 0.022 $kg.m^{-2}.s^{-1}$ and the average biomass consumption rate was measured (by weighing) to 0.032, 0.033 and 0.034 $kg.m^{-2}.s^{-1}$. The air/biomass ratio on dry basis was 0.69, 0.67 and 0.65 for respectively pine, miscanthus and wheat straw. The equivalence ratio (ER) which is defined as the actual air/biomass ratio relative to the stoichiometric air/biomass ratio was calculated to respectively 0.13, 0.11, and 0.11. The higher ER for the woody biomass shows that less woody biomass was consumed to sustain the OZ propagation under the same air flux. The OZ consumed 11 to 13 % of the stoichiometric combustion air to provide energy for the process.

The average propagation velocity of the oxidation zone in beds of the three biomasses can be calculated from the measured biomass consumption rate and the bulk density of the biomasses, as follows:

$$V_{OZ} = \frac{\dot{m}_b}{\rho_b} \quad (18)$$

The propagation velocity was calculated to 0.30, 0.35, 0.39 cm.min^{-1} for pine, miscanthus and wheat straw (Table 22). The difference in velocity is explained mainly by the difference in the bulk density of the biomasses, respectively 657, 584 and 549 kg.m^{-3}. Indeed, in the previous work, Daouk et al. carried out experiments with pine wood chips and pellets in continuous operating mode and showed that the propagation velocity was inversely proportional to the wood bulk density [1]. This result was found in a good agreement with other authors who studied the effect of density on the velocity of the oxidation zone [72,78,92].

	Pine	Miscanthus	Wheat straw
Average propagation velocity (cm.min^{-1})	0.30	0.35	0.39

Table 22. Average propagation velocity in the three biomass beds during continuous operation

IV.4. Compositions of the oxidative pyrolysis products

Oxidative pyrolysis products include char (solid residue), condensates (pyrolytic liquid products) and permanent gases. Composition of permanent gases were determined directly by the micro-GC analyses during the experiments. Samples of char and condensates were analyzed after the experiments. For the char, proximate and ultimate analyses were carried out. The composition of condensates was presented in terms of water fraction and elemental composition calculated by the elemental balance. Karl Fisher Titration method was applied to determine the water content in the condensates. The compositions of the products supported the establishment of the mass and energy balance (presented in Section IV.4).

IV.4.1. Composition of the char

Proximate and ultimate analyses of the chars from the oxidative pyrolysis of the three biomasses are presented in Table 23.

High ash content is one characteristic of the produced char from the herbaceous and agricultural residues biomasses compared to char from woody biomass. Ash is known to cause fouling and

sintering problems in industrial CHP biomass plants. Here, ash content were 10.7 % and 25.2 % for miscanthus and wheat straw chars, and 1.1 % only for char from pine pellets.

The produced chars were all rich in carbon since they contained 94.8, 92.5 and 92.4 % for pine, miscanthus and wheat straw, respectively. The oxygen content of the char from pine, miscanthus and wheat straw chars was 3.1, 5.2 and 4.3 %, respectively. High carbon and low oxygen contents were responsible for the high values of the Lower Heating Value (LHV) of the resulting chars, i.e. 34.1, 33.2 and 33.3 $MJ.kg^{-1}$ (Table 23).

Char	Pine	Miscanthus	Wheat straw
Proximate analysis (%m, db)			
Ash	1.1	10.7	25.2
Volatile matter	2.7	4.7	3.7
Fixed carbon	96.3	84.7	71.1
Ultimate analysis (%m, daf)			
C	94.8	92.5	92.4
H	1.6	1.7	1.9
N	0.6	0.7	1.6
O (by difference)	3.0	5.1	4.1
LHV ($MJ.kg^{-1}$, daf)	34.1	33.2	33.3

Table 23. Ultimate and proximate analyses of chars from oxidative pyrolysis in continuous mode (air mass flux of 0.022 $kg.m^{-2}.s^{-1}$)

IV.4.2. Composition of the permanent gases

Composition of the permanent gases were analyzed by the Micro-GC system (Table 24). Concentration of nitrogen (about 45 to 55 %) in sampled gas was not taken into account in the Table 24.

Gas fraction (%m)	Pine	Miscanthus	Wheat straw
CO_2	56.9	64.7	67.0
CO	32.8	25.5	23.6
H_2	2.3	2.2	2.1
CH_4	5.2	5.1	5.1
C_2H_4	2.1	1.6	1.3
C_2H_6	0.7	0.9	1.0
LHV ($MJ.kg^{-1}$)	10.0	8.9	8.5

Table 24. Composition of the permanent gases from oxidative pyrolysis in continuous mode, air mass flux of 0.022 $kg.m^{-2}.s^{-1}$, (N_2 free)

Regarding the composition of the permanent gases from oxidative pyrolysis of the biomasses, CO_2 was the dominant gas, varying from 55 % to 67 %. The high content of CO_2 was responsible for the low heating values of the permanent gases of about 8.5-10 $MJ.kg^{-1}$. CO was the second main permanent gas, accounting from 24 % to 33 %.

IV.4.3. Composition of the condensates

The composition of the condensates is presented here in terms of water content and elemental composition (Table 25.). Water content in condensates was determined by the Karl Fisher titration method using the METTLER TOLEDO V20 system. Because the condensates sampling remained questionable and problematic, the elemental composition of the condensates was determined from the elemental balance based on composition (C and H) and char yield, permanent gases and biomass. The oxygen content of condensates was calculated by difference.

	Pine	Miscanthus	Wheat straw
Water fraction %m	48.8	46.4	46.6
C	63.9	59.5	57.0
H	4.3	5.5	6.2
O	31.8	35.2	36.9
LHV ($MJ.kg^{-1}$)	13.6	14.9	15.9

Table 25. Analyses of condensates from the oxidative pyrolysis in continuous mode, air mass flux of 0.022 $kg.m^{-2}.s^{-1}$

Water content in the condensates from oxidative pyrolysis of the biomasses was about 46-49 %. Water content included both drying water from biomass and water from pyrolysis/oxidation reactions. High amounts of water was responsible for the low heating values of condensates from oxidative pyrolysis, i.e. 13.6 $MJ.kg^{-1}$ for pine, 14.9 $MJ.kg^{-1}$ for miscanthus and 15.9

$MJ.kg^{-1}$ for wheat straw. However, without considering the aqueous phase of the condensates, the heating value of the condensates was 23.2 $MJ.kg^{-1}$ for pine, 22.4 $MJ.kg^{-1}$ for miscanthus and 22.0 $MJ.kg^{-1}$ for wheat straw. Furthermore, comparing the water yield in the condensates from oxidative pyrolysis and the inert one, Milhé et al. [59] showed that pyrolysis water yield was 15 to 27 %m higher in the case of oxidative pyrolysis.

IV.5. Mass and energy balance

IV.5.1. Mass balance

Mass balance was established by knowing mass flowrates of all inlet and outlet components as listed as below:

Inlet:

- Biomass
  - Biomass, daf
  - Moisture
  - Ash
- Air
  - O_2
  - N_2

Outlet:

- Char
  - Char, daf
  - Ash
- Condensates
  - Organic condensates
  - Pyrolysis water
  - Drying water
- Permanent gases
  - CO_2, CO, H_2, CH_4, C_2H_4, C_2H_6
  - N_2

Figure 58 shows the mass balance for miscanthus pellets oxidative pyrolysis in continuous mode.

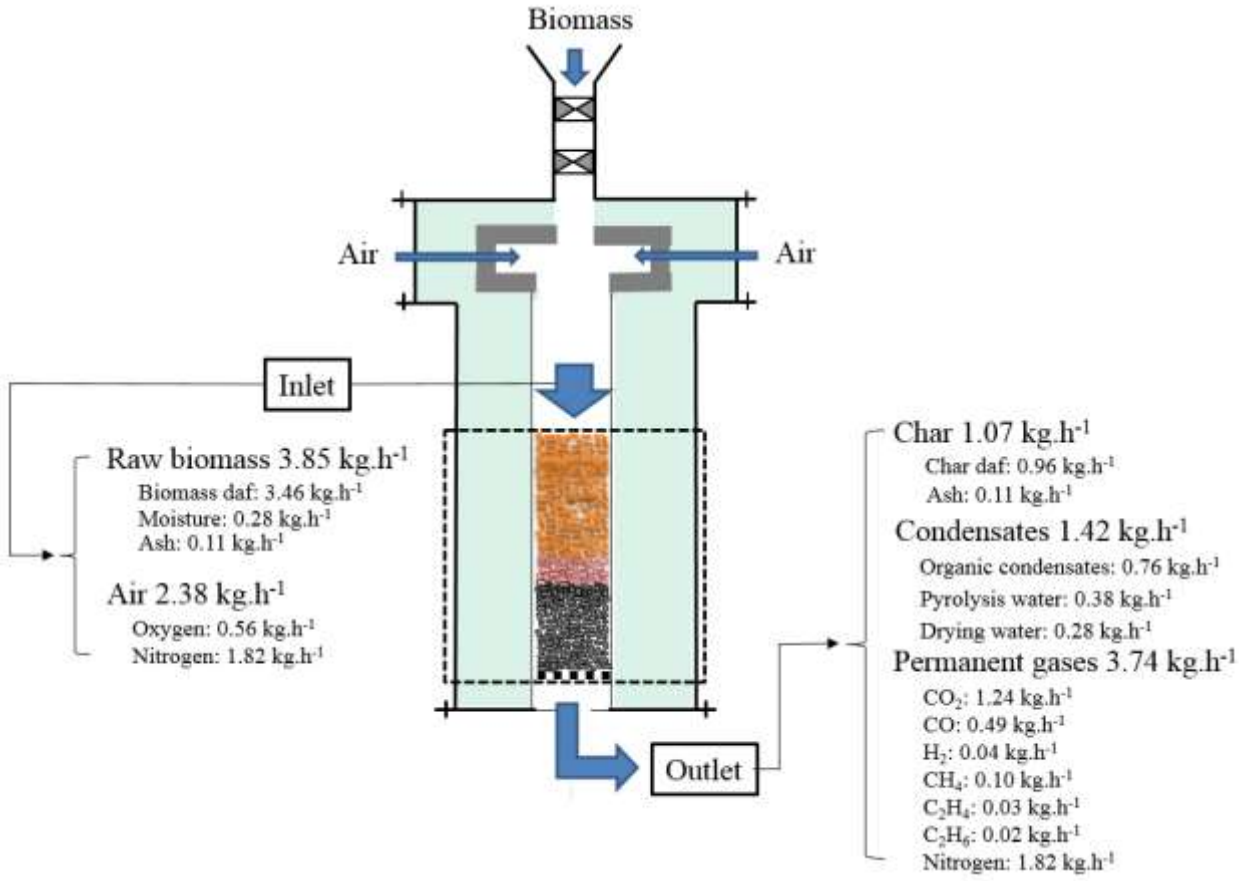

Figure 58. Mass balance case of miscanthus oxidative pyrolysis in continuous mode

Fixing an air flowrate of 34 NL.min^{-1} (2.38 kg.h^{-1}), we measured the mass flowrate of the raw biomass consumed to 3.85 kg.h^{-1}. At the outlet, we measured the flowrate of char to 1.07 kg.h^{-1} and permanent gases to 3.74 kg.h^{-1}. Condensates flowrates was calculated by difference between the inlet and outlet to 1.42 kg.h^{-1}.

The summary of the mass balance for the three biomasses is given in Table 26.

Flow rates ($kg.h^{-1}$)			Pine	Miscanthus	Wheat straw
Inlet	Biomass, daf		3.48	3.46	3.40
	Water (biomass)	H_2O	0.21	0.28	0.33
	Oxygen (from air)	O_2	0.56	0.56	0.56
	Nitrogen (from air)	N_2	1.82	1.82	1.82
	Ash (from biomass)		0.01	0.11	0.30
Outlet	Char, daf		0.74	0.96	1.03
	Condensates		0.95	0.76	0.78
	Pyrolysis water		0.69	0.38	0.35
	Drying water		0.21	0.28	0.33
	Permanent gases	CO_2	0.94	1.24	1.20
		CO	0.54	0.49	0.42
		H_2	0.04	0.04	0.04
		CH_4	0.09	0.10	0.09
		C_2H_4	0.04	0.03	0.02
		C_2H_6	0.01	0.02	0.02
	Nitrogen		1.82	1.82	1.82
	Ash (from char)		0.01	0.11	0.30

Table 26. Inlet and outlet flow rates ($kg.h^{-1}$) of the oxidative pyrolysis of the three biomasses

To facilitate the comparison of the results from different types of biomass, we present here the yields in daf (Figure 59). The yields of the char (Y^{Char}), condensates ($Y^{Condensates}$) and permanent gases ($Y^{Permanent\ gases}$) were calculated as a percentage of the mass of biomass in daf basis.

Note that the sum of the measured yields exceeded 100% because oxygen from the air reacted inside the bed and was recovered in the pyrolysis products [1,59].

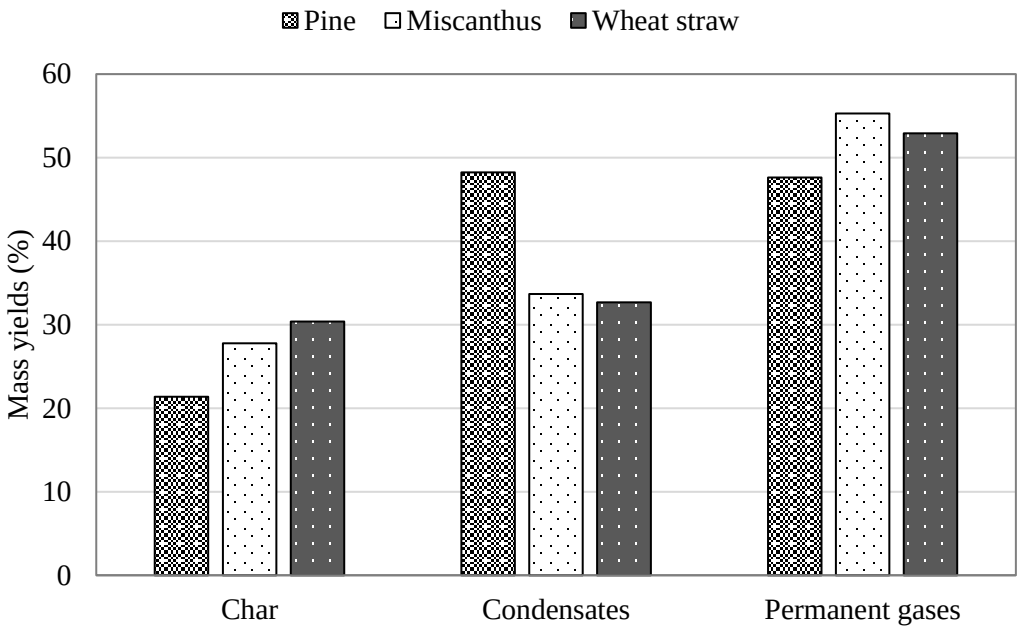

Figure 59. Mass yields (daf) of the oxidative pyrolysis products from different biomasses, 0.022 kg.m^{-2}.s^{-1} air flux

As shown in Figure 59, the char yield of pine, miscanthus and wheat straw was 21 %, 28 % and 30 %, respectively. The permanent gas yield ranged from 47 to 55 %, and the highest yield was obtained from pine pyrolysis. Condensates yield was found to be for pine, miscanthus and wheat straw char to 48 %, 34 % and 33 %, respectively. The difference in temperature between the beds of about 20°C cannot explain for the difference in the char yields. The best assumption to explain these measured differences in products yields is the difference in the ash content (0.3 %, 3.0 %, and 8.2 %). Indeed, it is known that biomass particles shrink during pyrolysis and the ash tends to concentrate on the external surface thereby creating a thin layer of ash surrounding the particle. The catalytic effects of the ash layer might accelerate secondary char-forming reactions (i.e. condensation, cross-linking and repolymerisation) and favored the cracking of heavy organic compounds. Consequently, a high ash content might be responsible for a high char yield and a low condensates yield, as observed by other authors [93–101].

IV.5.2. Repartition of energy in the products

This section presents the energy repartition in the products- char, condensates and permanent gases- from the oxidative pyrolysis of the three biomasses.

The energy yields are expressed as follows:

$$E_Y^{Char} = \frac{LHV^{Char}}{LHV^{Biomass}} Y^{Char} \quad (19)$$

$$E_Y^{Condensates} = \frac{LHV^{Condensates}}{LHV^{Biomass}} Y^{Condensates} \quad (20)$$

$$E_Y^{Permanent\ gases} = \frac{LHV^{Permanent\ gases}}{LHV^{Biomass}} Y^{Permanent\ gases} \quad (21)$$

where:

- Y^{Char}, $Y^{Condensates}$ and $Y^{Permanent\ gases}$ are yields of char, condensates and permanent gases;
- LHV^{Char}, $LHV^{Condensates}$, $LHV^{Permanent\ gases}$ and $LHV^{Biomass}$ are the lower heating values of char, condensates and permanent gases and biomass, respectively;

Figure 60 shows the energy repartition in the products from the oxidative pyrolysis of pine pellets.

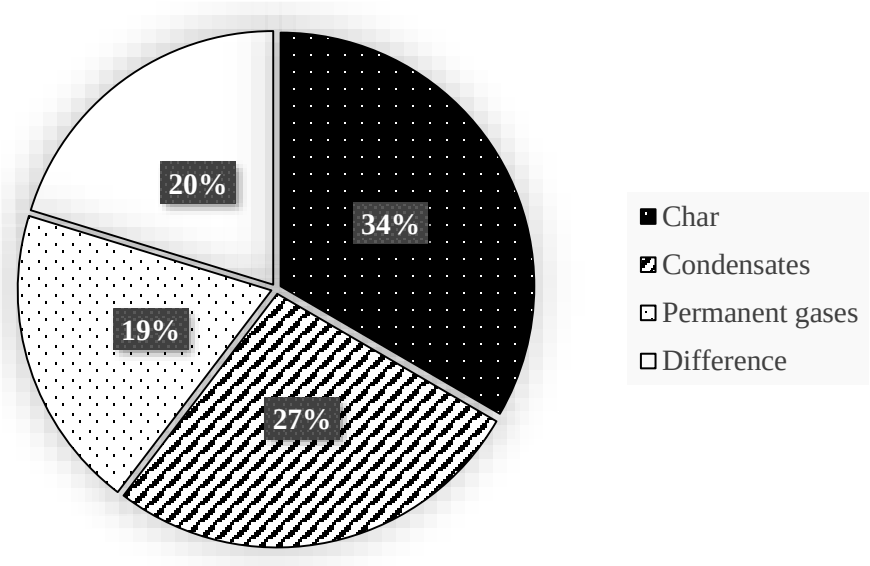

Figure 60. Energy repartition in the products from the oxidative pyrolysis of pinewood pellets, 0.022 kg.m^{-2}.s^{-1} air flux (daf)

As illustrated in Figure 60, energy repartition in the case of pinewood oxidative pyrolysis was 34 % for char, 27 % for condensates and 19 % for permanent gases. The remaining energy to reach 100 % is the sum of sensible heat, latent heat and losses. In the case of pinewood pellets, the difference was found to 20 %, i.e. 4.4 MJ.kg^{-1} of pine pellets (daf). In the same reactor, Milhé et al. [29] operated with wood chips and obtained a lower value of this difference of 7.4%, i.e. 1.5 MJ.kg^{-1} of dry wood chips.

Energy repartition in the products from the oxidative pyrolysis of the biomasses is presented in Figure 61.

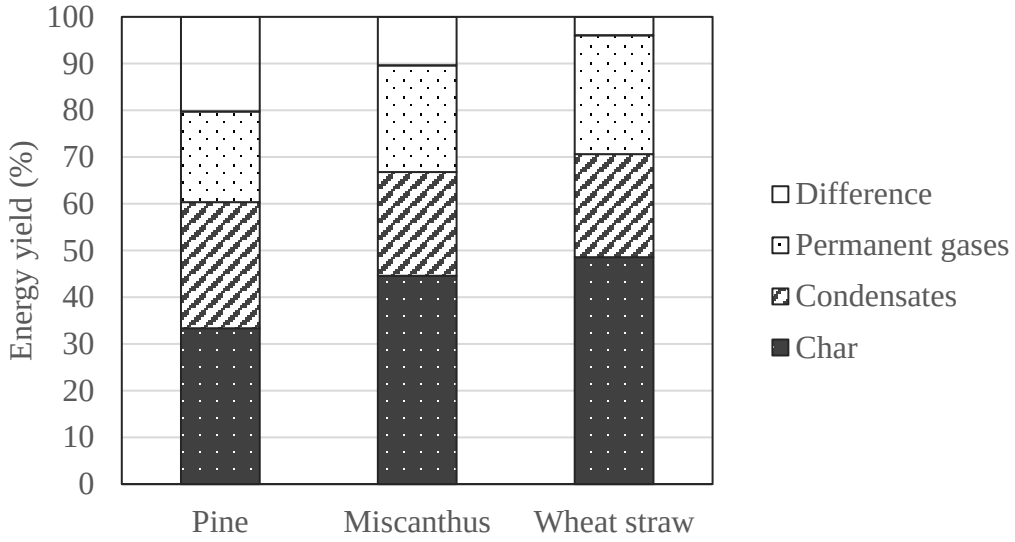

Figure 61. Energy yields of the oxidative pyrolysis products from different biomasses, continuous mode and 0.022 kg.m^{-2}.s^{-1} air flux

Char was the most important product as its energy yield accounted for about 33, 45 and 49 % for respectively pine, miscanthus and wheat straw. Permanent gases was the second important product with their energy yields in the range of 19-25 %. Energy yield of condensates was about 22-27 %.

The difference to reach 100% was found to 20, 10 and 4 % in the cases of pine, miscanthus and wheat straws, respectively. However, one should note that this estimation of the enthalpy of reaction depends on the accuracy of mass balance and heating value measurement. For biomass, char and permanent gases, measurement of heating value is accurate. However, it was not the case for the condensates because its heating value was calculated theoretically from the composition based on elemental balance. The imprecision of 5 % was found in the elemental balance and of 10% in the determination of water fraction. Thus, calculation of the reaction enthalpy based on the repartition of energy in the products is questionable. To support discussion and valorization of the experimental results, we decided to set up a detailed enthalpy balance. This point is detailed in the next section.

IV.6. Detailed enthalpy balance establishment

The initial objectives of the establishment of a detailed enthalpy balance were to:

- Validate experiments;

- Support discussion by comparing energy fluxes calculated;
- Quantify sensitivity of some thermodynamic and experimental data on global balance;
- Potentially determine some imprecise experimental data.

IV.6.1. Methodology

Enthalpy exists in three forms: standard of formation, sensible and latent. The considered domain for the enthalpy balance is presented in Figure 62.

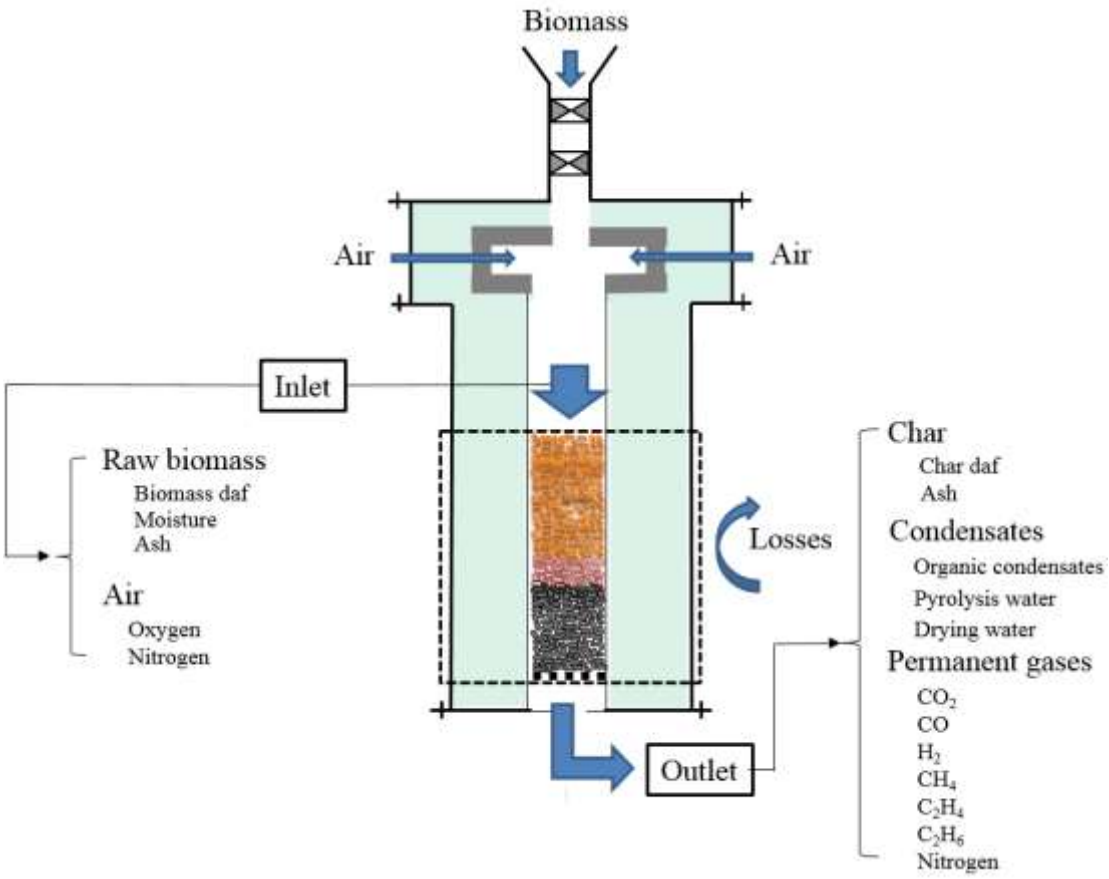

Figure 62. Simplified sketch for enthalpy balance establishment

Enthalpy balance is expressed by the following equation:

$$\dot{h}_{bio}^{Ti} + \dot{h}_{water(d)}^{Ti} + \dot{h}_{air}^{Ti} + \dot{h}_{Ash}^{Ti} = \dot{h}_{char}^{To} + \dot{h}_{gas}^{To} + \dot{h}_{cond}^{To} + \dot{h}_{water(d)}^{To} + \dot{h}_{water(p)}^{To} + \dot{h}_{Ash}^{To} + Losses \quad (22)$$

The mass flux of water have been splitted into drying water (d) and pyrolysis water (p).

$\dot{h}_j^T$ [J.s^{-1}] is the enthalpy flux of j at temperature T, expressed as:

$$\dot{h}_j^T = \dot{m}_j . h_j^T \quad (23)$$

where:

- T_i and T_o [K] are the inlet and outlet temperatures determined from the experiments;
- $\dot{m}_j$ [kg.s^{-1}], mass flux of j, determined from the measurements;
- h_j^T [J.kg^{-1}], enthalpy of j at T (K).

Note that h_j^T and $\dot{m}_j$ can be expressed respectively in [J.mol^{-1}] and [mol.s^{-1}].

The enthalpy of a compound j is expressed:

$$h_j^T = h_j^0 + \int_{298}^{T} C_p^j . dT + \Delta H_j \quad (24)$$

where:

- ΔH_j [J.kg^{-1}] is the latent heat of vaporization of j
- h_j^0 [J.kg^{-1}] is the standard formation enthalpy of compound j.
- C_p^j [J.kmol^{-1}.K^{-1}] is the heat capacity of compound j as a function of temperature.

The following section details the determination of the standard enthalpy of formation and the heat capacity.

IV.6.1.1. Determination of standard enthalpy of formation

- Water and permanent gases and ash

The standard enthalpy of water, permanent gases and ash (supposing SiO_2) were directly taken in the Perry's Chemical Engineering Handbook [23] (Appendix B).

- Biomass, char (daf) and condensates

Based on the combustion reaction, the standard enthalpy of biomass, char and condensates were calculated from their heating values and composition. Biomass, char and condensates were expressed by the simplified formula of a hydrocarbon $C_xH_yO_z$. The stoichiometric combustion of biomass and char is written:

$$C_xH_yO_z + n\ O_2 = x\ CO_2 + \frac{y}{2}.H_2O \quad (25)$$

Thus, the standard enthalpy of the hydrocarbon $C_xH_yO_z$ was calculated as follows:

$$h^0_{\mathrm{CxHyOz}} = x.h^0_{CO_2} + \frac{y}{2}.h^0_{H_2O(l)} + HHV_{\mathrm{CxHyOz}}.M_{\mathrm{CxHyOz}} \quad (26)$$

where:

- HHV_{CxHyOz} [J.g^{-1}] is the higher heating value of $C_xH_yO_z$ on daf.
- M_{CxHyOz} [g.mol^{-1}] is the molar mass of $C_xH_yO_z$.

We assumed that the char and condensates have a chemical formula based on C_6 as a derived material of biomass $(C_6H_{10}O_5)_n$. Their chemical formulas were determined from the composition (CHO) of the biomasses and the products (Table 27). The HHV of biomass, char and condensates are also given in the table.

Chemical formula HHV, J.g^{-1}	Biomass	Char	Condensates
Pine	$C_6H_{9.67}O_{3.72}$	$C_6H_{1.19}O_{0.14}$	$C_6H_{12.72}O_{3.75}$
	23.28	34.43	23.49
Miscanthus	$C_6H_{8.92}O_{3.36}$	$C_6H_{1.30}O_{0.25}$	$C_6H_{23.76}O_{5.66}$
	22.07	33.51	23.58
Wheat straw	$C_6H_{9.15}O_{3.21}$	$C_6H_{1.43}O_{0.21}$	$C_6H_{29.83}O_{6.90}$
	22.30	33.71	23.10

Table 27. Chemical formula and heating values of biomass, char and condensates from oxidative pyrolysis in continuous mode, air mass flux of 0.022 kg.m^{-2}.s^{-1}

Therefore, the standard enthalpies of biomass, char and condensates from oxidative pyrolysis in continuous mode are given in Table 28.

Standard enthalpy of formation (at 25°C, 1atm), kJ.mol^{-1}	Biomass	Char	Condensates
Pine	-448.80	71.05	-772.76
Miscanthus	-656.36	46.69	-1349.01
Wheat straw	-507.68	24.16	-1705.43

Table 28. Standard enthalpy of formation of biomass, char and condensates from oxidative pyrolysis in continuous mode, air mass flux of 0.022 kg.m^{-2}.s^{-1}

IV.6.1.2. Determination of heat capacity

The heat capacities of water and permanent gases as function of temperature were taken from the Perry's Chemical Engineering Handbook [23] for temperature in range of 273-1200K. Heat capacities of biomass and char were found from literature [22,102]. Heat capacity of Ash was chosen as the heat capacity of SiO_2. The heat capacities as function of temperature of these components are given in Appendix C.

The heat capacity of condensates as a complex mixture is difficult to determine. We considered condensates as a mixture of Acetic acid, Methanol, and Benzene (33.33 % for each) as follows:

$$Cp = \overline{C_1} + \overline{C_2} * T + \overline{C_3} * T^2 \quad (J.kmol^{-1}.K^{-1}) \tag{27}$$

The coefficients $\overline{C_1}$, $\overline{C_2}$ and $\overline{C_3}$ are the average values determined from Perry's Chemical Engineering Handbook [23] (Table 29).

$J.kmol^{-1}.K^{-1}$	Acetic acid	Methanol	Benzene
C_1	139640	105800	129440
C_2	-320.8	-362.23	-169.5
C_3	0.8985	0.9379	0.64781

Table 29. Components for determination of the heat capacity of condensates

IV.6.1.3. Determination of the heat losses

Heat losses were estimated from the measurement of the external wall temperature during the experiments:

$$Heat\ losses = h.S.\Delta T \tag{28}$$

The convective heat transfer coefficient (h) was considered to 15 $W.m^{-2}.K^{-1}$ as usual in natural convection. The external dimensions of the considered domain for the estimation of the heat losses was 0.65 m height and 0.6 m external diameter. In order to measure the temperature at the reactor wall, we installed three thermocouples t1, t2, and t3 at the same elevation as the thermocouples T5, T6, T7, respectively (Figure 63). Typical wall temperature profiles in the beds of the three biomass are shown in Figure 63. We observe the wall temperature increased during about 250 to 300 min before stabilizing between 30 and 60°C.

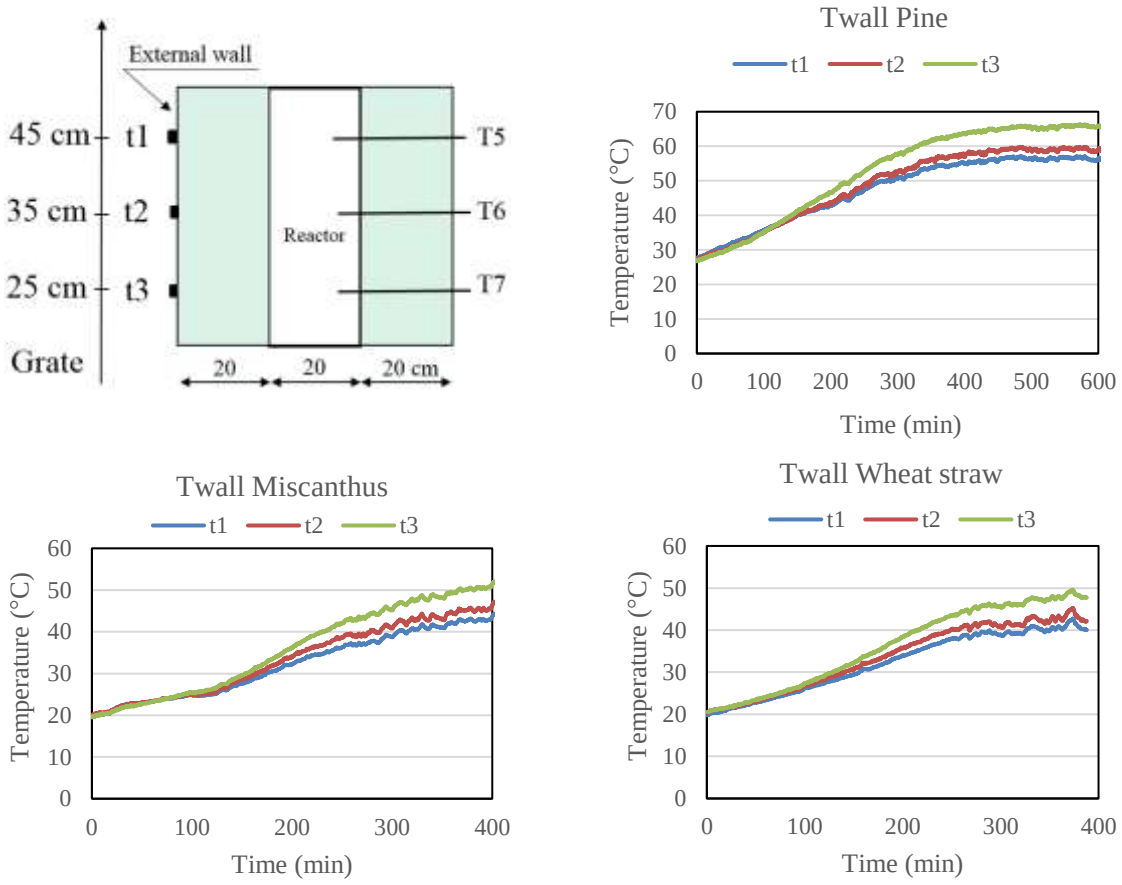

Figure 63. Wall thermocouple positions and typical profiles of wall temperature in the beds of the three biomasses

Based on this figure, we plotted the average wall temperature during experiments for the different biomasses (Figure 64). The average wall temperature during the stationary period was measured to 53, 35 and 39°C for pine, miscanthus and wheat straw. One should note that, external (ambient) temperatures were 27, 20 and 20°C for pine, miscanthus and wheat straw as experiments were not performed the same day. Thus, the heat loss fluxes were calculated to 0.60, 0.22 and 0.34 kW, equivalent to 3.5%, 1.5% and 2.5% of the inlet power of pine, miscanthus and wheat straw, respectively. The difference in the heat losses is difficult to explain, as the bed temperatures are similar for the three biomasses. The non-achievement of the stationary regime in the external wall temperature could be the main reason. However, the contribution of the heat losses is quite small in the enthalpy balance.

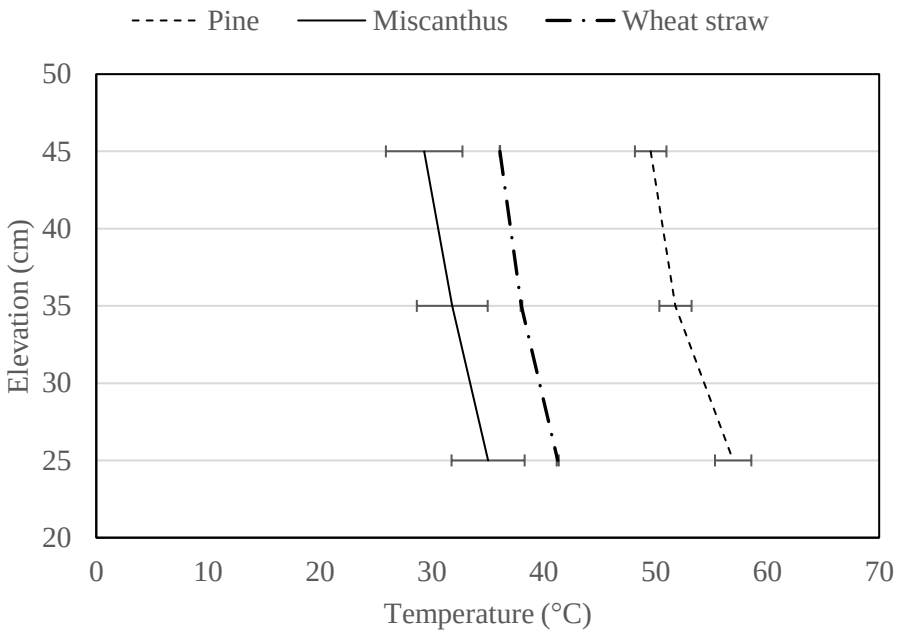

Figure 64. Profile of the average temperature measured at the external surface of the reactor wall during stabilizing period of experiments

IV.6.2. Results

We considered an inlet temperature of T_i = 25°C, and an outlet temperature of T_o = 700°C.

The enthalpy balance is rewritten:

$$\dot{m}_{biomass}.h^0_{bio} + \dot{m}_{water(d)}h^0_{water(d)} = + \dot{m}_{char}\left(h^0_{char} + \int_{298}^{993} C_p^{char}.dT\right) + \sum_i \dot{m}_{gas_i}\left(h^0_{gas_i} + \int_{298}^{993} C_p^{gas_i}.dT\right) + \dot{m}_{cond}\left(h^0_{cond} + \int_{298}^{993} C_p^{cond}.dT\right) + \dot{m}_{water(d)}\left(\int_{298}^{993} C_p^{water}.dT + \Delta H_{latent}\right) + \dot{m}_{water(p)}\left(h^0_{water} + \int_{298}^{993} C_p^{cond}.dT\right) + \dot{m}_{ash}\int_{298}^{993} C_p^{ash}.dT + Heat\ losses \quad (29)$$

We observe that the closures of the enthalpy balances were 18.19, -8.01 and 9.97 % for respectively pine, miscanthus and wheat straw (Table 30). Detail of the enthalpy balance for each biomass is given in Appendices D, E and F. In the following, we focus on the contribution of the standard enthalpy and sensible heat on the balance closure.

- Standard enthalpy of formation

The standard enthalpy fluxes are also detailed in Table 30.

			Standard enthalpy of formation fluxes (at 25°C, 1 atm) (kW)			Total enthalpy fluxes (kW)		
			Pine	**Miscanthus**	**Wheat straw**	**Pine**	**Miscanthus**	**Wheat straw**
Inlet	Biomass, daf		-3.07	-4.68	-3.61	-3.07	-4.68	-3.61
	Water (moisture)		-0.94	-1.21	-1.44	-0.94	-1.21	-1.44
	Oxygen (from air)		0.00	0.00	0.00	0.00	0.00	0.00
	Nitrogen (from air)		0.00	0.00	0.00	0.00	0.00	0.00
	Ash (from biomass)		0.00	0.00	0.00	0.00	0.00	0.00
	Total					-4.01	-5.89	-5.05
Outlet	Char, daf		0.19	0.16	0.09	0.23	0.22	0.16
	Condensates		-1.41	-1.53	-1.73	0.10	-0.59	-0.89
	Pyrolysis water		-3.04	-1.68	-1.54	-2.74	-1.52	-1.39
	Drying water		-0.94	-1.21	-1.44	-0.71	-0.92	-1.09
	Permanent gases	CO_2	-2.35	-3.08	-2.99	-2.15	-2.82	-2.74
		CO	-0.60	-0.54	-0.46	-0.48	-0.43	-0.38
		H_2	0.00	0.00	0.00	0.10	0.11	0.10
		CH_4	-0.11	-0.13	-0.12	-0.06	-0.07	-0.06
		C_2H_4	0.02	0.02	0.01	0.02	0.02	0.01
		C_2H_6	-0.01	-0.01	-0.01	-0.01	-0.01	-0.01
	Nitrogen	N_2	0.00	0.00	0.00	0.36	0.36	0.36
	Ash (from char)		0.00	0.00	0.00	0.00	0.01	0.04
	Heat losses					0.60	0.22	0.34
		Total				-4.74	-5.42	-5.56
Closure (%)						18.19	-8.01	9.97

Table 30. Detailed standard enthalpy of formation and total enthalpy fluxes for the three biomasses oxidative pyrolysis

Regarding this table, it is noticeable that the standard enthalpies of biomass and condensates play a major role in the global enthalpy balance. Moreover, these standard enthalpies are very sensitive to some experimental data, in particular:

- HHVs and compositions of biomass, char and condensates;

- Water fraction.

Therefore, in the next section (IV.6.3), we will investigate the sensitivity of these experimental data to the enthalpy balance closure.

- Sensible heat

The sensible heats are detailed in Table 31.

			Sensible heat fluxes (kW)			**Total enthalpy fluxes (kW)**		
			Pine	**Miscanthus**	**Wheat straw**	**Pine**	**Miscanthus**	**Wheat straw**
Inlet	Biomass, daf		0.00	0.00	0.00	-3.07	-4.68	-3.61
	Water (moisture)		0.00	0.00	0.00	-0.94	-1.21	-1.44
	Oxygen (from air)		0.00	0.00	0.00	0.00	0.00	0.00
	Nitrogen (from air)		0.00	0.00	0.00	0.00	0.00	0.00
	Ash (from biomass)		0.00	0.00	0.00	0.00	0.00	0.00
	Total					-4.01	-5.89	-5.05
Outlet	Char, daf		0.04	0.06	0.07	0.23	0.22	0.16
	Condensates		1.50	0.93	0.84	0.10	-0.59	-0.89
	Pyrolysis water		0.30	0.17	0.15	-2.74	-1.52	-1.39
	Drying water		0.09	0.12	0.14	-0.71	-0.92	-1.09
	Permanent gases	CO_2	0.19	0.25	0.24	-2.15	-2.82	-2.74
		CO	0.11	0.10	0.09	-0.48	-0.43	-0.38
		H_2	0.10	0.11	0.10	0.10	0.11	0.10
		CH_4	0.05	0.06	0.06	-0.06	-0.07	-0.06
		C_2H_4	0.00	0.00	0.00	0.02	0.02	0.01
		C_2H_6	0.00	0.00	0.00	-0.01	-0.01	-0.01
	Nitrogen	N_2	0.36	0.36	0.36	0.36	0.36	0.36
	Ash (from char)		0.00	0.01	0.04	0.00	0.01	0.04
	Heat losses					0.60	0.22	0.34
			Total			-4.74	-5.42	-5.56
Closure (%)						18.19	-8.01	9.97

Table 31. Detailed sensible heat and total enthalpy fluxes for the three biomasses oxidative pyrolysis

The sensible heat of condensates plays a major role in the global balance. Moreover, this type of energy flux is sensitive to heat capacity of condensates whose value was difficult to define based on our experiments and literature. Therefore, this sensitivity of this constant will be also investigated in the next section.

IV.6.3. Sensitivity analysis of the enthalpy balance

In this sensitivity analysis, we focused on the following parameters:

- HHV of biomass;
- HHV of condensates;
- Composition of biomass (index H/C ratio);
- Composition of condensates (index H/C ratio);
- Water fraction in condensates;
- Heat capacity of condensates.

We compared the closure of the enthalpy balance with the reference value (REF) for the investigated parameters (listed above) with the closure when varying these parameters in a range of 5 or 10 % (Table 32). The deviations of the parameters proposed are relevant regarding our experiments. Results will be presented with the Miscanthus.

HHV ($MJ.kg^{-1}$)	H/C ratio	Water in condensates	$\int CpdT$
5	5	10	10

Table 32. Deviation of the parameters (%) of the parameters for the sensitivity analysis

IV.6.3.1. HHV of biomass

First, we investigated impact of the heating value of biomass. Table 33 shows that a 5 % error in the HHV measurement represent a +23 % difference in the standard enthalpy. This result was found similar to the finding in the work of Peduzzi et al. [103]. Then, an error of +23 % in the standard enthalpy results in a very big error (+252 %) in the enthalpy balance closure. Thus, heating value of the biomass greatly affects the enthalpy balance.

HHV ($MJ.kg^{-1}$)	REF	REF +5 %	Variation (%)
	22.07	23.17	
H° ($kJ.mol^{-1}$)	-656.36	-507.57	+23
Enthalpy balance closure (%)	-8.01	12.18	+252

Table 33. Sensitivity of the HHV of biomass on standard enthalpy of formation and on enthalpy balance closure

IV.6.3.2. HHV of condensates

Regarding the impact of the heating value of condensates, one should note that this value was calculated from the composition (CHO) of the condensates following Channiwala and Parikh [16]. Table 34 shows that a mistake of 5 % in the calculation of the heating value implies an error in the standard enthalpy of +16 %, and then a difference in the enthalpy balance closure of -53 %.

HHV ($MJ.kg^{-1}$)	REF	REF +5 %	Variation (%)
	23.58	24.76	
H° ($kJ.mol^{-1}$)	-1349.01	-1129.08	+ 16
Enthalpy balance closure (%)	-8.01	-12.24	- 53

Table 34. Sensitivity of the HHV of condensates on its standard enthalpy of formation and on enthalpy balance closure

IV.6.3.3. Composition of biomass

Results concerning the influence of the composition of biomass and condensates on the standard enthalpy and the enthalpy balance are given in Table 35. Here we presented the composition of biomass in terms of the index H/C ratio (Table 27). An error of 5 % in the index H/C ratio of biomass results in a difference of -10 % on the standard enthalpy and in of -82 % on the enthalpy balance closure.

Index H/C ratio	REF	REF +5 %	Variation (%)
	1.49	1.56	
H° ($kJ.mol^{-1}$)	-656.36	-719.92	-10
Enthalpy balance closure (%)	-8.01	-14.58	-82

Table 35. Sensitivity of the index H/C ratio of biomass on its standard enthalpy of formation and on enthalpy balance closure

IV.6.3.4. Composition of condensates

Similar to the composition of biomass, we presented the composition of condensates in terms of index H/C ratio. One should note here is that the composition C and H of the condensates were calculated based on the elemental balance.

Index H/C ratio	REF	REF +5 %	Variation (%)
	3.96	4.16	
H° ($kJ.mol^{-1}$)	-1349.01	-1518.34	-13
Enthalpy balance closure (%)	-8.01	-4.76	+41

Table 36. Sensitivity of the index H/C ratio of condensates on its standard enthalpy of formation and on enthalpy balance closure.

As Table 36 shows, an error of 5 % in the index H/C ratio in composition of condensates results in a difference of -13 % on the standard enthalpy and in of +41 % on the enthalpy balance closure; the error is compensated by another factor.

IV.6.3.5. Water fraction in the condensates

Water fraction in the condensates not only affects the yield but also the composition of the condensates. Regarding the results in Table 37, an error of 10 % in the water fraction determination results in the difference in the enthalpy balance closure of +45 %.

Water in condensates	REF	REF +10 %	Variation (%)
	46.37	51.01	
Enthalpy balance closure (%)	-8.01	-4.45	+45

Table 37. Sensitivity of the water fraction in the condensates on the enthalpy balance closure

IV.6.3.6. Heat capacity of the condensates

As mentioned before, condensates is a complex mixture thus it was difficult to determine its heat capacity. We considered it as a mixture of Acetic acid, Methanol and Benzene. Then, heat capacity of the condensates was determined as the average value of all the components in the mixture. Table 38 shows the sensitivity of the heat capacity of the condensates on the closure of enthalpy balance. It is shown that the heat capacity has a lower impact: an error of 10 % in the determination of the heat capacity results in a difference of only -20 % in the enthalpy balance closure.

$\int CpdT$	REF	REF +10 %	Variation (%)
	4.42	4.87	
Enthalpy balance closure (%)	-8.01	-9.60	-20

Table 38. Sensitivity of the heat capacity on the enthalpy balance closure

To sum up, heating value, composition, water fraction and heat capacity of the condensates greatly affect the enthalpy balance. A small error in heating value and composition of biomass results in a significant change in the enthalpy balance. Water fraction was also an influencing parameter. Moreover, a high precision in the determination of these parameters remains today difficult to obtain. Thus, regarding its high sensitivity to some parameters, the enthalpy balance

is not relevant to compare our experiments and to investigate the role of biomass nature on the oxidative pyrolysis in a fixed bed.

IV.7. Conclusions

The aim of the study in continuous mode was to investigate the behavior of oxidative pyrolysis of woody biomass, herbaceous and agricultural residues biomass pellets in a downdraft continuous fixed bed to reproduce the pyrolysis process as existing in some industrial staged gasifiers.

This work has been performed in the fixed bed reactor of 20 cm I.D with an air flux of 0.022 $kg.m^{-2}.s^{-1}$. The procedure of this operation mode consisted in maintaining a stable oxidation zone (OZ) at the middle of the biomass bed. This zone tended to propagate upward opposed to the biomass and air flows - but could be kept still by removing char at the bottom. Such operating conditions were achieved using temperature measurement as an indicator of the elevation of the oxidation zone. We fed biomass into the reactor and measured its consumption rate to about 4.0 $kg.h^{-1}$ as well as collected and measured the char flow rate at the bottom of the reactor. Condensates and permanent gases were collected and analyzed via a Micro GC system adapted from the Tar protocol. After experiments, char was analyzed.

Air/biomass ratio was measured to 0.69, 0.67 and 0.65 for pine, miscanthus and wheat straw. The propagation of the oxidation zone consumed about 12 % of the stoichiometric combustion air to provide energy for the autothermal pyrolysis process. However, the propagation velocity was found lower in bed of pine than in beds of other biomasses. The bed temperature seemed to have an inverse trend. In stable continuous fixed bed conditions, oxidative pyrolysis of miscanthus and wheat straw pellets produced more char than those of wood pellets: char yields on daf were 28 % for miscanthus and 30 % for wheat straw, compared to 21 % for wood pellets. This is a result of the difference in ash content and process temperature.

Enthalpy balance has been also established to detail the distribution of the enthalpy components including sensible heat, latent heat, and standard enthalpy of formation. A sensitivity analysis has been performed to quantify the accuracy of the enthalpy balance. Our conclusion is that enthalpy balance is too imprecise to support the comparison between the biomasses. Indeed, accuracy of some experimental data and thermodynamic values (enthalpy of formation) did not allow establishing a relevant enthalpy balance.

This conclusion has to be considered carefully when setting up a process model. Moreover, improvement of accuracy of some influencing parameters (experimental or theoretical) is a necessary step in the future in order to set up relevant enthalpy models.

- Page intentionally left blank -

CHAPTER V

OXIDATIVE PYROLYSIS OF BIOMASS BATCH OPERATING CONDITIONS

Compared to continuous mode, the batch operation mode allowed a fine characterisation of the Oxidation Zone (OZ), in particular the measurement of propagation velocity, thickness and compaction.

The propagation of an OZ in a fixed bed is often referred as "smoldering". In this chapter, we investigated the forced counter-current smoldering configuration in a pyrolysis downdraft fixed bed reactor in "batch" operating conditions. Injecting a low air flux of 0.022 $kg.m^{-2}.s^{-1}$ at the top of reactor, we ignited an oxidation zone at the bottom of the reactor and followed it propagation in a fixed bed of biomass of 80 cm (Figure 65).

Influence of the biomass properties on the main OZ features was investigated through three biomass pellets: pine, miscanthus and wheat straws.

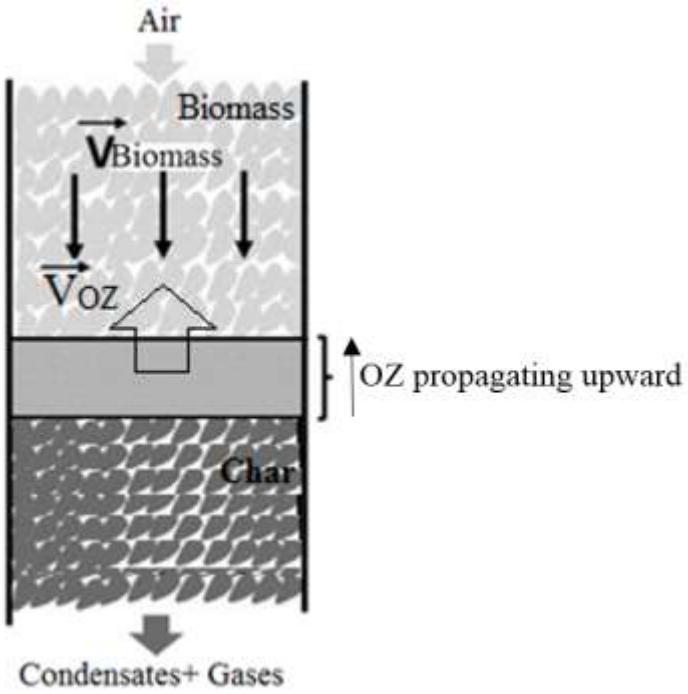

Figure 65. Propagation of the oxidation zone in a fixed bed

This chapter presents, first, the experimental procedure in batch operating conditions. Then, methods set up for the characterization of oxidation zone in a fixed bed are detailed. Finally, the main results obtained in the batch mode are presented and discussed.

V.1. Experimental procedure

The procedure in batch mode includes:

- ignition of the oxidation zone at the bottom of the reactor;
- monitoring of the OZ and sampling of permanent gases and condensates;
- stop of the experiment and data collection.

The ignition step was carried out in the same way as in the continuous mode (Chapter IV).

After the ignition step, the OZ propagated upward. It was monitored by the increase in temperature observed every 10 cm by the thermocouples. We measured the propagation from 15 cm to 65 cm above the grate. Note that the sampling line was operated when the OZ propagation was supposed stabilized: i.e. when it reached 25 cm.

When the OZ exceeded 65 cm, the experiment was ended by switching air to Nitrogen to stop the oxidation reactions and to evacuate the remaining volatiles matters.

Data such as temperature, flow rate, bed height, and pressure were recorded during the experiments for subsequent processing and analysis.

V.2. Methods for the characterization of the oxidation zone

V.2.1. Bed compaction

During the propagation of the OZ, the bed height was measured continuously by a laser beam. An example of the height recorded is shown in Figure 66.

The decrease observed was due to the compaction of the bed during OZ propagation. When the OZ propagated from the bottom of the reactor to about 100 min, no significant bed compaction was observed. Between 100 and 280 min, when the OZ propagated from T7 to T5, the bed compacted linearly versus time (height slope was constant). Note that at around the end of the experiment, the measured bed height fluctuated. This phenomenon is caused by disturbance in the measurement from the laser systemt, due to radiation of hot OZ when it reaches the bed surface.

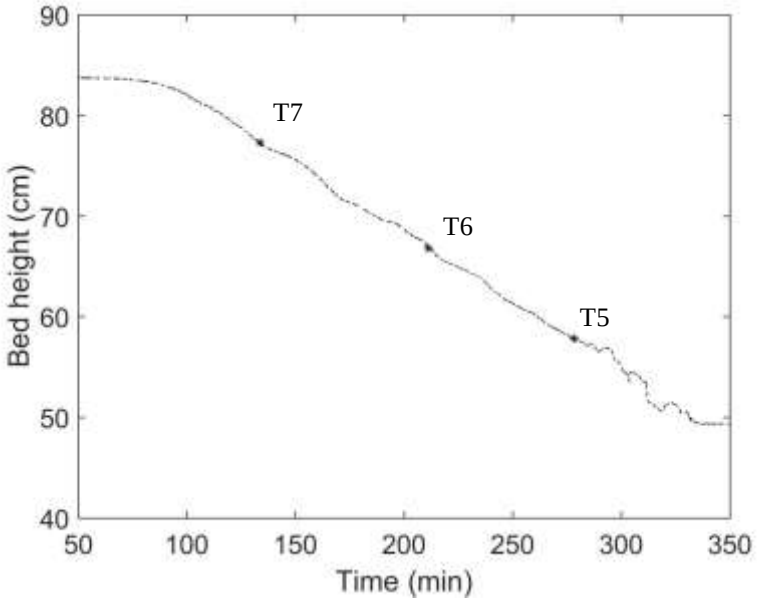

Figure 66. Bed height measurement in a batch experiment with pine pellets, 0.022 kg·m^{-2}s^{-1} air flux

We calculated the *bed compaction rate, C(t),* versus time as follows:

$$C(t) = \frac{h(t_0) - h(t)}{h(t_0)} \tag{30}$$

where $h(t_0)$ is the bed height when the OZ is in a low position (T7, 25 cm from the grate).

For example, as shown in Figure 66, the bed height when the OZ is at T7, T6 and T5 was measured to 77.3, 66.8 and 57.8 cm, respectively. Thus, the bed compaction rate of the pine bed when the OZ was at T7, T6 and T5 was 0 %, 14 % and 25 % respectively.

V.2.2. Propagation velocity

In the counter-current smoldering configuration, the OZ propagates upwards, and the compaction tends the OZ to go downward. Consequently, as illustrated in Figure 67, we defined two velocities:

- *The apparent propagation velocity, Voz/reactor*, as the OZ upward velocity related to an external fixed point (reactor).

- *The effective propagation velocity, Voz/biomass*, as the velocity of the OZ related to the virgin biomass. This velocity refers to a term commonly referred in the literature as "front propagation velocity", "ignition velocity" or "flame speed".

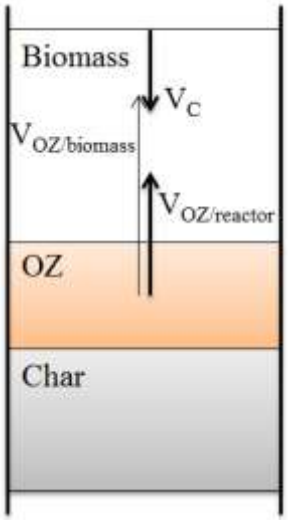

Figure 67. Schematic representation of OZ propagation velocities and compaction velocity

- ***Effective propagation velocity ($V_{OZ/biomass}$)***

Considering the compaction of the bed, the effective velocity was calculated from the measured apparent velocity according to Equation (31):

$$V_{OZ/biomass} = V_{OZ/reactor} + V_C \quad (31)$$

where *the compaction velocity* V_C is defined as the downward velocity of the virgin biomass bed caused by compaction in the OZ.

- ***Compaction velocity (V_C)***

Assuming no compaction in the virgin biomass bed, the compaction velocity was calculated as the derivative of the total bed height versus time (Figure 68).

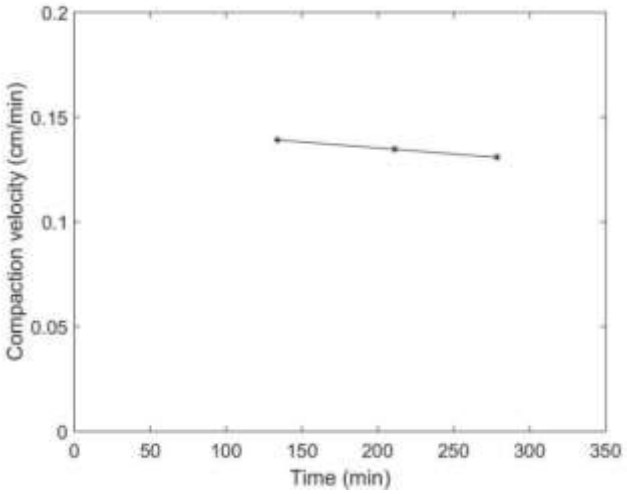

Figure 68. Compaction velocity determination

- ***Apparent propagation velocity ($V_{OZ/reactor}$)***

In the literature, a method to determine the apparent propagation velocity of the oxidation zone was first proposed by Ohlemiller and Lucca [69]. They measured the propagation velocity (in beds of wood fibers and poluisocyanurate) by measuring the propagation time between two consecutive thermocouples. The detection of the OZ at the thermocouples location was based on an abitrary temperature threshold of 250°C. Later on, this method was commonly used by other authors [71,72,76]. However, the choice of the threshold (reference) temperature differs between the authors. Mahapatra and Dasappa [76] performed smoldering in a fixed bed gasifier of wood chips and they chose 773k (500°C) as the reference temperature. Porteiro et al. [71] chose a reference of 700°C to measure the propagation velocity in a fixed bed combustor of different biomass types.

In this study, as we performed smoldering under a very slow air mass flux of 0.022 $kg.m^{-2}.s^{-1}$, we tested and compared several criteria based on temperature measurements to locate the OZ. We concluded that the maximum derivative of the temperature $(dT/dt)_{max}$ was the most relevant and repeatable criteria. Thus, the oxidation zone was said to be located at a given thermocouple T_i when *dTi/dt* was maximum.

Moreover, we defined the *passage time* t_{OZ}^{i} as the time coresponding to the passage of the OZ at the elevation of thermocouple T_i.

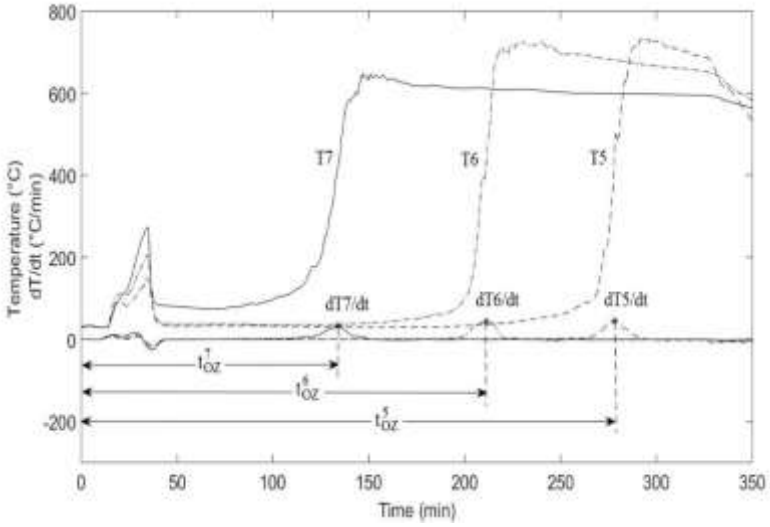

Figure 69. Determination of the passage time of the OZ

Knowing the distance between two thermocouples (10 cm), it was then possible to plot the elevation of the oxidation zone in the reactor versus time (Figure 70-a). The apparent propagation velocity was calculated as the derivative (Figure 70-b).

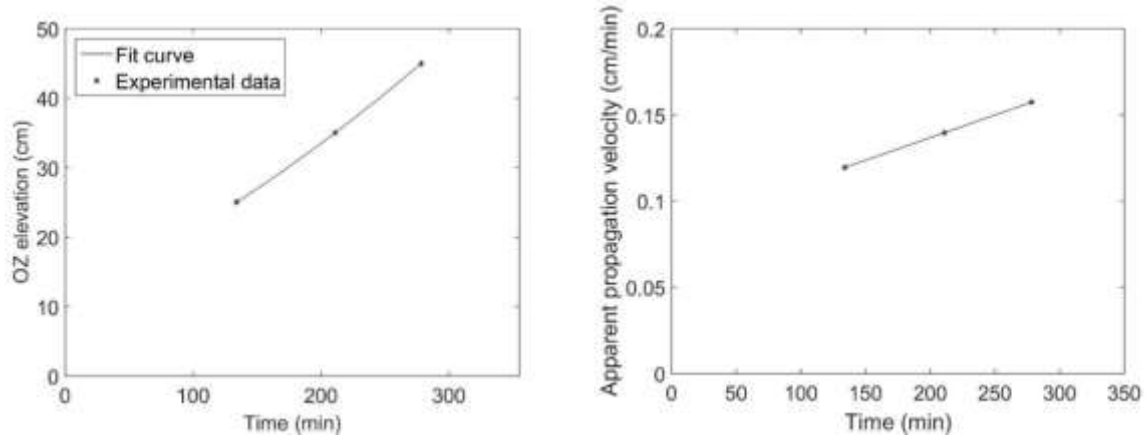

(a) (b)

Figure 70. Determination of the apparent propagation velocity: (a) OZ propagation; (b) OZ apparent propagation velocity

- ***Effective propagation rate or biomass consumption rate***

We also defined the effective propagation rate, $\dot{m}_{OZ}$ (kg.s^{-1}.m^{-2}), as the flux of biomass consumed by the oxidation zone during its propagation, according to Equation 32:

$$\dot{m}_{OZ} = V_{OZ/biomass} \cdot \rho_{biomass} \quad (32)$$

Where $\rho_{biomass}$ (kg.m^{-3}) is the bulk density of the biomass.

Figure 71 presents an example of the propagation velocities and effective propagation rate of the OZ when it propagates in a bed of pine pellets.

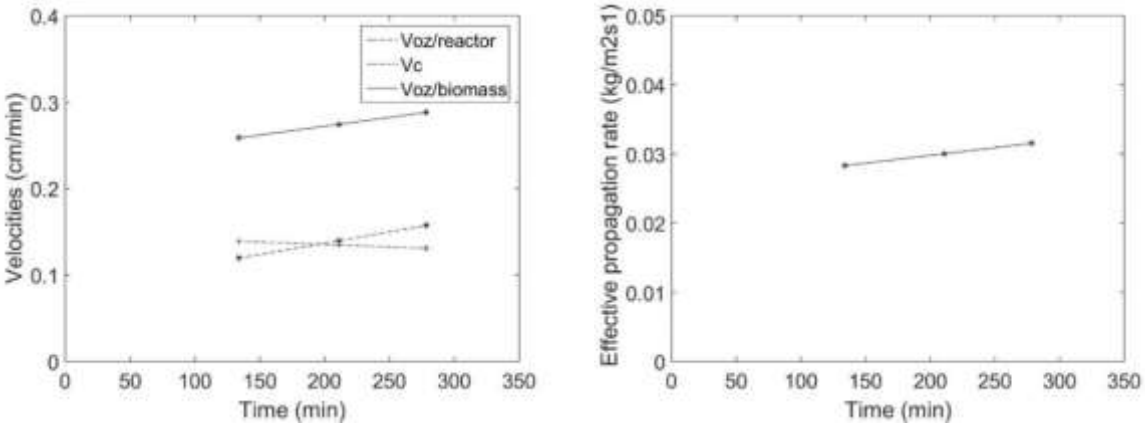

(a) (b)

Figure 71. Propagation velocities and effective propagation rate of the oxidation zone, bed of pine pellets, air mass flux of 0.022 kg.m^{-2}.s^{-1}: (a) Apparent, effective, and compaction velocities; (b) Effective propagation rate

In the objective of methods validation, the average effective propagation rate calculated from velocities measurement (Equation 32) has to be compared to the average biomass flux determined by weighing.

V.2.3. OZ Thickness

To measure the OZ thickness, we proposed to locate the top and the bottom surfaces of the OZ based on changes in temperature. The derivative of the temperature versus time "dT/dt" was proposed as the criterion. The OZ top surface t_{OZ}^{top} was detected at a given thermocouple (elevation) when dT/dt > 5°C.min^{-1} while the bottom surface t_{OZ}^{bottom} was detected when the temperature started to decrease, i.e. dT/dt < 0 (Figure 72). The criteria of 5°C.min^{-1} was chosen to avoid inherent temperature fluctuations at low temperature.

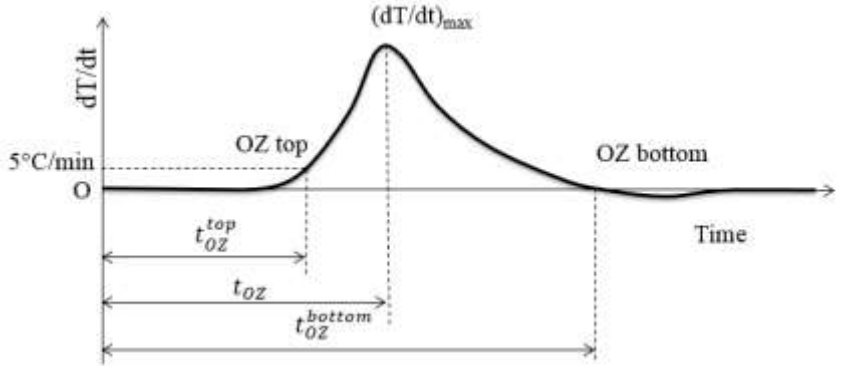

Figure 72. The passage time of the OZ top and bottom surfaces at a given thermocouple

Then, the OZ thickness δ_{OZ} was calculated as follows:

$$\delta_{OZ} = (t_{OZ}^{bottom} - t_{OZ}^{top}).V_{OZ/reactor} \quad (33)$$

V.2.4. Temperature profile

We paid a particular attention to the maximum temperature of the OZ as an important process parameter. Maximum bed temperature was detected and plotted along the bed height. Figure 73 presents the maximum temperature profile along a bed of pine pellets.

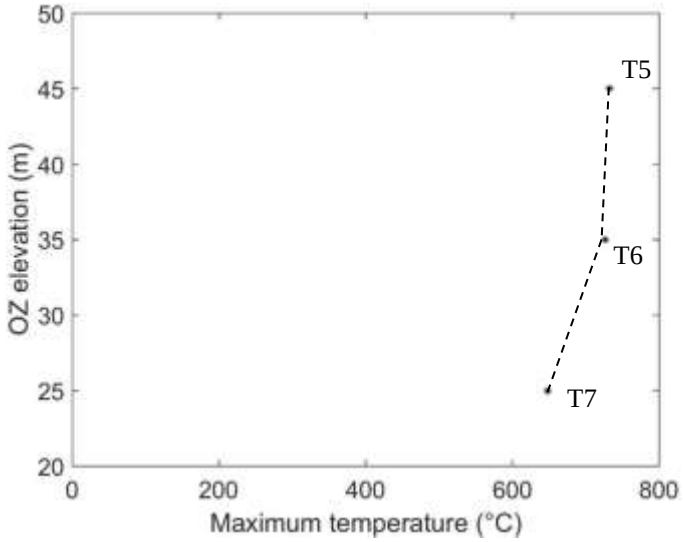

Figure 73. Maximum temperature profile along the bed of pine pellets, when OZ propagated from T7 to T5, 0.022 kg.m^{-2}.s^{-1} air flux

The maximum temperature was about 650-720 °C. Temperature was slightly lower at the bottom of the bed.

Based on the temperature profile versus time at a given thermocouple and knowing the propagation velocity of the oxidation zone, we calculated the temperature profile along the fixed bed, assuming a stationary regime. Figure 74 presents the calculated temperature profile when the oxidation zone was at T6 (35 cm from the grate). A cold zone of biomass bed with temperature of about 50°C exists above the OZ. Below the OZ, there is a hot zone with temperature in the range of 650-700°C.

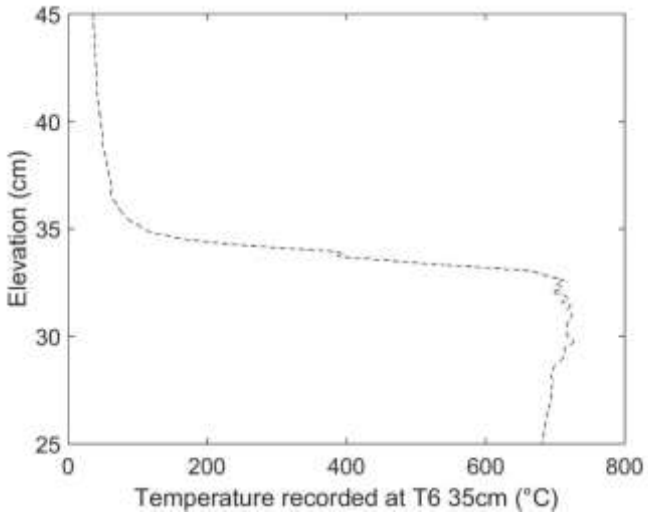

Figure 74. Temperature profile along the fixed bed of biomass when the OZ is at 35 cm from the grate

V.2.5. Data processing

Experimental data recorded from acquisition devices, i.e. temperature and bed height (laser beam), contained measuring noises. Consequently, the calculations of the velocities, which were based on the derivative of these values, were problematic. Therefore, we developed two numerical tools for the data treatment: a fitting method and a filtering (or smoothing) method. The two methods are detailed in Appendix G.

To illustrate the advantage of using the numerical tools in this study, Figure 75 shows the determination of the compaction velocity with and without data processing.

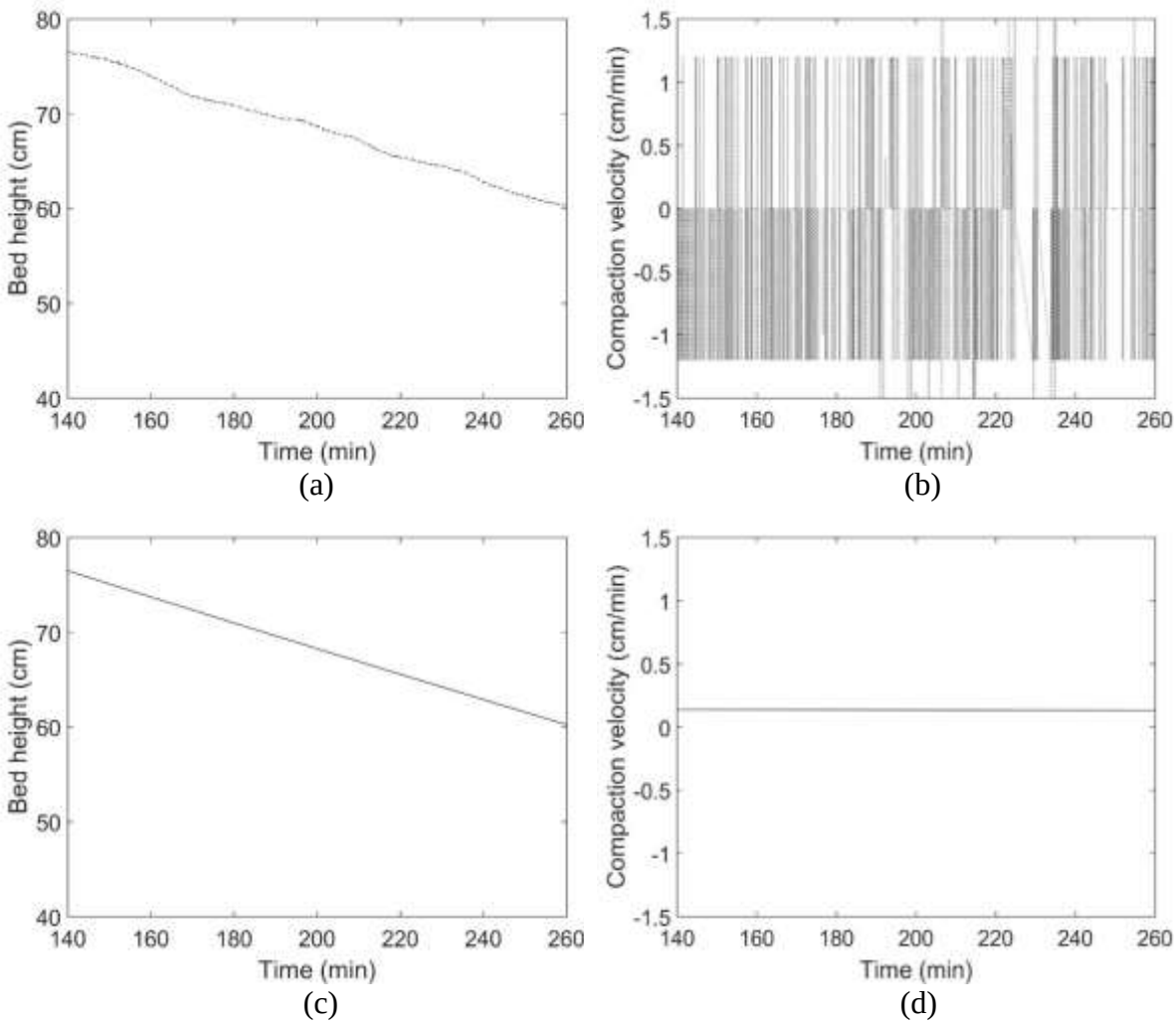

Figure 75. Data of bed height before and after treatment with Matlab®: (a) Raw data of bed height from laser beam system; (b) Derivative of bed height curve before smoothing; (c) Bed height after smoothing; (d) Derivative of bed height curve after smoothing

As shown Figure 75-a, despite slight fluctuation in the values of the bed height, the estimation of the derivative (compaction velocity) is not possible (Figure 75-b). In contrast, data after smoothing (Figure 75-c) provides a nice profile of the derivative values; the average

compaction velocity (for example, in case of pine pellets) is then determined to 0.14 $cm.min^{-1}$ (Figure 75-d).

V.3. Results and discussion

V.3.1. Air/biomass ratio and equivalent ratio

The air mass flux was the same for all three biomasses (0,022 $kg.m^{-2}.s^{-1}$). We measured the average biomass consumption rate by weighing for each type of biomass (Table 39). The biomass consumption rate, air/biomass ratio and equivalence ratio are presented on a dry ash-free basis (daf) to facilitate the comparison.

	Pine	Miscanthus	Wheat straw
Air mass flux ($kg.m^{-2}.s^{-1}$)	0.022	0.022	0.022
Average biomass consumption rate ($kg.m^{-2}.s^{-1}$)	0.029	0.034	0.035
Air/biomass ratio	0.76	0.64	0.63
Air/biomass stoichiometry	5.39	5.66	5.34
Equivalence ratio	0.14	0.11	0.12

Table 39. Air/biomass ratio and equivalence ratio during oxidative pyrolysis of the three biomasses

The air/biomass ratio on daf basis was 0.76, 0.64 and 0.63 respectively for pine, miscanthus and wheat straw. The equivalence ratio (ER), defined as the actual air/biomass ratio relative to the stoichiometric air/biomass ratio, was calculated to be respectively, 0.14, 0.11, and 0.12. In the other words, that is to say that the OZ consumes respectively 14, 11 and 12% of the stoichiometric combustion air to provide energy for the autothermal pyrolysis process.

The higher ER for the woody biomass than for the herbaceous biomasses shows that less woody biomass is consumed to sustain the OZ propagation under the same air flux.

Compared to the ERs in continuous operation mode (0.13, 0.12 and 0.12), one could recognize that there is no significant difference between the two operation modes.

V.3.2. Bed compaction rate

Compaction occurred in our experiments during the OZ propagation in all three biomass pellet beds. The compaction rate, plotted versus the elevation of the OZ, is shown in Figure 76.

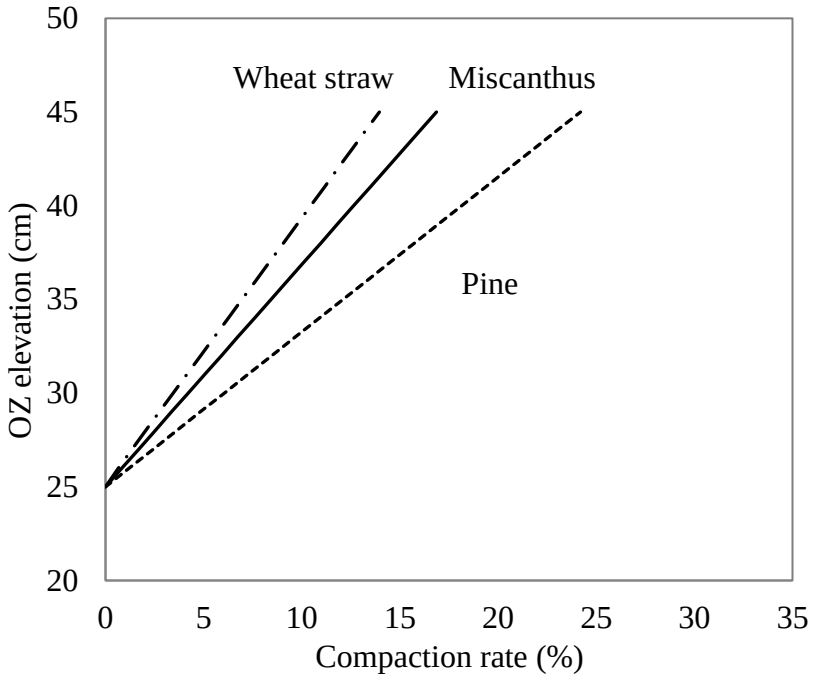

Figure 76. Bed compaction rate in different pellet beds with 0.022 kg.m^{-2}.s^{-1} air flux

It is shown that at the end of the experiment, i.e. OZ at 45 cm from the grate, the compaction rate was 24 %, 17 %, and 14 % for the pine, miscanthus and wheat straw beds, respectively. Compaction can be caused by shrinkage, fragmentation, and rearrangement of biomass particles during the conversion, as the consequences of a number of coupled chemical and mechanical phenomena [78,104].

However, as shown in Figure 66, bed compaction was linear, revealing that the bed was quite static and that the impacts of particle rearrangment, and fragmentation may not be significant. Thus, particle shrinkage is clearly the main phenomenon responsible for bed compaction.

In order to determine particle shrinkage, we measured the average diameter of biomass pellets to 6.08 mm, 6.28 mm, 5.56 mm, and the average diameter of the char after oxidative pyrolysis to be 4.35 mm, 4.80 mm, 4.37 mm, for pine, miscanthus and wheat straw, respectively (Figure 77). The reduction in particle diameter was then calculated to 28 %, 24 % and 21 %. These values are in line with several studies focussed on particle shrinkage of pelletized biomass during pyrolysis, in a temperature range of 300-800 °C [105,106]. The difference in ash content may explain the differences in the shrinkage of the three biomasses. Indeed, the higher the ash content, the less the particle shrinks during pyrolysis.

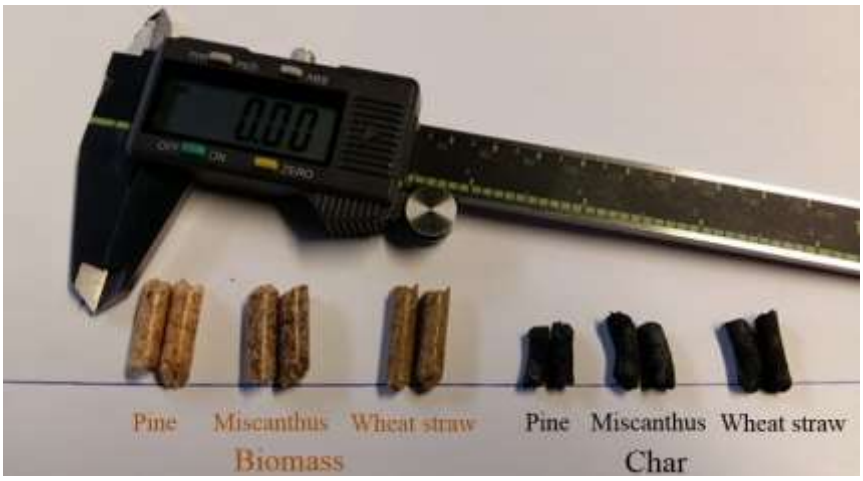

Figure 77. Measurement of particle size of the biomasses and the produced chars

Moreover, the particle volume shrinkage was calculated to 63 %, 55 % and 51 % for pine, miscanthus and wheat straw, respectively. It was considerably higher than the measured compaction rate of the bed. This observation shows that, as the char bed is static, the rearrangment of the particle does not occur efficiently and that the intra-particle porosity was consequently considerably higher in the char beds than in the biomass beds.

V.3.3. Propagation velocity of the oxidation zone

Effective propagation velocity was calculated from both temperature and bed height measurement (Section V.2.2). Here, we present the profile of the effective propagation velocity in the three-biomass beds. These velocities can be considered constant along the studied zone, as regards to the accuracy of the experiments (Figure 78).

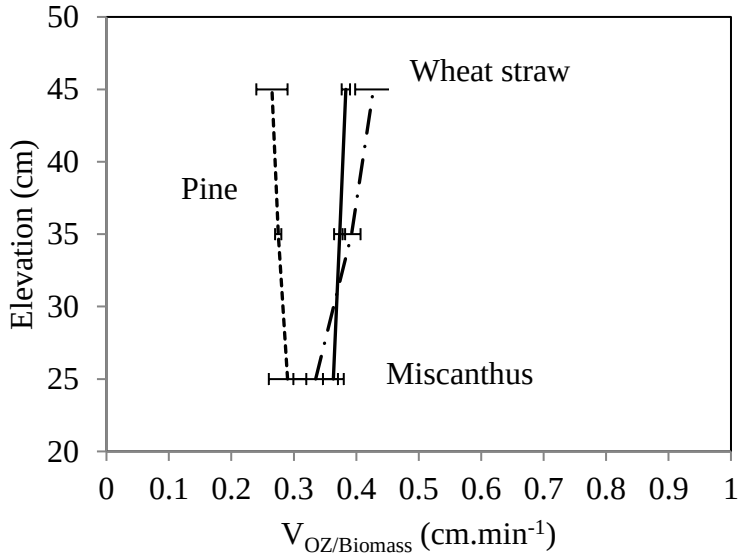

Figure 78. Propagation velocity in different pellet beds, 0.022 kg.m^{-2}.s^{-1} air flux

The profile of the wheat straw pellet bed suggests that the stationary regime was not fully reached at a distance of 35 cm from the grate, compared to the two other biomass pellet beds (Figure 78). The average effective velocity is 0.28, 0.37, and 0.39 $cm.min^{-1}$ in the beds of pine, miscanthus and wheat straw pellets, respectively. It is clearly lower in the wood pellet bed than in the two other beds.

Explaining the difference in OZ propagation velocity is complex because it is controlled by many factors related to biomass/bed properties. In our tests, bed bulk density, ranged from 549 $kg.m^{-3}$ for wheat straw pellets to 657 $kg.m^{-3}$ for wood pellets, could affect the velocity. Porteiro et al. [71] compared velocities in a wide range of bulk densities, under higher air flux than in the present study. They showed that velocity decreased from 2.5 $cm.min^{-1}$ to 0.7 $cm.min^{-1}$ with an increase in bulk density from 150 to 350 $kg.m^{-3}$. Above this density range, velocity decreased much more slowly and remained close to 0.5 $cm.min^{-1}$. Indeed, the same authors measured a slight drop (of about 5 %) in velocity in the pellets beds when the bulk density was increased from 600 to 700 $kg.m^{-3}$. Compared to our experiment, their results show that in the same range of bed density, lower propagation velocities (from 0.28 to 0.39 $cm.min^{-1}$) are obtained with low air flux. We obtained a sharper decrease in the propagation velocity, i.e. of about 25%, when we changed the bulk density from 549 $kg.m^{-3}$ with wheat straw pellets to 657 $kg.m^{-3}$ with wood pellets. The higher sensitivity of the propagation velocity to the bulk density that we observed could be explained by our specific very low airflow conditions. Nevertheless, we believe that other properties of the biomass have a greater impact. Indeed, the ash in the biomass, which influences the thermal properties of the bed (conductivity or emissivity) and reaction kinetics (inhibition and/or catalytic effects), is certainly the main factor responsible for the difference measured in the propagation velocity between woody and herbaceous biomass.

Based on the propagation velocity, cross-sectional area of the reactor and biomass density, the effective propagation rate was calculated to 0.031, 0.036, 0.036 $kg.m^{-2}.s^{-1}$. These values are in agreement with the average biomass consumption rates measured by weighing (Table 39). This agreement validates the method for the determination of effective velocity.

Furthermore, the OZ propagation velocity was found similar for both batch and continuous operation modes. For sure, one should remind that the determination of the propagation velocity in batch mode based on temperature and bed height measurement has a higher accuracy.

V.3.4. Thickness of the oxidation zone

The thickness of the oxidation zone has been measured based on the apparent propagation velocity and the passage time of the oxidation zone at a given thermocouple. Figure 79 presents the OZ thickness along the height of the three biomasses beds.

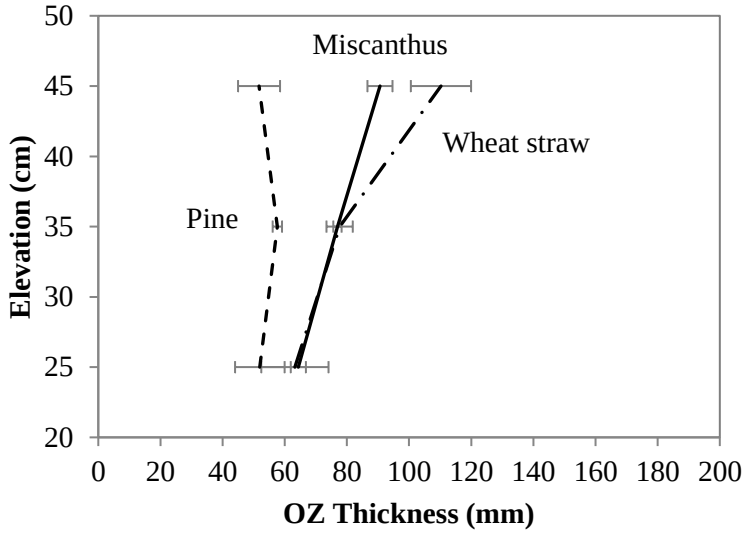

Figure 79. OZ thickness in different pellet beds with 0.022 kg.m^{-2}.s^{-1} air flux

The OZ thickness, was measured to 57 mm for the pine bed and 78 mm for miscanthus and wheat straw bed. The higher density in woody biomass than other herbaceous biomass can explain this difference. Indeed, Yang et al [107] showed that the fuel material density mainly affects the reaction zone thickness. In a given volume, high-density fuels have more combustible mass, they require more energy to heat up to reach the ignition temperature. Thus, denser biomass produces a thinner reaction zone. In contrast, light material tends to lose temperature easily by radiation as it has a smaller heat capacity per unit of volume and produces a thicker reaction zone.

In addition, the thickness of the OZ increased until a distance of 35 cm above the grid, and then stabilized in the wood bed showing that stationary propagation was reached. In the case of wheat straw, the stationary regime seems not to be completely reached.

Our results can be compared with the literature. Porteiro et al. [75] measured the thickness of the reaction front (similar to what we call the oxidation zone in our work) during counter-current smouldering in a bed of wood pellets with a density of 690 kg.m^{-3}. They assumed that the main processes occuring in the reaction front do not overlap and are defined by threshold temperatures. They described a reaction front with three different zones: drying zone,

devolatilisation zone, and char reaction zone corresponding to the threshold temperatures of 100 °C, 500 °C, and Tmax, respectively. Their results showed that the thickness of each of the two first zones was about 5 mm whatever the air flux. The thickness of the char reaction zone they measured ranged from 10 to 15 mm with an air flux greater than 0.12 $kg.m^{-2}.s^{-1}$. But when the air flux was reduced to 0.07 $kg.m^{-2}.s^{-1}$ the thickness of the char reaction zone increased to 40 mm. In the present work, the thickness of the OZ we measured based on the derivative of the temperature should be compared to the sum of the three zones defined by Porteiro et al. To summarise, when propagating under a low air flux (0.022 $kg.m^{-2}.s^{-1}$), the global OZ was slightly thicker than with a higher air flux, 57 mm compared to 50 mm in the work of Porteiro et al. [75].

V.3.5. Temperature field

Bed temperature measurement allows drawing the temperature profiles along the fixed bed at a given position of the oxidation zone. In detail, based on the data of the bed temperature at a given thermocouple and the propagation velocity of the oxidation zone (presented in the previous section), we plotted the temperature profile of the bed height when the OZ was at 35 cm (Figure 80).

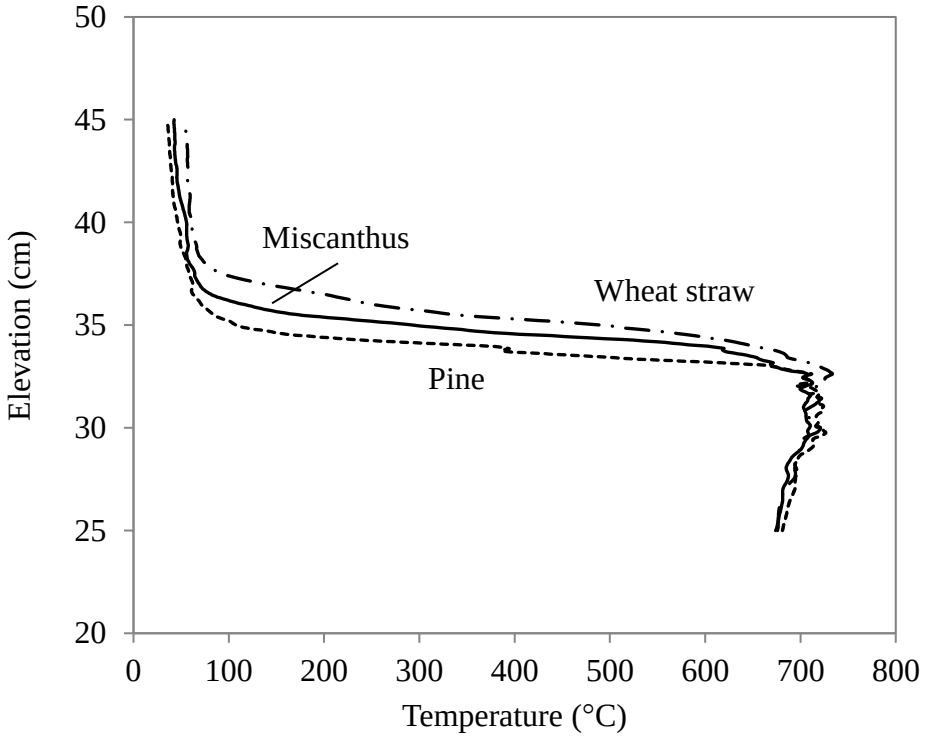

Figure 80. Temperature profile in different pellet beds with 0.022 $kg.m^{-2}.s^{-1}$ air flux. OZ at 35 cm height

Comparing the three biomasses, it is remarkable that no difference in temperature was observed, despite significant differences particularly in properties such as ash content or heating value. The temperature increased from 50 °C to a peak of around 720 °C, and then decreased slowly and regularly along the char bed. This decrease is due to heat losses through the reactor walls and possibly some endothermic reactions in char bed.

Comparing the bed temperature in the two operation modes, it is noticeable that there was no significant difference between them. Under a small air flowrate of 0.022 $kg.m^{-2}.s^{-1}$, maximum temperature was found to about 720°C for both modes and for all the studied biomasses.

Comparing our results with the previous studies on smoldering in literature, the maximum temperatures of a propagation front have been reported to be higher than 800 °C [69,72,73]. The reason is that the experiments were generally carried out in conditions close to stoichiometric combustion to fit with fixed bed incinerator. In our experiments, oxidative pyrolysis was performed in high sub-stoichiometric conditions, using only 11 % to 14 % of the stoichiometric combustion air, which resulted in a lower peak temperature. These temperature profiles, associated with OZ velocity and thickness provide information on the heating rate, which is known to strongly influence the yields of the pyrolysis products. The average heating rate was calculated to be 20-35 °C/min in all the experiments.

V.3.6. Product yields and mass balance

Mass balances were determined from the experimental results by considering the products entering and leaving the oxidation zone in the beds for the three different biomasses (Table 40). The values presented are the average of at least three tests for each biomass. Discrepancy in the measured flow-rates was below 10 % for a given experiment. In the table, the total inlets and outlets masses were the same because the flow rates of the condensates were calculated by difference.

Flow rates ($kg.h^{-1}$)			Pine	Miscanthus	Wheat straw
Inlet	Biomass, daf		3.17	3.77	3.80
	Water (biomass)		0.22	0.31	0.36
	Oxygen (from air)		0.56	0.56	0.56
	Nitrogen (from air)		1.85	1.85	1.85
	Ash (from biomass)		0.01	0.12	0.34
Outlet	Char, daf		0.59	0.92	1.01
	Condensates (by difference)		1.70	1.35	1.62
	Drying water	H_2O	0.22	0.31	0.36
	Permanent gases	CO_2	0.90	1.29	1.17
		CO	0.15	0.58	0.36
		H_2	0.03	0.04	0.03
		CH_4	0.31	0.10	0.12
		C_2H_4	0.03	0.03	0.03
		C_2H_6	0.01	0.02	0.02
	Nitrogen		1.85	1.85	1.85
	Ash (from char)		0.01	0.12	0.34

Table 40. Inlet and outlet flow rates ($kg.h^{-1}$) of the oxidative pyrolysis of the three biomasses

The yield of the char, condensates and permanent gases were calculated as a percentage of the mass of dry ash-free biomass and plotted in Figure 81. Note that the sum of the measured yields (char, condensates, permanent gases) exceeded 100 % because oxygen from the air reacts inside the bed and is recovered in the pyrolysis products.

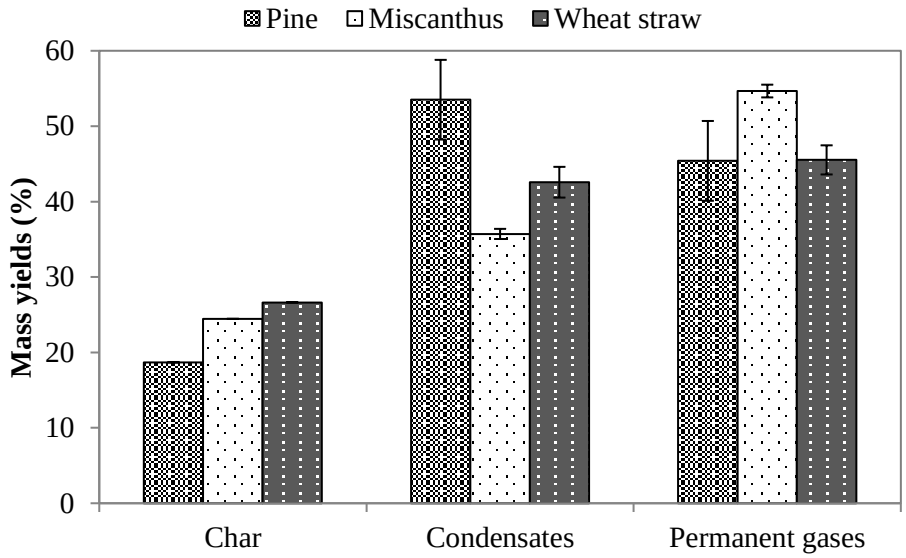

Figure 81. Mass yields (daf) of the oxidative pyrolysis products from different biomasses, 0.022 kg.m^{-2}.s^{-1} air flux

As can be seen in Figure 81, the yield of pine, miscanthus and wheat straw char was 18.7, 24.5 and 26.6 %, respectively. The yield of permanent gas ranged from 46 to 54 %, and the highest yield was obtained from miscanthus pyrolysis. The yield of condensates from the pine pyrolysis was significantly higher, 53.5 %. However, these differences cannot be explained by the difference in peak temperatures and heating rates during pyrolysis as we showed that these values were the same for the three biomasses. The differences in the ash content of the biomasses is probably the main reason as discussed in Chapter IV.

Comparing each yield of the products separately between the two operation modes, with regarding the experimental error of about 10 % as shown in the previous works [1,59], no significant difference was found. For example for the char yield, one could say that in both operation modes, it was measured to about 20, 25 and 28 % for pine, miscanthus and wheat straw, respectively.

V.3.7. Oxidative pyrolysis products

V.3.7.1. Char

The chars produced by oxidative pyrolysis of the three biomasses were all rich in carbon: 94.4, 91.2 and 88.5 % for pine, miscanthus and wheat straw, respectively. High carbon and low oxygen contents are responsible for the high heating values of the resulting chars. The oxygen content of the produced pine, miscanthus and wheat straw chars was 3.3, 6.6 and 8.1 %, respectively. This result can be explained by the catalytic effects of ash on the formation of the

secondary char by the condensation/polymerization of the primary tar and the interaction between the resulting volatiles and char. Indeed, Song et al. [108] showed that during the adsorption and subsequent conversion of tar molecules by char, some O-containing species originating from tar are transferred to the char and form additional O-containing structures in the char matrix.

Charcoal	Pine	Miscanthus	Wheat straw
Proximate analysis (%m, db)			
Ash	1.5	11.2	25.0
Volatile matter	6.8	6.4	9.5
Fixed carbon	91.8	82.4	65.5
Ultimate analysis (%m, daf)			
C	94.4	91.2	88.5
H	2.0	1.8	1.8
N	0.4	0.5	1.6
O (by difference)	3.3	6.6	8.1
LHV ($MJ.kg^{-1}$, daf)	33.4	33.1	31.8

Table 41. Proximate and ultimate analysis of the char produced by oxidative pyrolysis of the three biomasses, 0.022 $kg.m^{-2}.s^{-1}$ air flux

Some specific elements in the ash play an important role in the biomass pyrolysis process. As reported in the literature [94,99,101], Potassium in particular has a significant influence on the char formation stage by increasing the char yield [79,109]. What is more, the reactivity of the alkaline metal compounds decreases in the presence, ranked in order of importance of K, Na, Ca, Mg, Al, Zn, Fe. Regarding the three biomasses studied here, Table 19 shows that the amounts of Al, Zn and Fe are very small compared to those of K and Ca. Thus, the high concentration of Potassium may explain its impact on the pyrolysis yields of three different biomasses.

Regarding the influence of ash on char oxidation reactions, some authors [110–113] have also demonstrated the catalytic effect of ashes on char oxidation reactions. However, we observed in this study that the yield of char from oxidative pyrolysis of ash-rich (herbaceous) biomass was higher than the yield of low-ash biomass (wood). This observation along with the findings

from several works [75][59][114] suggest that there was almost no significant oxidation of char during oxidative pyrolysis under a low air mass flux of 0.022 $kg.m^{-2}.s^{-1}$. This conclusion is of importance with respect to the OZ propagation phenomena as it shows that only oxidation of volatile matter provides the energy for the process.

V.3.7.2. Permanent gases

Composition of the permanent gases, measured by the MicroGC system, is presented in Figure 82.

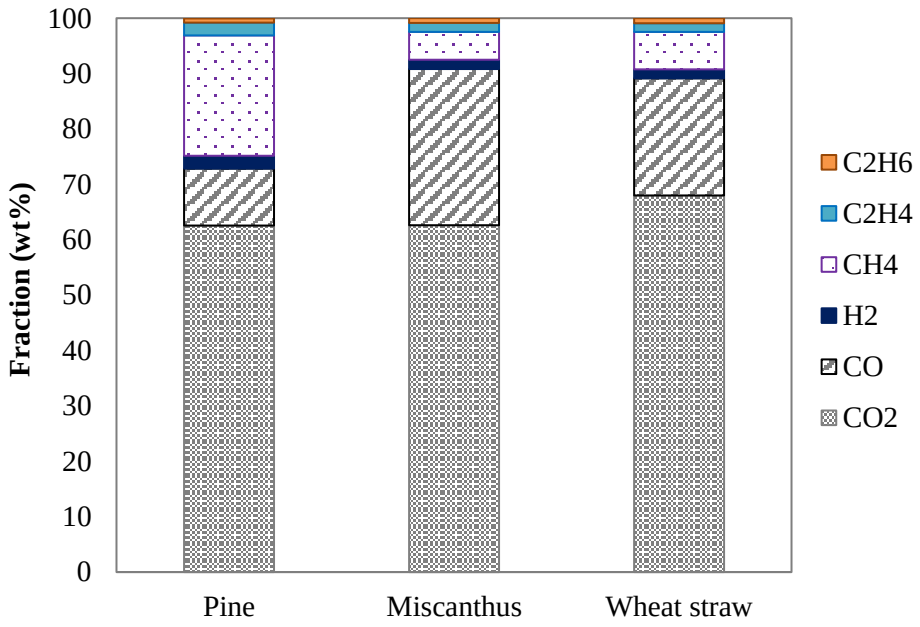

Figure 82. Composition of the permanent gases from oxidative pyrolysis of the three biomasses

Regarding the composition of the permanent gases from oxidative pyrolysis of three biomasses, CO_2 is the dominant gas, varying from 62 to 68 %. The high content of CO_2 is responsible for the low heating values of the permanent gases of pine, miscanthus and wheat straw, measured to 6.16, 13.54 and 12.95 $MJ.kg^{-1}$, respectively. The amounts of CO and CO_2 in woody biomass were lower than those of other biomasses. It can be explained by the catalytic effects of the ash. Indeed, some authors [94,115–117] have also observed higher yields of CO_2 and CO with higher ash content in biomass during pyrolysis. Pan et al [94] indicated that the increase in total yield of the catalyzed formation of carbon dioxide could be explained by decarboxylation of uranic acids alone.

V.3.7.3. Organic condensates

The condensates are presented in terms of water content and elemental composition (Table 42). Water content in the condensates from oxidative pyrolysis of the three biomasses varied from 42 to 57 %. Water content includes water from both biomass drying and oxidative pyrolysis reactions. High amounts of water are responsible for the low heating values of condensates from oxidative pyrolysis.

	Pine	Miscanthus	Wheat straw
Water fraction (%m)	56.94	56.85	42.56
C	30.92	38.26	38.39
H	2.4	6.18	5.58
O (by difference)	66.68	55.55	56.02
LHV ($MJ.kg^{-1}$)	6.16	13.54	12.95

Table 42. Composition of condensates

The composition of the organic condensates presented here by the elemental analysis (CHO) of the condensates was calculated from the elemental balance. Regarding the oxygen content in the condensates, it is clear that oxygen content for pine was higher than that for miscanthus and wheat straw experiments. This observation can be explained by the difference of ash content between the biomasses. Indeed, Williams et al [115] showed that the ash in biomass acts as a catalyst to convert the oxygen in the pyrolysis oil to H_2O at the lower temperatures and to CO and CO_2 at the higher temperatures. It is thus shown a good agreement with our observation here as CO and CO_2 is higher while oxygen content in the condensates are lower in cases of miscanthus and wheat straw than those in case of pine wood.

In addition, concerning the water yield in the products, Milhé et al. [59] showed that pyrolysis water yield was 15 to 27 %m higher in oxidative pyrolysis than in inert ones, as a result of oxidation reactions.

V.3.8. Repartition of energy in the products

Repartition of energy in the products can be calculated from the mass yields and calorific values of the products. Results are shown in Figure 83.

In case of the oxidative pyrolysis of pine, 35 % of the energy content in the biomass is recovered in the permanent gases, 30 % in the char, and 16 % in the condensates. However, in cases of oxidative pyrolysis from non-woody biomasses, miscanthus and wheat straw, energy yields

were measured to respectively 21 % and 18 % in permanent gases, 39 % and 41 % in char, and for 31 % and 33 % in condensates. The differences in the composition of the oxidative pyrolysis products presented in the previous sections explain the differences in their repartition of energy.

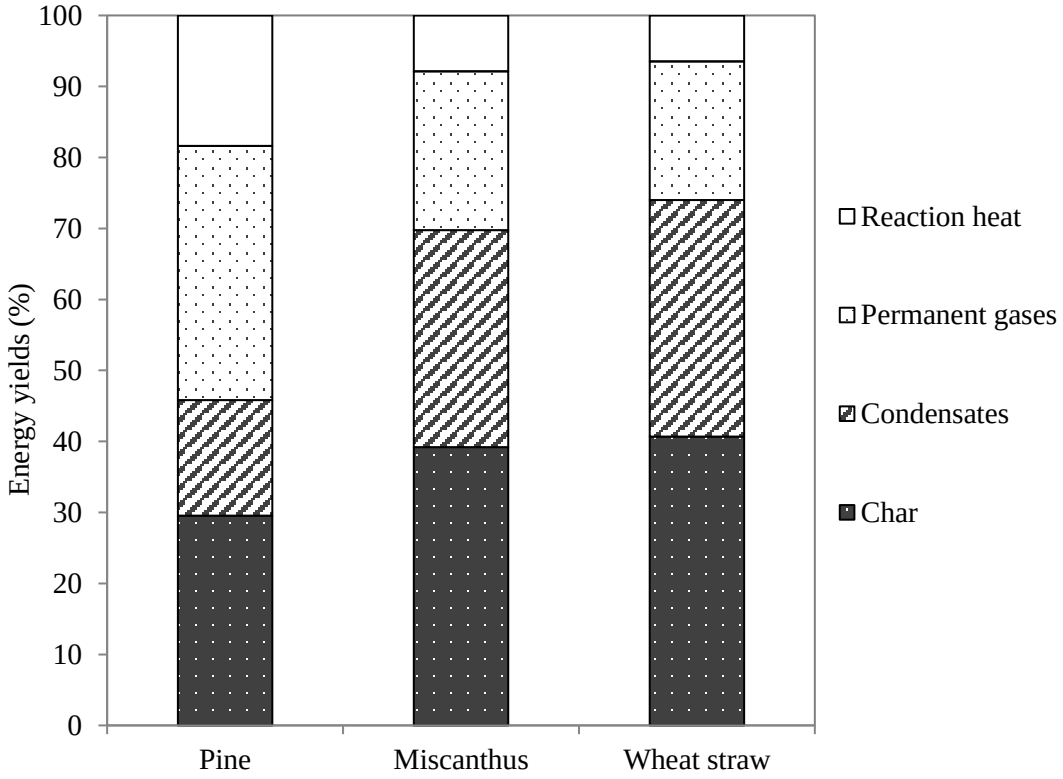

Figure 83. Energy yields of the oxidative pyrolysis products from different biomasses, 0.022 kg.m^{-2}.s^{-1} air flux

The remaining energy to reach 100 % corresponds to the reaction heat or reaction enthalpy of the oxidative pyrolysis. It is the sum of the sensible heat contained in the pyrolysis products, latent heat of water vaporization, and the heat losses through the reactor wall. It is considerably higher in pine pellets bed, 20 % compared to about 8 to 9 % in the cases of wheat straws and miscanthus. The reason is that the equivalence ratio (ER) was higher with wood than with the two others biomasses and thus favored the oxidation reactions. In addition, as air contains majority amount of nitrogen, higher ER in pine means that more nitrogen was injected in the reactor. In this case, the additional oxygen injected was partly used to heat up the related additional nitrogen. This explains why the sensible heat is higher in the case of wood pellets. We can see in the detailed enthalpy balance (presented in Chapter IV) that the sensible heat of nitrogen contributed significantly the output enthalpy flux. The higher nitrogen is, the higher sensible heat is and thus the higher is the reaction enthalpy to sustain propagation.

V.4. Conclusions

In this chapter, oxidative pyrolysis was performed in batch operation conditions to better access and quantify some features of the oxidation zone.

A new method was developed to measure the oxidation zone propagation velocity and thickness. The velocities and thicknesses were shown to be 25 % lower when the oxidation zone propagates in a fixed bed of pine wood pellets, mainly due to differences in ash content and bulk density. In this case, less biomass was required to sustain propagation of the oxidation zone resulting in a higher ER. For the oxidative pyrolysis of the three biomasses, ER ranged from 0.11 to 0.14.

In low air flux conditions, the peak temperature in the oxidation zone was around 720°C, and was shown to be unaffected by the nature of the biomass. Significant compaction took place in the bed, ranging from 15 to 30 % for the three biomasses, the biomass with the highest ash content being the least sensitive to compaction.

Ash was shown to have the most impact on process performance from two points of view:

- from the thermal point of view, since it affected the propagation velocity due to the inert mass fraction it introduced to the oxidation zone.

- from the chemical point of view, since it influenced the yields and compositions of the resulting products due to a catalytic effect on primary and secondary pyrolysis reactions.

- Page intentionally left blank -

GENERAL CONCLUSION

In line with a series of researches which have been carried out at CIRAD, this PhD focused on the oxidative pyrolysis in a fixed bed as the first step of the staged gasification process. More specifically, we investigated the influence of the biomass nature on the process performance and behavior through the three different types of biomass pellets: pine as a representative for forestry residues; miscanthus as a representative for herbaceous energy crops; and wheat straw as a representative for agricultural residues.

Oxidative pyrolysis occurs in a fixed bed and is controlled by an Oxidation Zone (OZ) that propagates upward towards the raw biomass. This zone produces char, condensates and gas for the next steps of gasification process and provides energy necessary for the pyrolysis process. Understanding and control this zone was the general scientific objectives of this PhD thesis.

An experimental study had been performed in a fixed bed reactor of 20 cm diameter and 1.6 m height. This reactor was adapted to be operated in both continuous or batch mode. The continuous mode enabled to reproduce the operation mode as existing in an industrial gasifier; the batch mode was set up to allow a fine characterisation of the OZ features.

In both operation modes, the oxidative pyrolysis was performed under an airflow of 34 $NL.min^{-1}$ equivalent to 0.022 $kg.m^{-2}.s^{-1}$ as in the pyrolysis step of staged gasifiers. Biomass was fed at the top of the reactor and the produced char, condensates and gas were collected at the bottom of the reactor and analyzed.

The oxidative pyrolysis behaves globally similar when using herbaceous, agricultural residues and wood pellets. However, in the case of wood pellets, less biomass was required to sustain propagation of the OZ, resulting in a higher equivalence ratio (ER). The propagation of the OZ consumed about 12 % of the stoichiometric combustion air to provide energy for the autothermal pyrolysis process for all the biomasses. The air/biomass ratio was found to be about 0.65-0.70. Peak temperatures of the oxidation zone was measured to around 720°C with a good repeatability.

In addition, mass and enthalpy balances were established and a sensitivity study was performed. The weak of accuracy of some experimental and thermodynamic data caused difficulties to establish a relevant enthalpy balance. However, this sensitivity study is of importance regarding future development of numerical models based on enthalpy.

Results in batch mode were globally the same as the ones in continuous mode. However, the batch mode experiments allowed a fine characterization of the OZ and in particular, the measurement of propagation velocity, thickness and compaction. An original methodology and data treatment tools were set up.

The average OZ velocity was measured to 0.28, 0.37 and 0.39 $cm.min^{-1}$ for pine, miscanthus and wheat straw respectively. The average OZ thickness was measured to 57 mm for pine pellets bed, 78 mm for miscanthus and wheat straw pellets beds. Velocity and thickness were 25% lower when the OZ propagates in a fixed bed of pine pellets than in herbaceous and agricultural pellets beds. Significant compaction took place in the bed and was determined to be in range of 15 to 30 % for the three biomasses. It was found higher in the case of pine pellets bed than in other biomass beds.

Ash was shown to have a significant impact on process performance from two points of view:

- from the thermal point of view, since it affected the propagation velocity due to the inert mass fraction it introduced to the OZ.

- from the chemical point of view, since it influenced the yields and compositions of the resulting products due to a catalytic effect on primary and secondary pyrolysis reactions.

To sum up, these works provide a useful experimental database to understand the oxidative pyrolysis of biomass in a downdraft fixed bed reactor and to support modelling. Regarding the development of gasification technologies, future works should keep on the investigation on the extension of the usable biomass to low-density biomasses such as rice husk, and corncob or to polluted biomasses such as municipal solid wastes.

REFERENCES

[1] E. Daouk, L. Van de Steene, F. Paviet, E. Martin, J. Valette, S. Salvador, Oxidative pyrolysis of wood chips and of wood pellets in a downdraft continuous fixed bed reactor, Fuel. 196 (2017) 408–418. doi:10.1016/j.fuel.2017.02.012.

[2] W. Van de Kamp, P. De Wild, U. Zielke, M. Suomalainen, H. Knoef, J. Good, T. Liliedahl, C. Unger, M. Whitehouse, J. Neeft, H. van den Hoek, J. Kiel, Tar measurement standard for sampling and analysis of tars and particles in biomass gasification product gas, Proceedings of the 14th European Biomass Conference and Exhibition. (2005) 791–794.

[3] Oxidative pyrolysis of various biomasses in a fixed bed : yields , composition and properties of the products, (n.d.) 720.

[4] Salman Zafar, An Introduction to Biomass Energy, (2018) http://www.bioenergyconsult.com/biomass-energy-int.

[5] G. Fischer, L. Schrattenholzer, Global bioenergy potentials through 2050, 20 (2001) 151–159.

[6] M. Parikka, Global biomass fuel resources, 27 (2004) 613–620. doi:10.1016/j.biombioe.2003.07.005.

[7] GLOBAL BIOMASS POTENTIAL TOWARDS 2035, (2016).

[8] B. Feedstocks, Biomass Feedstocks, Biofuels. (2009) 45–85. doi:10.1007/978-1-84882-011-1_2.

[9] A. V. Bridgwater, Thermal biomass conversion 2009, (n.d.).

[10] S. Wang, G. Dai, H. Yang, Z. Luo, Lignocellulosic biomass pyrolysis mechanism: A state-of-the-art review, Progress in Energy and Combustion Science. 62 (2017) 33–86. doi:10.1016/j.pecs.2017.05.004.

[11] P. Harmsen, W. Huijgen, Literature Review of Physical and Chemical Pretreatment Processes for Lignocellulosic Biomass, (2010) 1–49.

[12] C.R. To, Cutting-edge research for a greener sustainable future, 9262 (2013). doi:10.1039/c2gc36364j.

[13] I. Obernberger, F. Biedermann, W. Widmann, R. Riedl, Concentrations of inorganic elements in biomass fuels and recovery in the different ash fractions, Biomass and Bioenergy. 12 (1997) 211–224. doi:10.1016/S0961-9534(96)00051-7.

[14] Phyllis 2 (2014) Database for biomass and waste. Energy Research Centre, Netherlands., (n.d.).

[15] D.J. Roddy, C. Manson-Whitton, Biomass gasification and pyrolysis, in: Comprehensive Renewable Energy, 2012: pp. 133–153. doi:10.1016/B978-0-08-087872-0.00514-X.

[16] S.A. Channiwala, P.P. Parikh, A unified correlation for estimating HHV of solid, liquid and gaseous fuels, Fuel. 81 (2002) 1051–1063. doi:10.1016/S0016-2361(01)00131-4.

[17] C. Di Blasi, Modeling chemical and physical processes of wood and biomass pyrolysis, Progress in Energy and Combustion Science. 34 (2008) 47–90. doi:10.1016/j.pecs.2006.12.001.

[18] V. Hankalin, T. Ahonen, R. Raiko, On Thermal Properties of a Pyrolysing Wood Particle, Process Engineering. (2009) 1–20.

[19] S. Harada, T., Hata, T., Ishihara, Thermal constants of wood during the heating process measured with the laser flash method, Journal of Wood Science. Vol. 44 (1998) 425–435.

[20] A. Koufopanos, C. A., Maschio, G. & Lucches, Kinetic modeling of the pyrolysis of biomass and biomass components, Canadian Journal of Chemical Engineering. Vol. 67 (1989) 75–84.

[21] B.M. Jenkins, Physical properties of biomass. In: Kitani, O., Hall, C.W. (Eds.), Biomass Handbook. Gordon & Breach, Science Publishers, Amsterdam. (1989).

[22] C. Dupont, R. Chiriac, G. Gauthier, F. Toche, Heat capacity measurements of various biomass types and pyrolysis residues, Fuel. 115 (2014) 644–651. doi:10.1016/j.fuel.2013.07.086.

[23] Robert H. Perry, Perry's Chemical Engineers' Handbook, Seventh, n.d.

[24] S. Kumar, S.K. Shukla, A Review on Recent Gasification Methods for Biomethane Gas Production, International Journal of Energy Engineering. 6 (2016) 32–43. doi:10.5923/s.ijee.201601.05.

[25] Guide Biomasse-Energie, (1994).

[26] I. Obernberger, Reached developments of biomass combustion technologies and future outlook, Proceedings of the 17th European Biomass Conference. (2009) 20–37.

[27] G. Brem, ★Cofiring and co-processing biomass with coal, Thermal Net. (2008). http://ec.europa.eu/energy/intelligent/projects/sites/iee-

projects/files/projects/documents/thermalnet_cofiring_and_co_processing_biomass_with_coal.pdf.

[28] I. Obernberger, Biomass combustion-current status and future development, (n.d.).

[29] M. Milhé, PYROLYSE DE PLAQUETTES FORESTIERES EN LIT FIXE CONTINU, (n.d.).

[30] R. Warnecke, Gasification of biomass: Comparison of fixed bed and fluidized bed gasifier, Biomass and Bioenergy. 18 (2000) 489–497. doi:10.1016/S0961-9534(00)00009-X.

[31] L.G.P. Van de steene, Veille technologique communacation personnele, (n.d.).

[32] A. Dufour, Optimisation de la production d'hydrogène par conversion du méthane dans les procédés de pyrolyse / gazéification de la biomasse, (2007).

[33] A. V. Bridgwater, Review of fast pyrolysis of biomass and product upgrading, Biomass and Bioenergy. 38 (2012) 68–94. doi:10.1016/j.biombioe.2011.01.048.

[34] M.I. Jahirul, M.G. Rasul, A.A. Chowdhury, N. Ashwath, Biofuels production through biomass pyrolysis- A technological review, Energies. 5 (2012) 4952–5001. doi:10.3390/en5124952.

[35] H. Yang, Characteristics of hemicellulose , cellulose and lignin pyrolysis, 86 (2007) 1781–1788. doi:10.1016/j.fuel.2006.12.013.

[36] F.X. Collard, J. Blin, A review on pyrolysis of biomass constituents: Mechanisms and composition of the products obtained from the conversion of cellulose, hemicelluloses and lignin, Renewable and Sustainable Energy Reviews. 38 (2014) 594–608. doi:10.1016/j.rser.2014.06.013.

[37] W.U. Yi-min, Z. Zeng-li, L.I. Hai-bin, H.E. Fang, Low temperature pyrolysis characteristics of major components of biomass, Journal of Fuel Chemistry and Technology. 37 (2009) 427–432. doi:10.1016/S1872-5813(10)60002-3.

[38] S. Salvador, C. Couhert, J. Commandre, Failure of the component additivity rule to predict gas yields of biomass in flash pyrolysis at 950 8 C, Biomass and Bioenergy. 33 (2009) 316–326. doi:10.1016/j.biombioe.2008.07.003.

[39] Q. Liu, C. Lv, Y. Yang, F. He, L. Ling, Study on the pyrolysis of wood-derived rayon fiber by thermogravimetry – mass spectrometry, 733 (2005) 193–202. doi:10.1016/j.molstruc.2004.01.016.

[40] T. Hosoya, H. Kawamoto, S. Saka, Solid/liquid- and vapor-phase interactions between

cellulose- and lignin-derived pyrolysis products, Journal of Analytical and Applied Pyrolysis. 85 (2009) 237–246. doi:10.1016/j.jaap.2008.11.028.

[41] M.L. Boroson, J.B. Howard, J.P. Longwell, W.A. Peters, Product yields and kinetics from the vapor phase cracking of wood pyrolysis tars, AIChE Journal. 35 (1989) 120–128. doi:10.1002/aic.690350113.

[42] Thèse Milhé 2013.pdf, (n.d.).

[43] J. Rath, G. Staudinger, Cracking reactions of tar from pyrolysis of spruce wood, 80 (2001).

[44] Liden, A.G., F. BerrutiI, and D.S. Scott, A kinetic model for the production of liquids from the flash pyrolysis of biomass., Chemical Engineering Communications. 65(1) (1988) 207–221.

[45] Font, R., A. Marcilla, J. Devesa, and E. Verdù, Kinetic study of the flash pyrolysis of almond shells in a fluidized bed reactor at high temperatures, Journal of Analytical and Applied Pyrolysis. 27(2) (1993) 245–273.

[46] and L. Cozzani, V., C. Nicolella, L. Petarca, M. Rovatti, Tognotti, A Fundamental Study on Conventional Pyrolysis of a Refuse-Derived Fuel, Ind. Eng. Chem. Res.,. 34(6) (1995) 2006–2020.

[47] Baumlin, S., F. Broust, M. Ferrer, N. Meunier, E. Marty, and J. Lédé, The continuous self stirred tank reactor: measurement of the cracking kinetics of biomass pyrolysis vapours., Chemical Engineering Science. (2005).

[48] A.N. Garcia, Kinetic study of the flash pyrolysis of municipal solid waste in a fluidized bed reactor at high temperature, 31 (1995).

[49] Morf, P., P. Hasler, and T. Nussbaumer, Mechanisms and kinetics of homogeneous secondary reactions of tar from continuous pyrolysis of wood chips., Fuel. (2002) 843–853.

[50] Fagbemi, L., L. Khezami, and R. Capart, Pyrolysis products from different biomasses: application to the thermal cracking of tar., Applied Energy. (2001).

[51] T.A. Milne, R.J. Evans, N. Abatzaglou, Biomass Gasifier "'Tars'": Their Nature, Formation, and Conversion, 1998. doi:10.2172/3726.

[52] and W.A.P. Michael L. Boroson, Jack B. Howard, John P. Longwell, Heterogeneous cracking of wood pyrolysis tars over fresh wood char surfaces, Energy & Fuels. (1989) 735–740.

[53] S. Baumlin, F. Broust, M. Ferrer, N. Meunier, E. Marty, J. Lédé, The continuous self stirred tank reactor : measurement of the cracking kinetics of biomass pyrolysis vapours, 60 (2005) 41–55. doi:10.1016/j.ces.2004.07.057.

[54] L. Fagbemi, L. Khezami, R. Capart, Pyrolysis products from different biomasses, Applied Energy. 69 (2001) 293–306. doi:10.1016/S0306-2619(01)00013-7.

[55] P. Morf, P. Hasler, T. Nussbaumer, Mechanisms and kinetics of homogeneous secondary reactions of tar from continuous pyrolysis of wood chips q, 81 (2002).

[56] Q. Sun, S. Yu, F. Wang, J. Wang, Decomposition and gasification of pyrolysis volatiles from pine wood through a bed of hot char, Fuel. 90 (2011) 1041–1048. doi:10.1016/j.fuel.2010.12.015.

[57] M. Amutio, G. Lopez, R. Aguado, M. Artetxe, J. Bilbao, M. Olazar, Kinetic study of lignocellulosic biomass oxidative pyrolysis, Fuel. 95 (2012) 305–311. doi:10.1016/j.fuel.2011.10.008.

[58] A. Anca-Couce, N. Zobel, A. Berger, F. Behrendt, Smouldering of pine wood: Kinetics and reaction heats, Combustion and Flame. 159 (2012) 1708–1719. doi:10.1016/j.combustflame.2011.11.015.

[59] M. Milhé, L. van de Steene, M. Haube, J.-M. Commandré, W.-F. Fassinou, G. Flamant, Autothermal and allothermal pyrolysis in a continuous fixed bed reactor, Journal of Analytical and Applied Pyrolysis. 103 (2013) 102–111. doi:10.1016/j.jaap.2013.03.011.

[60] E. Daouk, L. Van de Steene, F. Paviet, S. Salvador, Oxidative Pyrolysis of a Large Wood Particle : Effects of Oxygen Concentration and of Particle Size, Chemical Engineering Transactions. 37 (2014) 73–78. doi:10.3303/CET1437013.

[61] X.H. Pham, B. Piriou, S. Salvador, J. Valette, L. Van de Steene, Oxidative pyrolysis of pine wood, wheat straw and miscanthus pellets in a fixed bed, Fuel Processing Technology. 178 (2018) 226–235. doi:10.1016/j.fuproc.2018.05.029.

[62] T.J. Ohlemiller, Modeling of smoldering combustion propagation, Progress in Energy and Combustion Science. 11 (1985) 277–310. doi:10.1016/0360-1285(85)90004-8.

[63] W.L.H. Hallett, Packed bed combustion: An overview, Combustion Institute Canadian Section Spring Meeting. (2005).

[64] E.R. Carvalho, C.A. Gurgel Veras, J.A. Carvalho, Experimental investigation of smouldering in biomass, Biomass and Bioenergy. 22 (2002) 283–294. doi:10.1016/S0961-9534(02)00005-3.

[65] F. De Souza Costa, D. Sandberg, Mathematical model of a smoldering log, Combustion and Flame. 139 (2004) 227–238. doi:10.1016/j.combustflame.2004.07.009.

[66] M.A. Nolter, D.H. Vice, Looking back at the Centralia coal fire: A synopsis of its present status, International Journal of Coal Geology. 59 (2004) 99–106. doi:10.1016/j.coal.2003.12.008.

[67] Y. Bin Yang, A.N. Phan, C. Ryu, V. Sharifi, J. Swithenbank, Mathematical modelling of slow pyrolysis of segregated solid wastes in a packed-bed pyrolyser, Fuel. 86 (2007) 169–180. doi:10.1016/j.fuel.2006.07.012.

[68] Y.B. Yang, V.N. Sharifi, J. Swithenbank, Effect of air flow rate and fuel moisture on the burning behavior s of biomass and simulated municipal solid wastes in packed beds, Fuel. 83 (2004) 1553–1562. doi:10.1016/j.fuel.2004.01.016.

[69] T.J. Ohlemiller, D.A. Lucca, An experimental comparison of forward and reverse smolder propagation in permeable fuel beds, Combustion and Flame. 54 (1983) 131–147. doi:10.1016/0010-2180(83)90027-5.

[70] M. Fatehi, M. Kaviany, Adiabatic reverse combustion in a packed bed, Combustion and Flame. 99 (1994) 1–17. doi:10.1016/0010-2180(94)90078-7.

[71] J. Porteiro, D. Patiño, J. Collazo, E. Granada, J. Moran, J.L. Miguez, Experimental analysis of the ignition front propagation of several biomass fuels in a fixed-bed combustor, Fuel. 89 (2010) 26–35. doi:10.1016/j.fuel.2009.01.024.

[72] C. Ryu, Y. Bin Yang, A. Khor, N.E. Yates, V.N. Sharifi, J. Swithenbank, Effect of fuel properties on biomass combustion: Part I. Experiments—fuel type, equivalence ratio and particle size, Fuel. 85 (2006) 1039–1046. doi:10.1016/j.fuel.2005.09.019.

[73] J. Porteiro, D. Patiño, J. Moran, E. Granada, Study of a fixed-bed biomass combustor: Influential parameters on ignition front propagation using parametric analysis, Energy and Fuels. 24 (2010) 3890–3897. doi:10.1021/ef100422y.

[74] D. Shin, S. Choi, The combustion of simulated waste particles in a fixed bed, Combustion and Flame. 121 (2000) 167–180. doi:10.1016/S0010-2180(99)00124-8.

[75] J. Porteiro, D. Patiño, J.L. Miguez, E. Granada, J. Moran, J. Collazo, Study of the reaction front thickness in a counter-current fixed-bed combustor of a pelletised biomass, Combustion and Flame. 159 (2012) 1296–1302. doi:10.1016/j.combustflame.2011.10.007.

[76] S. Mahapatra, S. Dasappa, Experiments and analysis of propagation front under

gasification regimes in a packed bed, Fuel Processing Technology. 121 (2014) 83–90. doi:10.1016/j.fuproc.2014.01.011.

[77] S. Zhao, Y. Luo, Y. Su, Y. Zhang, Y. Long, Experimental investigation of the oxidative pyrolysis mechanism of pinewood on a fixed-bed reactor, Energy and Fuels. 28 (2014) 5049–5056. doi:10.1021/ef500612q.

[78] J.J. Saastamoinen, R. Taipale, M. Horttanainen, P. Sarkomaa, Propagation of the ignition front in beds of wood particles, Combustion and Flame. 123 (2000) 214–226. doi:10.1016/S0010-2180(00)00144-9.

[79] Y.B. Yang, H. Yamauchi, V. Nasserzadeh, J. Swithenbank, Effects of fuel devolatilisation on the combustion of wood chips and incineration of simulated municipal solid wastes in a packed bed☆, Fuel. 82 (2003) 2205–2221. doi:10.1016/S0016-2361(03)00145-5.

[80] E. Daouk, Études Expérimentale et Numérique de la Pyrolyse Oxydante de la Biomasse en Lit Fixe., (2015).

[81] E. Daouk, Etudes Expérimentale et Numérique de la Pyrolyse Oxydante de la Bioimasse en Lit Fixe, (2015).

[82] Y. Li, H. Liu, High-pressure densification of wood residues to form an upgraded fuel, Biomass and Bioenergy. 19 (2000) 177–186. doi:10.1016/S0961-9534(00)00026-X.

[83] N. Kaliyan, R. Vance Morey, Factors affecting strength and durability of densified biomass products, Biomass and Bioenergy. 33 (2009) 337–359. doi:10.1016/j.biombioe.2008.08.005.

[84] J. Vinterbäck, Pellets 2002: the first world conference on pellets, (n.d.). doi:10.1016/j.biombioe.2004.05.005.

[85] P. Gilbert, C. Ryu, V. Sharifi, J. Swithenbank, Bioresource Technology Tar reduction in pyrolysis vapours from biomass over a hot char bed, Bioresource Technology. 100 (2009) 6045–6051. doi:10.1016/j.biortech.2009.06.041.

[86] A. Sultana, A. Kumar, D. Harfield, Development of agri-pellet production cost and optimum size, Bioresource Technology. 101 (2010) 5609–5621. doi:10.1016/j.biortech.2010.02.011.

[87] V.K. Verma, S. Bram, F. Delattin, P. Laha, I. Vandendael, A. Hubin, J. De Ruyck, Agro-pellets for domestic heating boilers: Standard laboratory and real life performance, Applied Energy. 90 (2012) 17–23. doi:10.1016/j.apenergy.2010.12.079.

[88] L. Van De Steene, De la description fine de la gazéification en lit fixe à l'optimisation des procédés étagés - HDR, (2014).

[89] Gabriel TEIXEIRA, Gazéification de charbon de granules de bois : comportement thermochimique et mécanique d'un lit fixe continu, (2012) 234.

[90] F. Mermoud, Gazéification de charbon de bois à la vapeur d'eau : de la particule isolée au lit fixe continu, (2006) 221. http://ethesis.inp-toulouse.fr/archive/00000353/.

[91] Mettler Toledo, Good Titration Practice ™ in Karl Fischer Titration, GTP KF Brochure. (2011) 98. http://fr.mt.com/dam/LabDiv/Campaigns/TestingLabs2013/moisture/package/gtp-karl-fischer-EN.pdf.

[92] A. Rostami, J. Murthy, M. Hajaligol, Modeling of smoldering process in a porous biomass fuel rod, 83 (2004) 1527–1536. doi:10.1016/j.fuel.2003.11.018.

[93] C.A. Zaror, I.S. Hutchings, D.L. Pyle, N. Stiles, Secondary char formation pyrolysis of biomass in the catalytic, 64 (1985) 990–994.

[94] W.P. Pan, G.N. Richards, Influence of metal ions on volatile products of pyrolysis of wood, Journal of Analytical and Applied Pyrolysis. 16 (1989) 117–126. doi:10.1016/0165-2370(89)85011-9.

[95] R. Fahmi, The effect of alkali metals on combustion and pyrolysis of Lolium and Festuca grasses , switchgrass and willow, 86 (2007) 1560–1569. doi:10.1016/j.fuel.2006.11.030.

[96] N. Tröger, D. Richter, R. Stahl, Effect of feedstock composition on product yields and energy recovery rates of fast pyrolysis products from different straw types, Journal of Analytical and Applied Pyrolysis. 100 (2013) 158–165. doi:10.1016/j.jaap.2012.12.012.

[97] K. Raveendran, A. Ganesh, K.C. Khilart, Influence of mineral matter pyrolysis characteristics on biomass, 74 (1995) 1812–1822.

[98] Y. Lee, J. Park, C. Ryu, K.S. Gang, W. Yang, Y.K. Park, J. Jung, S. Hyun, Comparison of biochar properties from biomass residues produced by slow pyrolysis at 500°C, Bioresource Technology. 148 (2013) 196–201. doi:10.1016/j.biortech.2013.08.135.

[99] W.F. DeGroot, F. Shafizadeh, The influence of exchangeable cations on the carbonization of biomass, Journal of Analytical and Applied Pyrolysis. 6 (1984) 217–232. doi:10.1016/0165-2370(84)80019-4.

[100] F. Ronsse, S. van Hecke, D. Dickinson, W. Prins, Production and characterization of slow pyrolysis biochar: Influence of feedstock type and pyrolysis conditions, GCB

Bioenergy. 5 (2013) 104–115. doi:10.1111/gcbb.12018.

[101] D.J. Nowakowski, J.M. Jones, R.M.D. Brydson, A.B. Ross, Potassium catalysis in the pyrolysis behavior of short rotation willow coppice, Fuel. 86 (2007) 2389–2402. doi:10.1016/j.fuel.2007.01.026.

[102] J.P. Tagutchou, Gazeification du Charbon de Plaquettes Forestières : Particule Isolée et Lit Fixe Continu, 2008.

[103] E. Peduzzi, G. Boissonnet, F. Maréchal, Biomass modelling: Estimating thermodynamic properties from the elemental composition, Fuel. 181 (2016) 207–217. doi:10.1016/j.fuel.2016.04.111.

[104] G. Teixeira, L. Van De Steene, E. Martin, F. Gelix, S. Salvador, Gasification of char from wood pellets and from wood chips: Textural properties and thermochemical conversion along a continuous fixed bed, Fuel. 102 (2012) 514–524. doi:10.1016/j.fuel.2012.05.039.

[105] R. Paulauskas, N. Striūgas, E. Misiulis, Experimental and theoretical investigation of wood pellet shrinkage during pyrolysis, (2014) 1–11.

[106] R. Paulauskas, N. Striūgas, K. Zakarauskas, A. Džiugys, L. Vorotinskienė, Investigation of regularities of pelletized biomass thermal deformations during pyrolysis, Thermal Science. OnLine-Fir (2017) 90–90. doi:doi.org/10.2298/TSCI160916090P.

[107] Y. YANG, C. RYU, A. KHOR, N. YATES, V. SHARIFI, J. SWITHENBANK, Effect of fuel properties on biomass combustion. Part II. Modelling approach—identification of the controlling factors, Fuel. 84 (2005) 2116–2130. doi:10.1016/j.fuel.2005.04.023.

[108] Y. Song, Y. Zhao, Destruction of tar during volatile-char interactions at low temperature, Fuel Processing Technology. 171 (2018) 215–222. doi:10.1016/j.fuproc.2017.11.023.

[109] W. Zhao, Z. Li, G. Zhao, F. Zhang, Q. Zhu, Effect of air preheating and fuel moisture on combustion characteristics of corn straw in a fixed bed, Energy Conversion and Management. 49 (2008) 3560–3565. doi:10.1016/j.enconman.2008.07.006.

[110] C. Zou, J. Zhao, X. Li, R. Shi, Effects of catalysts on combustion reactivity of anthracite and coal char with low combustibility at low / high heating rate, Journal of Thermal Analysis and Calorimetry. 126 (2016) 1469–1480. doi:10.1007/s10973-016-5806-y.

[111] Z. Shu, C. Zong-ding, C. Xu-jun, G. Xu-zhong, Effects of ash / K 2 CO 3 / Fe 2 O 3 on ignition temperature and combustion rate of demineralized anthracite, Journal of Fuel Chemistry and Technology. 42 (2014) 166–174. doi:10.1016/S1872-5813(14)60013-X.

[112] A. Williams, The role of metals in biomass char combustion, (2005).

[113] Z.A. Mayer, A. Apfelbacher, A. Hornung, A comparative study on the pyrolysis of metal- and ash- enriched wood and the combustion properties of the gained char, Journal of Analytical and Applied Pyrolysis. 96 (2012) 196–202.

[114] M. Kim, Y. Lee, J. Park, C. Ryu, T.I. Ohm, Partial oxidation of sewage sludge briquettes in a updraft fixed bed, Waste Management. 49 (2016) 204–211. doi:10.1016/j.wasman.2016.01.040.

[115] P.T. Williams, N. Nugranad, Comparison of products from the pyrolysis and catalytic pyrolysis of rice husks, Energy. 25 (2000) 493–513. doi:10.1016/S0360-5442(00)00009-8.

[116] G. Yildiz, F. Ronsse, R. Venderbosch, R. Van Duren, S.R.A. Kersten, W. Prins, Applied Catalysis B : Environmental Effect of biomass ash in catalytic fast pyrolysis of pine wood, "Applied Catalysis B, Environmental." 168–169 (2015) 203–211. doi:10.1016/j.apcatb.2014.12.044.

[117] I. Influencing, com Factors Related to Minerals and Ingredients Influencing the Distribution of Pyrolysates Derived from Herbaceous Biomass, 8 (2013) 1345–1360.

APPENDICES

A. Wood chips- raw biomass material and difficulties

We also attempted to perform several tests with wood chips as a raw biomass material. Wood chips selected in this study has similar composition as wood pellets, but density is different: 220 $kg.m^{-3}$ compared to 657 $kg.m^{-3}$ of wood pellets.

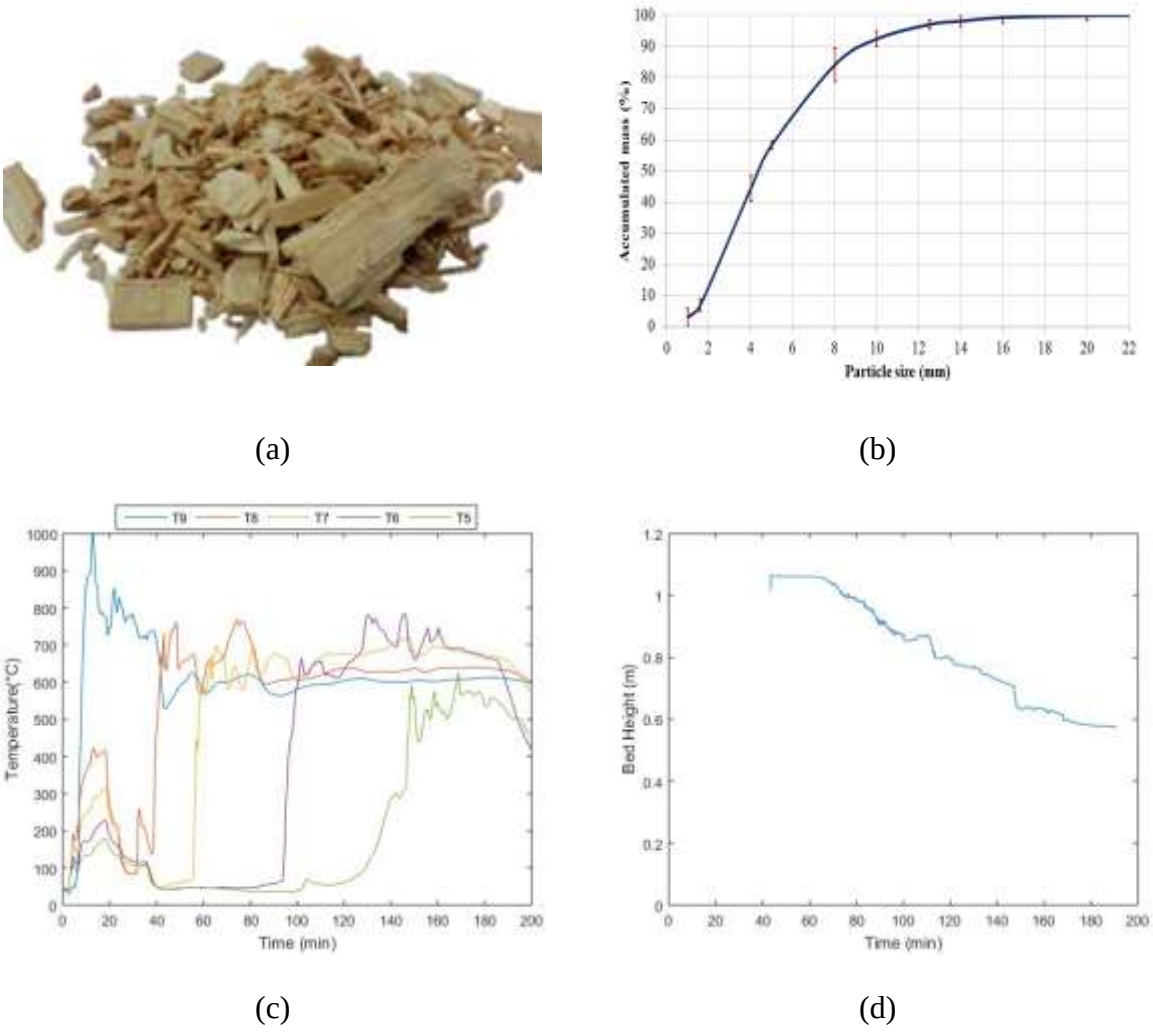

(a) (b)

(c) (d)

Figure 84. Wood chips and their difficulties with the tests in batch mode

(a) Wood chips particles (b) particle size distribution (c) bed temperature (d) bed height

As shown in Figure 84-a, the shape of the wood chips particles are inhomogeneous. While the wood pellets particles have homogeneous cylinder form, wood chips particle consists in various forms of the particle including cube, board, rod forms, etc.

The particle size distribution of the wood chips is determined by sieve analysis based on the standard « NF EN 15149-1: 2010 ». Sieve analysis is the common method to determine the granulometry distribution. It refers to the passing a known weight of sample material

successively through finer sieves and weighing the amount collected on each sieve to determine the percentage weight in each size fraction. For the wood chips, the sieve apertures of 1, 1.5, 4, 5, 8, 10, 12.5,14, 16 and 20 mm were chosen. A horizontally oscillating screen system including standard sieves equipped with a mechanical oscillating system at BioWooEB- CIRAD were used. About 8L of wood sample were used and placed in the coarsest sieve. The operation period of each analysis is 15 minutes to ensure the complete passing of particles. After this period, each sieve was weighed by a balance with a precision of 0.1 g; results are presented in Figure 84-b.

Particles with size in range of 1.6 to 4 mm and from 5 to 8 mm are dominants in wood chips sample. In addition, an important value of the particle size distribution is the index D50, the median particle size distribution. The D50 is the size of particle that splits the distribution with half above and half below this diameter. This value is a common data referring to the particle size distributions. For the wood chips used in this study, D50 was determined to 4.3 mm.

Regarding the bed temperature obtained in the beds of wood chips (Figure 84-c), after the ignition step followed by T9, as the oxidation zone propagates in the fixed bed, temperature reaches T8, T7, T6 and T5 consequently. However, unlike the case of the wood pellets, the form of the temperature profile versus time is unpredicted. Moreover, the times for the oxidation zone reaches these thermocouple positions vary between the tests. Consequently, the determination of the propagation velocity is difficult and has a high uncertainty. This problem can be explained by the low density of the biomass as indicated in the work of Porteiro et al. [71].

In addition, bridging within the bed is observed during the test with the wood chips. As shown in Figure 84-d, at the moment of 100 min, the bridging occurred and the bed height remained stable. Five minutes later, the bed height was suddenly reduced by about 5 cm. This phenomenon occurred again at the moment of 150 min. Bridging is common phenomenon occurs in downdraft fixed bed reactor. It causes the aggregate of the biomass particles thus reduces the intraparticle convective flow. Consequently, it forms channeling and stagnant solid movement in the reactor. This phenomenon can be overcome thanks to the help of mechanical actions like shaking, vibrating the reactor. However, in this study, the oxidation zone propagates in the fixed bed of biomass naturally, i.e. without any impact of external forces. The determination of the propagation velocity of the oxidation zone is based on the bed height measurement. Thus, the bridging caused by the low density of the wood chips is the big problem for this study.

High uncertainty the determination of the propagation velocity and the bridging problem bother the fine characterization of the oxidation zone in a fixed bed of biomass. Thus, in this study, we decided to choose biomass in pellet form.

B. Standard enthalpy of formation of water and permanent gases

Compound	h_i^0 (kJ.mol^{-1})
H_2	0
N_2	0
O_2	0
CH_4	-74.52
CO	-110.53
CO_2	-393.51
H_2O (vapor)	-241.81
H_2O (liquid)	-285.80
C_2H_4	52.3
C_2H_6	-84.7
Ash	0

C. Heat capacity as function of temperature

($kJ.mol^{-1}.K^{-1}$)	Cp(T)	References
CH_4	(5.34+0.0115*T)*4.1855	[23]
O_2	(8.27+0.000258*T-187700*T^{-2})*4.1855	[23]
CO	(6.62+0.0012*T)*4.1855	[23]
CO_2	(10.34 + 0.00274*T-195500/T^2)*4.1855	[23]
H_2O(v)	(8.22+0.00015*T+0.00000134*T^2)*4.1855	[23]
H_2	(6.62+0.00018*T)*4.1855	[23]
N_2	(6.5+0.001*T)*4.1855	[23]
Char	(1.39+0.00036*T)*12.0305	[102]
C_2H_4	0.995+ 0.002565T	[23]
C_2H_6	1.008+ 0.003272T	[23]
Biomass	5.34*T-299	[22]
Ash	0.7	www.engineeringtoolbox.com

D. Detailed enthalpy balance for the case of pine oxidative pyrolysis

Pine			*Standard enthalpy of formation (at 25°C, 1 atm) (kW)*	*Sensible heat (kW)*	*Latent heat (kW)*	*Total enthalpy (kW)*
Inlet	Biomass, daf		-3.07	0.00	0.00	-3.07
	Water (moisture)		-0.94	0.00	0.00	-0.94
	Oxygen (from air)		0.00	0.00	0.00	0.00
	Nitrogen (from air)		0.00	0.00	0.00	0.00
	Ash (from biomass)		0.00	0.00	0.00	0.00
	Total		-4.01	0.00	0.00	-4.01
Outlet	Char, daf		0.19	0.04	0.00	0.23
	Condensates		-1.41	1.50	0.00	0.10
	Pyrolysis water		-3.04	0.30	0.00	-2.74
	Drying water		-0.94	0.09	0.13	-0.71
	Permanent gases	CO_2	-2.35	0.19	0.00	-2.15
		CO	-0.60	0.11	0.00	-0.48
		H_2	0.00	0.10	0.00	0.10
		CH_4	-0.11	0.05	0.00	-0.06
		C_2H_4	0.02	0.00	0.00	0.02
		C_2H_6	-0.01	0.00	0.00	-0.01
	Nitrogen	N_2	0.00	0.36	0.00	0.36
	Ash (from char)		0.00	0.00	0.00	0.00
	Total		-8.23	2.76	0.13	-5.34
Heat losses						0.60
Difference (%)						18.19

E. Detailed enthalpy balance for the case of miscanthus oxidative pyrolysis

Miscanthus			*Standard enthalpy of formation (at 25°C, 1 atm) (kW)*	*Sensible heat (kW)*	*Latent heat (kW)*	*Total enthalpy (kW)*
Inlet	Biomass, daf		-4.68	0.00	0.00	-4.68
	Water (moisture)		-1.21	0.00	0.00	-1.21
	Oxygen (from air)		0.00	0.00	0.00	0.00
	Nitrogen (from air)		0.00	0.00	0.00	0.00
	Ash (from biomass)		0.00	0.00	0.00	0.00
	Total		-5.89	0.00	0.00	-5.89
Outlet	Char, daf		0.16	0.06	0.00	0.22
	Condensates		-1.53	0.93	0.00	-0.59
	Pyrolysis water		-1.68	0.17	0.00	-1.52
	Drying water		-1.21	0.12	0.17	-0.92
	Permanent gases	CO_2	-3.08	0.25	0.00	-2.82
		CO	-0.54	0.10	0.00	-0.43
		H_2	0.00	0.11	0.00	0.11
		CH_4	-0.13	0.06	0.00	-0.07
		C_2H_4	0.02	0.00	0.00	0.02
		C_2H_6	-0.01	0.00	0.00	-0.01
	Nitrogen	N_2	0.00	0.36	0.00	0.36
	Ash (from char)		0.00	0.01	0.00	0.01
	Total		-8.00	2.19	0.17	-5.64
Heat losses						0.22
Difference (%)						-8.01

F. Detailed enthalpy balance for the case of wheat straw oxidative pyrolysis

Wheat straw			*Standard enthalpy of formation (at 25°C, 1 atm) (kW)*	*Sensible heat (kW)*	*Latent heat (kW)*	*Total enthalpy (kW)*
Inlet	Biomass, daf		-3.61	0.00	0.00	-3.61
	Water (moisture)		-1.44	0.00	0.00	-1.44
	Oxygen (from air)		0.00	0.00	0.00	0.00
	Nitrogen (from air)		0.00	0.00	0.00	0.00
	Ash (from biomass)		0.00	0.00	0.00	0.00
	Total		-5.05	0.00	0.00	-5.05
Outlet	Char, daf		0.09	0.07	0.00	0.16
	Condensates		-1.73	0.84	0.00	-0.89
	Pyrolysis water		-1.54	0.15	0.00	-1.39
	Drying water		-1.44	0.14	0.21	-1.09
	Permanent gases	CO_2	-2.99	0.24	0.00	-2.74
		CO	-0.46	0.09	0.00	-0.38
		H_2	0.00	0.10	0.00	0.10
		CH_4	-0.12	0.06	0.00	-0.06
		C_2H_4	0.01	0.00	0.00	0.01
		C_2H_6	-0.01	0.00	0.00	-0.01
	Nitrogen	N_2	0.00	0.36	0.00	0.36
	Ash (from char)		0.00	0.04	0.00	0.04
	Total		-8.19	2.09	0.21	-5.89
Heat losses						0.34
Difference (%)						9.97

G. Numerical tools for the experimental data treatment

1. Linear least squares fitting method

Linear least squares fitting technique is the simplest and most commonly applied form of linear regression and provides a solution to the problem of finding the best fitting straight line through a set of points.

To illustrate this method, let us consider a set of n data points (Figure 85), (x_i y_i) $1 \leq i \leq n$. For each value of x_i, we have a corresponding value $F(x_i)$, with $F(x_i) = \sum_{j=0}^{k} a_j x_i^k$, k is the degree of the polynomial F, $k \leq n$. The square deviations R^2 between $F(x_i)$ and y_i is calculated as:

$$R^2 = \sum_{i=1}^{n} (F(x_i) - y_i)^2 \tag{34}$$

Given a value of $k < n$, the set of the values of a_j is determined following the condition for R^2 to be minimum:

$$\frac{\partial(R^2)}{\partial a_j} = 0 \tag{35}$$

Now, we have a new set of data (x_i $F(x_i)$) following a continuous function F with degree of k from the discrete data (x_i y_i).

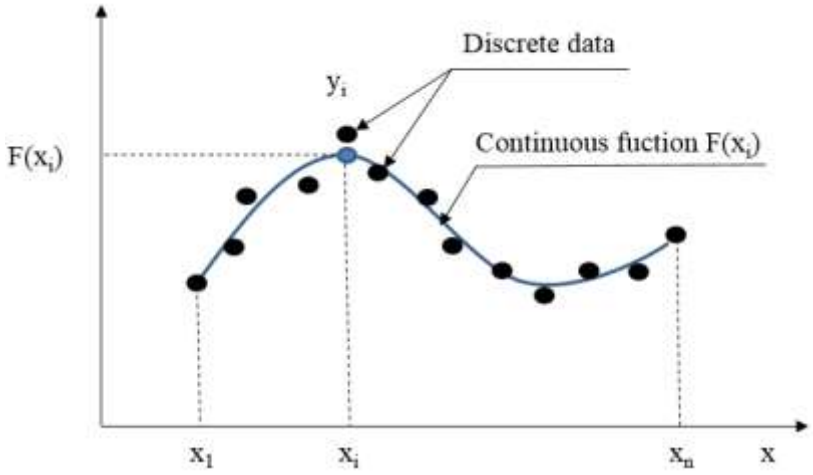

Figure 85. Linear least squares fitting method

Figure 70 shows an example of using this method to find the function of the OZ elevation propagation and then to determine the propagation velocity by its derivative.

In Matlab, we can apply this method with the program function *polyfit*, and the syntax: F= *polyfit (x, y, k)*. The function F(x) is the polynomial of degree k that best fit (in a least squares sense) the data (x, y).

2. Savitzky–Golay filter method.

When the signal is too complex, the simple fitting function is no longer suitable. A complex signal requires a fitting function with higher degree (>5) and thus the determination of the fitting function is more difficult and incorrect. In this case, other methods are proposed such as moving average method, Savitzky–Golay filter method. In this manuscript, we present the Savitzky–Golay filter method.

A Savitzky–Golay filter is a digital filter that can be applied to a set of digital data points for smoothing the data, that is, to increase the signal-to-noise ratio without greatly distorting the signal. This is achieved, in a process known as convolution, by fitting successive sub-sets of adjacent data points with a low-degree polynomial by the method of linear least squares. When the data points are equally spaced in the sub-sets, an analytical solution can be found, in the form of a single set of "convolution coefficients" that can be applied to all data sub-sets, to give estimates of the smoothed signal at the central point of each sub-set.

The method can be summarized in three steps:

- split the set of data into smaller sub-sets with the criteria: (i) the sub-sets have the same width and (ii) the sub-sets are convoluted (they have some common data).

- fit the data each the sub-set by the linear least squares fitting method.

- find the convolution coefficients between the successive sub-sets.

Figure 86 illustrates the Savitzky–Golay filter method applied for the set of n data points, (x_i y_i) $1 \leq i \leq n$.

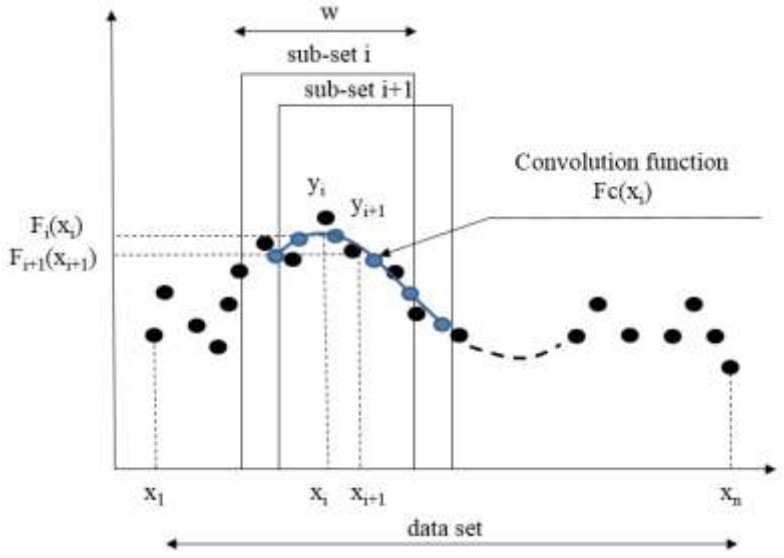

Figure 86. Savitzky–Golay filter method

The algorithm is implanted in Matlab® as the function *sgolayfilt*, with the syntax: *sgolayfilt (X, k, w).* X is the matrix containing the set of n data points (x_i y_i) $1 \leq i \leq n$; k is the degree of the interpolation polynomial and w is the width of the sub-set.

- Page intentionally left blank -

LIST OF FIGURES

LIST OF TABLES